

**MAGNETIC IRON OXIDE NANOCUBES – THE EFFECT OF SUBSTRATE
MODIFICATION, AND POST ASSEMBLY MANIPULATION ON THE FORMATION
OF A MONOLAYER**

Anya S. Chinniah

**A thesis presented to the faculty of Mount Holyoke College in partial fulfillment of the
requirements for the degree of Bachelor of Arts with Honors**

Department of Chemistry

Mount Holyoke College

South Hadley, Massachusetts

May 2021

This thesis was prepared under the directions of Dr. Himali Jayathilake, for 8
credits of independent study.

ACKNOWLEDGEMENTS

To professor Himali Jayathilake, words cannot express my appreciation and gratitude towards everything you have done to support me, whether it is in my research, my classes, my job applications, or my life. I could not have possibly asked for a better research mentor. Thank you for checking in on me when I was unwell, inviting me over for home cooked meals, and always making Mount Holyoke feel like my home away from home. You are incredibly kind, humble and know me and push me to reach my goals. Without your love and guidance, I could not have completed this project.

To professor Wei Chen, thank you for being a marvelous professor since day one and helping me discover my love for chemistry. Thank you for being a wonderful research mentor, and encouraging me to start research in the chemistry department. Without your advice and help, I would not have been able to write this thesis.

To professor Alan vanGiessen, thank you for being an incredible advisor, and guiding me through my four years at Mount Holyoke. Thank you for challenging me to think outside the box in your poisons class, and for helping me through Thermodynamics. Thank you for walking me through my different options when I was confused, and giving me an amazing recommendation to start me off on the next step of my journey.

To Sarah Kimele, I could not show more gratitude towards you and the TEM support you give me. I have enjoyed every moment spent talking about various subjects while imaging the iron (III) oxide nanocubes. Without your kindness, I would have never been able to finish this project and have the possibility to collect over 200 beautiful images. I really appreciate all the time and hard work you put into my project.

To professor Alan Werner, thank you for helping me integrate my love for chemistry into understanding different environmental problems posed by plastics in the environment. I appreciate the time and energy you spent on me helping me understand the different job opportunities for me as an environmental chemist.

To Sarah Andoh, thank you for being my peer mentor and guiding me through the first steps of my research. To Jennifer Taseneem, thank you for synthesizing the iron(III) oxide nanocubes, without which this project would not have been possible. Thank you both for all your previous work on this study, I could not have possibly come as far as I did with my research without it. I would also like to thank Maggie Minett, Katie Kolozsvari, Echo Jiang, Wenyun Wang, Jiuk Byun, Liz Hazen for being great research friends, and helping me brainstorm different ideas, without which my research would not be where it is today.

To my mother and father, without your unconditional love and support, I would not have the opportunity to come to the US to complete my undergraduate degree. Appa, thank you for being a remarkable role model and ma, thank you for guiding me through the most difficult of times, and believing in me when I did not believe in myself.

Finally, thank you to the Mount Holyoke Chemistry department, without which I could not have conducted this research or have completed my thesis

TABLE OF CONTENTS

	Page No.
ACKNOWLEDGEMENTS	i
TABLE OF CONTENTS	ii
LIST OF FIGURES AND TABLES	iv
ABSTRACT	1
1. INTRODUCTION	2
1.1 Nanoparticles and the History of Nanotechnology	2
1.2 Classification of Nanoparticles	2
1.3 Unique Nanoparticle Properties	3
1.4 Magnetic Nanoparticles	4
1.4.1 Coercivity and Superparamagnetism	5
1.5 Synthesis and Growth Mechanisms	6
1.5.1 Different Nanoparticle Synthesis Methods	7
1.5.2 La-Mer Mechanism	8
1.6 Monolayer Formation	9
1.7 Applications of Nanoparticles	10
1.7.1 Nanotechnology	10
1.7.2 Biomedical	11
1.7.3 Environmental	12
1.7.4 Data Science	13
1.8 Substrate Manipulation	14

1.8.1 Plasma Cleaning	14
1.8.2 Langmuir Blodgett Technique	15
1.8.3 Annealing	16
1.9 The goals of this Study	16
2. INSTRUMENTAL METHODS	18
2.1 Substrate Modification	18
2.1.1 Plasma Cleaning	18
2.1.2 Langmuir Trough	21
2.1.2.1 Langmuir-Schaefer Technique	22
2.1.2.2 Langmuir-Blodgett Technique	23
2.2 Preparation and Application of Nanocube Monolayer Films	23
2.2.1 Sonicating	23
2.2.2 Spin Coating	24
2.3 Post Assembly manipulation	25
2.3.1 Annealing	26
2.4 Characterization of Iron (III) Oxide (Fe_3O_4) Nanocubes	26
2.4.1 Fourier Transform Infra-Red (FTIR) Spectroscopy	26
2.4.2 UltraViolet Visible Spectroscopy	27
2.4.3 Dynamic Light Scattering (DLS)	28
2.4.4 Transmission Electron Microscopy (TEM)	28
3. EXPERIMENTAL METHODS	31
3.1 Synthesis	31
3.2 Confirmation of Magnetic Fe_3O_4 Nanoparticles	33

3.3 Transmission Electron Microscopy Grid Surface Manipulation:	34
3.3.1 Plasma Treatment	34
3.3.2 Cleaning of Langmuir Trough	35
3.3.3 Coating TEM Grid with HDA using the Langmuir Blodgett Technique	36
3.3.4 Coating TEM Grids with HDA using the Langmuir Schaefer Technique	38
3.4 Film Preparation	39
3.4.1 Sonication	39
3.4.2 Spin Coating	39
3.4.3 Annealing Procedure	40
3.5 Characterization Using TEM to Measure the Nanocube Size Distribution	41
4. RESULTS AND DISCUSSION	42
4.1 Magnetic Fe ₃ O ₄ nanocubes, and their characteristics	42
4.1.1 Decanoic acid surfactant coating	42
4.1.2 Size and shape analysis	43
4.1.3 Dynamic Light Scattering (DLS)	44
4.1.4 UV Visible Spectra	46
4.1.5 Fourier Transform Infrared Spectroscopy (FTIR)	47
4.2 Assembly of Magnetic Fe ₃ O ₄ Nanocubes, and modifications	47
4.2.1 Modifications of the substrate, and nanoparticles	48
4.2.1.1 Particles Annealed at 100 °C.	50
4.2.1.2 Particles Annealed at 125 °C	57
4.2.1.3 Particles Annealed at 150 °C	63

4.2.2 Particles spin cast onto TEM grids coated with HDA	70
5. CONCLUSIONS AND FUTURE WORK	73
6. REFERENCES	75
7. APPENDIX	82

LIST OF FIGURES AND TABLES

	Page No.
Figure 1: Schematic representation of unique, and modifiable nanoparticle properties ⁷	4
Figure 2: Schematic representation of magnetic nanoparticles coercivity through multi-domain and superparamagnetic domain levels	6
Figure 3: La Mer diagram schematic - reaction time vs. atom saturation. ²⁰	9
Figure 4: The formation of Maghemite (γ - Fe ₂ O ₃) monolayer. ²³	10
Figure 5: Applications of nanoparticles in different biological research studies including (a) substrate labeling, (b) sample concentration/separation, (c) substrate coding, and (d) signal transduction and amplification. ²⁶	11
Figure 6: Schematic representation of the variables used in this experiment	18
Figure 7: Schematic representation of surface oxidation, post plasma cleaning	19
Figure 8: Plasma cleaning a contaminated substrate. ⁴⁰	20
Figure 9: Langmuir Trough methods - Langmuir Blodgett and Langmuir Schaefer deposition techniques. ⁴¹	22
Figure 10: Before, and after sonication of the iron oxide nanoparticles suspended in a 3:1 Chloroform: Methanol dispersing agent	24
Figure 11: Schematic representation of the principle of the spin coating process for assembly of nanocube films. ⁴⁴	25
Figure 12: Layout of optical components in a basic TEM. ⁵³	29
Figure 13: Chemical structures of the reagents used in the synthesis of Fe ₃ O ₄ nanocubes: (a) iron acetylacetonate (b) decanoic acid (c) dibenzyl ether. ⁵⁴	31
Figure 14: Setup of the reaction vessel for the synthesis of nanocubes. ⁵⁴	32

Figure 15: Schematic representation of plasma treatment set up. ⁵⁵	35
Figure 16: Relationship between isotherm generated and phases of the packed HDA particles. ⁵⁶	37
Figure 17: Schematic diagram of compression barriers packing nanocubes into a solid layer for assembly using Langmuir-Blodgett technique. ⁵⁷	38
Figure 18: Schematic representation of drop-casting, and spin coating 10 µl of Fe ₃ O ₄ in 3:1 C: M solution onto a carbon TEM grid	40
Figure 19: Measuring the diameter size of a Fe ₃ O ₄ nanocube. ⁵⁴	41
Figure 20: Fe ₃ O ₄ nanocubes attraction to a neodymium magnet through a vial. ⁵⁴	42
Figure 21: Chemical structure of the decanoic acid used as the Fe ₃ O ₄ nanocube surfactant coating	43
Figure 22: Highly magnified image of magnetic Fe ₃ O ₄ nanocubes as seen in Image J	43
Figure 23: Size distribution histogram of magnetic Fe ₃ O ₄ nanocubes with a mean size of 15.50 ± 3.95 nm	44
Figure 24: DLS graph of magnetic Fe ₃ O ₄ nanocubes suspended in a 3:1 C: M dispersing agent with a mean diameter of 18.10 ± 6.30nm	45
Figure 25: UV Vis Spectra of pure 3:1 C:M solution, against Magnetic Fe ₃ O ₄ Nanocubes suspended in a 3:1 C: M Dispersing Agent	46
Figure 26: FTIR of the magnetic Fe ₃ O ₄ nanocubes with a peak at 579 cm ⁻¹ showing the presence of Fe ₃ O ₄	47
Figure 27: Highly magnified TEM image of iron oxide nanocubes suspended in a 3:1 C: M solution is taken on July 6th, 2017, and May 23rd, 2019 spin-cast on a carbon TEM grid with no surface modification	48
Figure 28: Carbon coated TEM grid, and an image of one square as viewed under Transmission Electron Microscopy	49
Figure 29: TEM image of Fe ₃ O ₄ nanocubes spin-cast onto a TEM grid with no surface modification, and no annealing at a magnification of 52,000x	50

Table 1: Fe ₃ O ₄ nanoparticles spin-cast on TEM Grids, with no surface modification, annealed at 100° C	51-52
Figure 30: (a) Nanocube percentage coverage of TEM grid with no surface modification annealed at 100° C against time with an average of 80.0 % (b) Mean nanocube size for nanocubes against annealing time with a mean length of 15.0 nm	53
Table 2: Fe ₃ O ₄ nanoparticles spin-cast on plasma cleaned TEM Grids, annealed at 100° C	54-55
Figure 31: (a) Nanocube percentage coverage of plasma cleaned TEM grid annealed at 100° C against time with an average of 43.5% (b) Mean nanocube size for nanocubes against annealing time with a mean length of 15.0 nm	56
Figure 32: 900x magnified TEM image of magnetic iron oxide nanoparticles spin-cast on Carbon Coated TEM grid for 1 minute at 6000 rpm under Nitrogen	57
Table 3: Fe ₃ O ₄ nanoparticles spin-cast on TEM Grids, with no surface modification, annealed at 125° C	58-59
Figure 33: Appearance of spherical particles on the TEM grid with no surface modification after annealing at 125° C for 6 hours.	60
Table 4: Fe ₃ O ₄ nanoparticles spin-cast on Plasma cleaned TEM Grids annealed at 125° C	61-62
Table 5: Fe ₃ O ₄ nanocubes spin-cast on TEM Grids with no surface modification, annealed at 150° C	63-64
Figure 34: (a) Nanocube percentage coverage of TEM grid with no surface modification annealed at 150° C against time with an average of 56.5% (b) Mean nanocube size for nanocubes against annealing time with a mean length of 15.0 nm	65
Figure 35: Highly magnified TEM image of spherical nanoparticles that was observed after annealing the TEM sample with no surface modification at 150° C for 24 hours	66

Table 6: Fe ₃ O ₄ nanoparticles spin-cast on Plasma cleaned TEM Grids annealed at 150 °C	66-68
Figure 36: (a) Nanocube percentage coverage of plasma cleaned TEM grid annealed at 150° C against time with an average of 20.0 % (b) Mean nanocube size for nanocubes against annealing time with a mean length of 15.6 nm	68
Figure 37: Highly magnified TEM image of spherical nanoparticles that was observed after annealing the plasma cleaned TEM sample at 150 °C for (a) 1.5 hours (b) 6 hours.	69
Table 7: Fe ₃ O ₄ nanocubes deposited on HDA Coated TEM grids using the LS technique at different magnifications	70-71
Table 8: Fe ₃ O ₄ nanocubes deposited on HDA Coated TEM grids using the LB technique at different magnifications	71

ABSTRACT

Over the last decade, nanoparticles have become particles of great research interest because of their inherent chemical compositions such as size, shape, ability to be coated by other molecules, and control over their magnetic properties. The Assembly of these particles into a monolayer allows their unique properties to be harnessed and applied in various fields of study. The goal of this study was to use various surface modification techniques to assemble magnetic iron oxide (Fe_3O_4) nanocubes suspended in a 3:1 chloroform: methanol dispersing agent, into a monolayer. By exploring literature on how changing different factors such as plasma cleaning, Langmuir-Blodgett (LB) technique, and annealing, the conditions optimal for the monolayer formation were characterized and verified using transmission electron microscopy (TEM) imaging and subsequent analysis. For the primary objective of nanoparticle assembly into monolayer films, the techniques of spin coating onto a carbon TEM substrate was used. The role of TEM grid modification using plasma cleaning and LB technique was explored to see the effect on the even distribution of the nanoparticles. Post-modification annealing on spin-coated nanoparticles was also explored and was projected to play a vital role in morphological stability and even particle distribution on the carbon TEM substrate. After annealing, the grids are imaged under TEM at different magnifications. Using the Java-based program, Image J, it was found that the nanocubes maintained their shape and the mean cubic length of 15.50 nm at temperatures ranging from 100 – 150 °C. The TEM grids with no surface modification, annealed at 100 °C showed the highest area coverage of 80%. The results so far indicate that plasma cleaning of TEM grids can hinder the formation of a uniform monolayer. This could be due to the unfavorable interaction between the hydrophobic decanoic acid coating of nanocubes and the hydrophilic TEM grid. The TEM grids coated with heptadecanoic acid (HDA) had a more evenly dispersed layer of nanocubes. This could be due to the favorable hydrophobic interactions between hydrocarbon chains of HDA and decanoic acid. The study reveals how different surface modification techniques affect the assembly of nanocubes into a monolayer formation. Further investigation is needed to confirm if annealing of nanocubes at 100° C on a hydrophobic substrate is the best modification to promote the formation of a uniform monolayer.

1. INTRODUCTION

1.1. Nanoparticles and the History of Nanotechnology

Over the last decade, nanoparticles have become particles of great research interest because of their inherent chemical compositions such as size, shape, and their ability to be coated by other molecules, that allow them to be applied in various fields of study. Nanotechnology is defined as the understanding and control of matter at dimensions between 1 and 100 nm where unique phenomena enable novel applications¹.

Although human exposure to nanoparticles has occurred throughout human history, it dramatically increased during the industrial revolution. The study of nanoparticles, however, is not new. The concept of a “nanometer” was first proposed by Richard Zsigmondy, the 1925 Nobel Prize Laureate in chemistry. He coined the term nanometer explicitly for characterizing particle size and he was the first to measure the size of particles such as gold colloids using a microscope². The beginning of the 21st century has seen an increased interest in the emerging fields of nanoscience and nanotechnology. In a timeframe of approximately half a century, nanotechnology has become the foundation for remarkable industrial applications and exponential growth. Today, nanotechnology impacts human life every day. The potential benefits are many and diverse.

1.2. Classification of Nanoparticles

Nanoparticles can be broadly classified into three groups - organic, inorganic, and magnetic nanoparticles. Organic nanoparticles may include carbon nanoparticles, such as fullerenes, while some of the inorganic nanoparticles may include nanoparticles such as

iron oxide, noble metal nanoparticles, such as silver and gold, and semiconductor nanoparticles such as titanium dioxide and zinc oxide.

There is a growing interest in inorganic nanoparticles as they provide superior material properties with functional versatility³. Due to their size features and surface chemistry modification, inorganic nanoparticles have been examined as potential tools for a variety of applications. Inorganic nanomaterials have been widely used for cellular delivery due to their versatile features like wide availability, rich functionality, good biocompatibility, the capability of targeted drug delivery, and controlled release of drugs.⁴

Magnetic nanoparticles are nanomaterials that consist of magnetic elements, such as iron, nickel, cobalt, chromium, manganese, gadolinium, and their chemical compounds. Magnetic nanoparticles are superparamagnetic because of their nanoscale size, offering great potentials in a variety of applications in their bare form or coated with a surface coating and functional groups chosen for specific uses.⁵

1.3. Unique Nanoparticle Properties

Several physical phenomena become more pronounced as the size of the system decreases. Certain phenomena may not come into play as the system moves from macro to micro-level but may be significant at the nanoscale. One example is the increase in surface area to volume ratio which alters the mechanical, thermal, and catalytic properties of the material. The increase in surface area to volume ratio leads to the increasing dominance of the behavior of atoms on the surface of the particle over that of those in the interior of the particle, thus altering the properties. The electronic and optical properties and the chemical reactivity of small clusters are completely different from the

better-known property of each component in the bulk or at extended surfaces. Some of the size-dependent properties of nanoparticles are quantum confinement in semiconductors, surface plasmon resonance in some metallic nanoparticles, and paramagnetism in magnetic nanoparticles.⁶

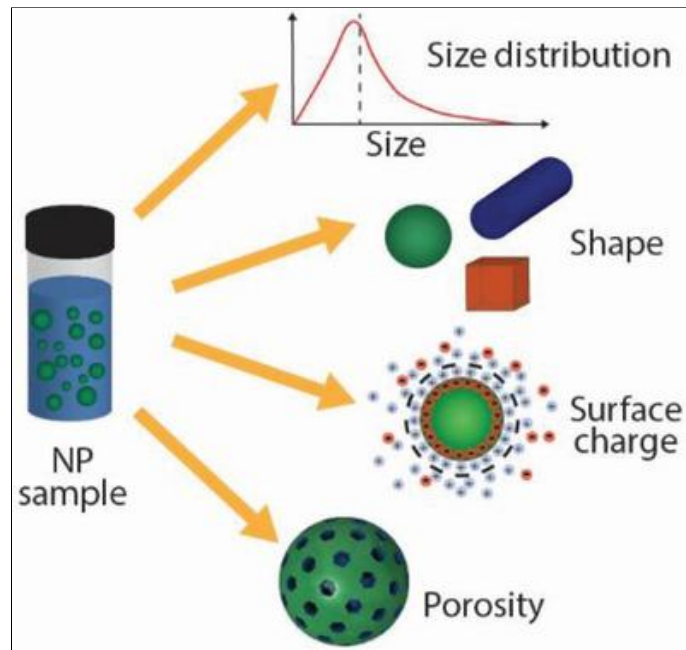


Figure 1: Schematic representation of unique, and modifiable nanoparticle properties⁷

1.4. Magnetic Nanoparticles

Magnetic nanoparticles represent an important class of functional nanoparticles because of their nanoscale properties and size-dependent magnetic applications.⁵ They show remarkable new phenomena such as high field irreversibility, high saturation field, superparamagnetism, extra anisotropy contributions, or shifted loops after field cooling. These phenomena arise from side effects and surface effects that dominate the magnetic

behavior of individual nanoparticles.⁸ They feature a magnetic ore such as iron, cobalt, or nickel along with a functioning group such as oxygen. Iron oxide nanoparticles (Fe_3O_4) and its oxidized state maghemite ($\gamma\text{-Fe}_2\text{O}_3$) are by far the most commonly employed nanoparticles for biomedical applications. Highly magnetic materials such as cobalt and nickel are susceptible to oxidation, resulting in high toxicity. Hence they are of little interest.⁹

1.4.1. Coercivity and Superparamagnetism

One of the most prominent features of magnetic nanoparticles is their size-dependent magnetic properties. Frenkel and Dorfman were the first to predict that a particle of ferromagnetic material below a critical size would consist of a single magnetic domain.¹⁰ A magnetic domain refers to a volume of ferromagnetic material in which all magnetons are aligned in the same direction by the exchange forces. This concept of domains distinguishes ferromagnetism from paramagnetism.

Coercivity is the ability of ferromagnetic material to withstand an external field without being demagnetized. It is found that as the size of the nanoparticle decreases, the number of magnetic domains reduces, and subsequently, the coercivity of the nanoparticles increases. However, when the size of single-domain particles further decreases below a critical diameter, the coercivity becomes zero, and such particles become superparamagnetic. What is unique about superparamagnetic nanoparticles is that they become magnetic in the presence of an external magnet, but revert to a nonmagnetic state when the external magnet is removed. This avoids an 'active' behavior of the particles when there is no applied field. Introduced in the living systems, particles are

'magnetic' only in the presence of an external field, which gives them unique advantages when working in biological environments.¹¹

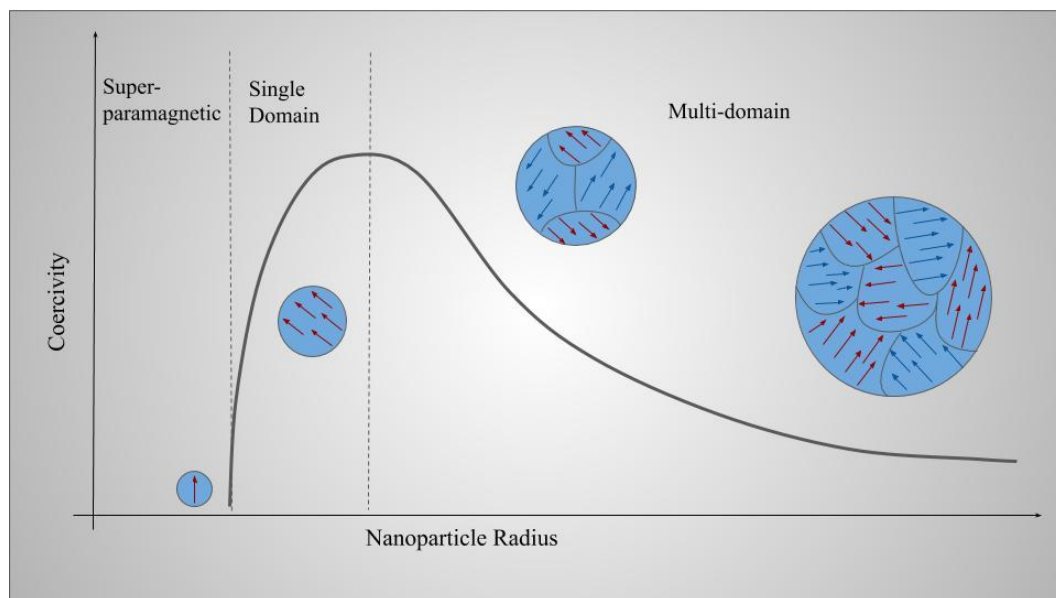


Figure 2: Schematic representation of magnetic nanoparticles coercivity through multi-domain and superparamagnetic domain levels

1.5. Synthesis and Growth Mechanisms

Despite the availability of several methods that are capable of producing nanoparticles at various stages of academic or commercial development such as plasma- or flame-based syntheses, the quality and consistency of nanoparticles can differ from process to process.¹² The inability of many processes to manufacture high-quality nanomaterials consistently and safely is in part due to inherent limitations of processes or lack of knowledge on particle-parameter behaviors. For example, processes that involve very high temperatures such as flame, combustion, or plasma processes result in phase separation or extensive agglomeration with low surface areas¹³. Some of these methods

also produce highly charged nanoparticles in the gas phase, which could potentially be hazardous to workers as they are airborne and present a potential inhalation hazard.¹⁴

1.5.1. Different Nanoparticle Synthesis Methods

A variety of physical and chemical methods can be utilized to synthesize nanoparticles, listed below:

The sol-gel technique is a wet-chemical technique used for the fabrication of metal oxides from a chemical solution which acts as a precursor for an integrated network (gel) of discrete particles or polymers. The precursor sol can be either deposited on the substrate to form a film, cast into a suitable container with the desired shape, or used to synthesize powders.¹⁵

Laser ablation is the process of removing material from a solid surface by irradiating it with a laser beam. At low laser flux, the material is heated by absorbed laser energy and evaporates or sublimates. At higher flux, the material is converted to plasma. The depth over which the laser energy is absorbed and the amount of material that is removed by a single laser pulse depends on the material's optical properties and the laser wavelength. Carbon nanotubes can be produced by this method.¹⁶

In the inert gas condensation synthesis method, different metals are evaporated in separate crucibles inside an ultra-high vacuum chamber filled with helium or argon gas at a typical pressure of few 100 pascals. As a result of interatomic collisions with gas atoms in the chamber, the evaporated metal atoms lose their kinetic energy and condense in the

form of small crystals which accumulate on a liquid nitrogen-filled cold finger. Ex: gold nanoparticles have been synthesized from gold wires.¹⁷

Solvothermal synthesis is a versatile low-temperature route in which polar solvents under pressure and at temperatures above their boiling points are used. Under solvothermal conditions, the solubility of reactants increases significantly, enabling the reaction to take place at a lower temperature.¹⁸

Chemical reduction, which is the reduction of an ionic salt in an appropriate medium in the presence of surfactant using reducing agents. Some of the commonly used reducing agents are sodium borohydride, hydrazine hydrate, and sodium citrate.¹⁹

1.5.2. La-Mer Mechanism

The magnetic iron oxide nanocubes used in this study were synthesized by the “La Mer Synthesis”.⁶ First is the decomposition using the heat where reducing agents work on the metal to break it down into many free atoms at reflux at a specified temperature. The second is the process of nucleation. Nucleation is a purely thermodynamic model which describes the process of the first step in a first-order phase transition. It describes the appearance of a new phase – the nucleus – in the metastable primary phase.²⁰ The free atoms arrange initially in a pattern resembling a crystal. It allows for new particles to grow on top and agglomerate forming the nanoparticles crystal shape/size depending on reagents and temperature duration. After the formation of the nanoparticles, a surfactant coating is used to cap further growth. This process occurs during synthesis, as well as at reflux. Capping molecules coat the nanoparticles that have been formed and cap them, stopping the growth at that specified temperature and

fostering repulsion between the nanoparticles creating stabilization. The concentration of capping molecules affects the size and shape of the nanoparticles.

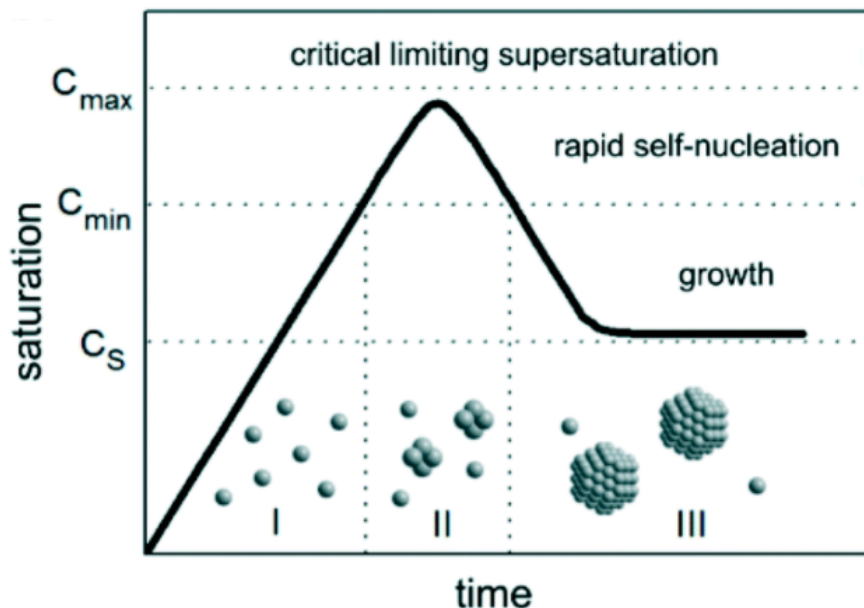


Figure 3: La Mer diagram schematic - reaction time vs. atom saturation.²⁰

1.6. Monolayer Formation

Recently, many attempts have been made to develop techniques and processes that would yield 'monodispersed colloids' consisting of uniform nanoparticles both in size and shape.²¹ For various biomedical applications, uniform iron oxide nanoparticles need surface modification processes to achieve biocompatibility and long-term stability.²² Nanoparticles possess unique properties associated with their core materials that differ from their bulk counterparts. Some of these properties are distinctive magnetic, photonic as well as electronic behavior. The assembly of these particles into a monolayer allows these unique behaviors to be harnessed and applied in a variety of industries.

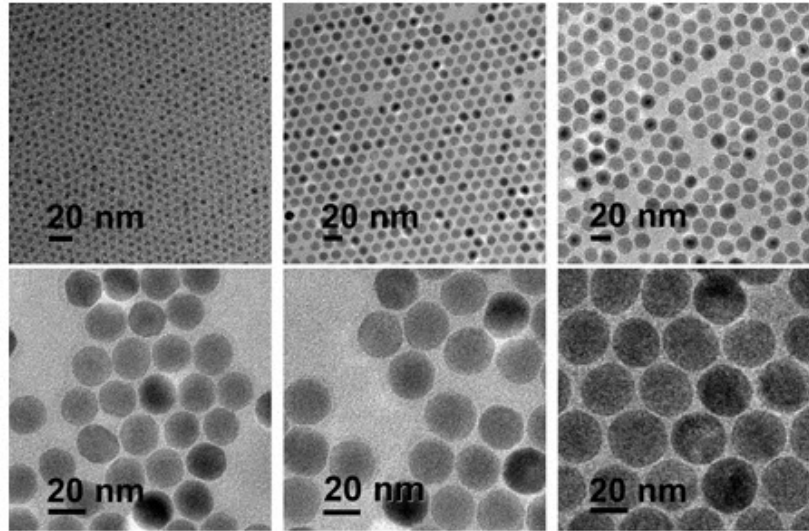


Figure 4: The formation of Maghemite (γ - Fe_2O_3) monolayer.²³

1.7. Application of nanoparticles

Nanoparticles applications span a wide range of industries including nanotechnology, biomedical applications, environmental applications, and data science applications. In this section, we see the various uses of nanoparticles in these different sectors.

1.7.1. Nanotechnology

Nanotechnology is recognized as an emerging enabling technology for the 21st century, in addition to the already established areas of information technology and biotechnology. This is because of the scientific convergence of physics, chemistry, biology, materials, and engineering at the nanoscale, and of the importance of the control of matter at the nanoscale on almost all technologies.²⁴ Nanoscience and nanotechnology have already been applied in various fields, such as computer electronics, communication, energy production, medicine, and the food industry. The nanoscale

devices are often manufactured with the view to imitate the nanodevices found in nature and include proteins, DNA, membranes, and other natural biomolecules.²⁵

1.7.2. Biomedical

Nanoparticles have a wide range of applications in the biomedical field. They are utilized in the detection of biomolecules, sample separation, purification and concentration, substrate coding, signal transduction, and amplification.²⁶

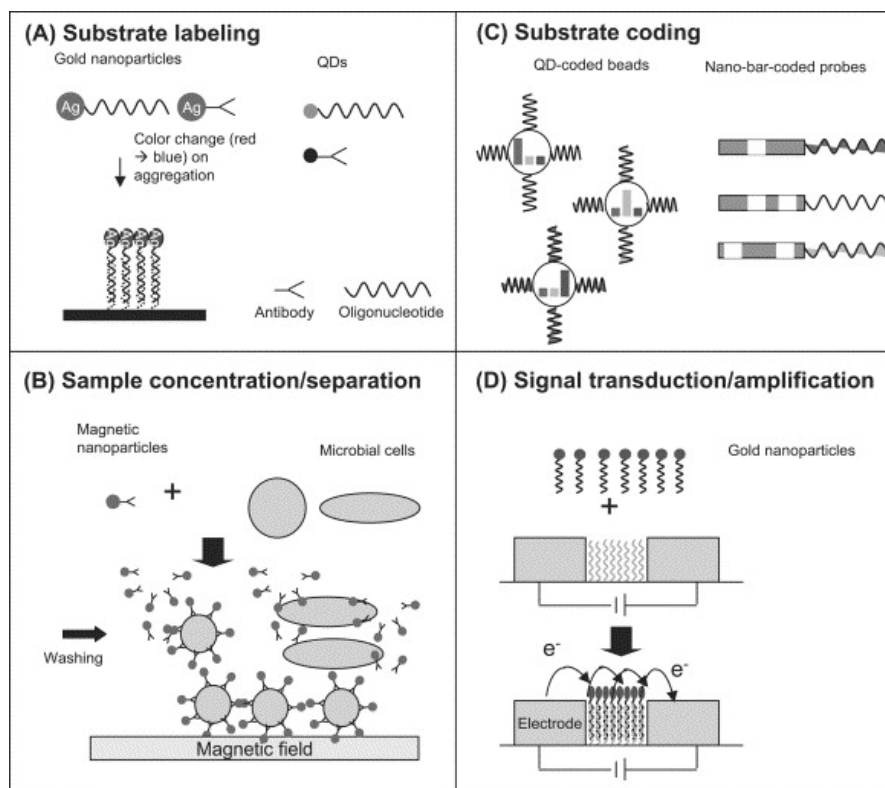


Figure 5: Applications of nanoparticles in different biological research studies including (a) substrate labeling, (b) sample concentration/separation, (c) substrate coding, and (d) signal transduction and amplification.²⁶

They have been used as signal reporters to detect biomolecules in DNA assay,

immunoassay, and cell bioimaging. Usually, they are derivatized with different functional groups such as nucleic acid-targeted oligonucleotide probes, antibodies, and protein to produce nanoprobess. Gold nanoparticle-based probes have been used in the identification of pathogenic bacteria in DNA-microarray technology.²⁷

Alternatively, nanoparticles can be utilized as fluorophores in fluorescence *in situ* hybridization. Quantum Dots attached to a specific oligonucleotide probe or immunoglobulin G have been used to successfully detect the human Y chromosome ²⁸, and to locate cancer markers in cellular imaging in cancer studies.²⁹

Magnetic nanoparticles are mainly used to assist the separation, purification, and concentration of different biomolecules. To do so, different capturing molecules such as antibodies and oligonucleotide probes can be immobilized on the surface of magnetic nanoparticles.²⁶

1.7.3. Environmental

Although there are fewer applications of nanoparticles in environmental studies than in biomedical studies, they have been used in a few sectors including microbial and monitoring detection, and chemical degradation, and source recovery.²⁶

The use of quantum dots as a fluorescence labeling system in microbial detection has been successfully demonstrated. Thiolated CdSe-core quantum dots could be conjugated with wheat germ agglutinin, a lectin that is commonly found in gram-positive bacteria.³⁰

The detection and monitoring of microorganisms can be further accelerated using nanoparticles in a fluorescence labeling system in microfluidic devices. For example, a simple microfluidic device has been developed for the rapid detection of viruses present in aqueous environments.³¹

Nanoparticle-based fluorescence reporting systems can be further developed to achieve rapid bacterial detection at the single-cell level. With the improvement in the fluorescence reporting system, the fluorescence intensity emitted by one *E. coli* O157 cell was sufficient to be detected using a normal spectrofluorometer in a conventional plate-based immunological assay.³²

Several studies have utilized bimetallic nanoparticles as an effective oxidant instead of granular zero-valency metal in the cleanup of environmental contaminants, mainly because (i) nanoparticles can diffuse or penetrate a contamination zone where microparticles cannot reach, and (ii) higher reactivity to redox-amenable contaminants than that of microsized particles can be obtained.³³

1.7.4. Data Science

Data storage is one area of technology where nanotechnology has been used even before the term nanotechnology became popular. The magnetic recording media - the disk that stores information in hard disk drives, used nanotechnology in the late 1990s, in the form of grains that are 15 nm or less in diameter (the grains in current technology are about 8 nm in diameter).³⁴

Flash-based memory chips used in computers and cameras today consist of semiconductor materials covered by an insulating oxide layer, which is only a few nanometres thick. Saving and deleting data on Flash storage media is only possible by using a phenomenon of quantum mechanics and this nanotechnology. The advantages of Flash-based memory chips, USB, and SSD cards would not be possible without the reduction in size beyond the nanometer barrier. But over the years, due to the increase in big data, other methods have been discovered that both minimize the storage space used and allow you to save more data in less space. With more and more companies creating massive amounts of data, research continues into the field of data storage; most of which use nanotechnology.³⁵

1.8. Substrate Manipulation

In an attempt to aid the formation of a smooth, and evenly dispersed iron oxide nanocube monolayer, substrate modification, and post-assembly manipulation can be utilized. In this study, modification techniques such as plasma cleaning, Langmuir trough, and annealing processes were utilized to promote the formation of the nanoparticle monolayer.

1.8.1. Plasma Cleaning

Plasma cleaning of solid surfaces is one of the hot topics of the very fast-developing field of plasma treatment of materials. Plasma cleaning has been implemented already in several industries such as semiconductor processing and microchip fabrication, metallurgy, the optical industry, dentistry, medical technologies, food packaging – to name just the most important areas.

Plasma cleaning is the process of removing all organic matter from the surface of an object through the use of an ionized gas called plasma. This is generally performed in a vacuum chamber utilizing oxygen and/or argon gas. The cleaning process is environmentally safe as there are no harsh chemicals involved. Plasma often leaves a free radical on the surface being cleaned to further increase the bondability of that surface.³⁶

The purpose of plasma cleaning in this study is to utilize the ability of oxygen plasma to increase the hydrophilicity of the substrate and subsequently promote the formation of a smooth monolayer.

1.8.2. Langmuir Blodgett Technique

Langmuir Blodgett's (LB) films have been the subject of scientific curiosity for most of the twentieth century. However, interest has grown significantly since the 1970s - a direct result of the work of Hans Kuhn and colleagues on the energy of transfer in multilayer systems. This introduced the idea of molecular engineering - using the LB technique to position certain molecular groups at a precise distance to others. In this way, new thin-film materials could be built up at the molecular level.³⁷

The LB deposition method offers a combination of controlled deposition, a wide range of substrates, and usability in ambient conditions. In an LB deposition process, a nanoparticle suspension is first deposited at the air/water interface, then, the resulting film is compressed to the desired surface pressure and particle density and then transferred onto a solid substrate by dipping the substrate into and through the particle layer. The deposition can then be repeated to fabricate alternating layer structures or performed at different speeds and temperatures.³⁸

The use of LB in this study is to coat the substrate of choice in a controlled manner with a hydrophobic compound to help enable the formation of a smooth monolayer.

1.8.3. Annealing

Several papers discuss the role of annealing in the alteration and manipulation of nanoparticle assembly. It is seen that self-assembled Pt nanoparticles evolution on *c*-plane sapphire was based on the control of annealing temperature and duration, in which the coherent effect of surface diffusion, surface energy minimization, Rayleigh instability, and Ostwald ripening lead to the formation of various configuration, size, and density of Pt nanoparticles.^{39,40,41}

1.9. The goal of this Study

The goal of this study is to use various surface modification techniques to assemble magnetic iron oxide nanoparticles suspended in a 3:1 chloroform: methanol dispersing agent into a monolayer. By exploring the literature on how changing different factors such as plasma cleaning, Langmuir, trough, and annealing, the conditions optimal for the monolayer formation are characterized and verified using transmission electron microscopy imaging and subsequent analysis.

For the primary objective of nanoparticle assembly into monolayer films, the techniques of spin coating onto a carbon TEM substrate are analyzed. The role of TEM grid modification using plasma cleaning and Langmuir trough is explored to see the effect on the even distribution of the nanoparticles. Post-modification annealing on spin

coating is also explored and is projected to play a vital role in morphological stability and even particle distribution on the carbon TEM substrate. The work in the study aims to gather more knowledge on the manipulation of the TEM grid substrate as well as annealing of magnetic iron oxide nanoparticles to understand the effect on the assembly of an even monolayer for a variety of different applications.

2. INSTRUMENTAL

2.1 Substrate Modification

In an attempt to aid the formation of a smooth, and evenly dispersed iron oxide nanocube monolayer, substrate modification, and post-assembly manipulation can be utilized. In this study, the substrate of choice, a carbon-based TEM grid is modified using plasma cleaning, and Langmuir trough techniques to alter the hydrophobic nature of the grid. Post manipulation of the substrate, the magnetic iron oxide nanocubes adhere to the substrate where they undergo post assembly manipulation via annealing processes.

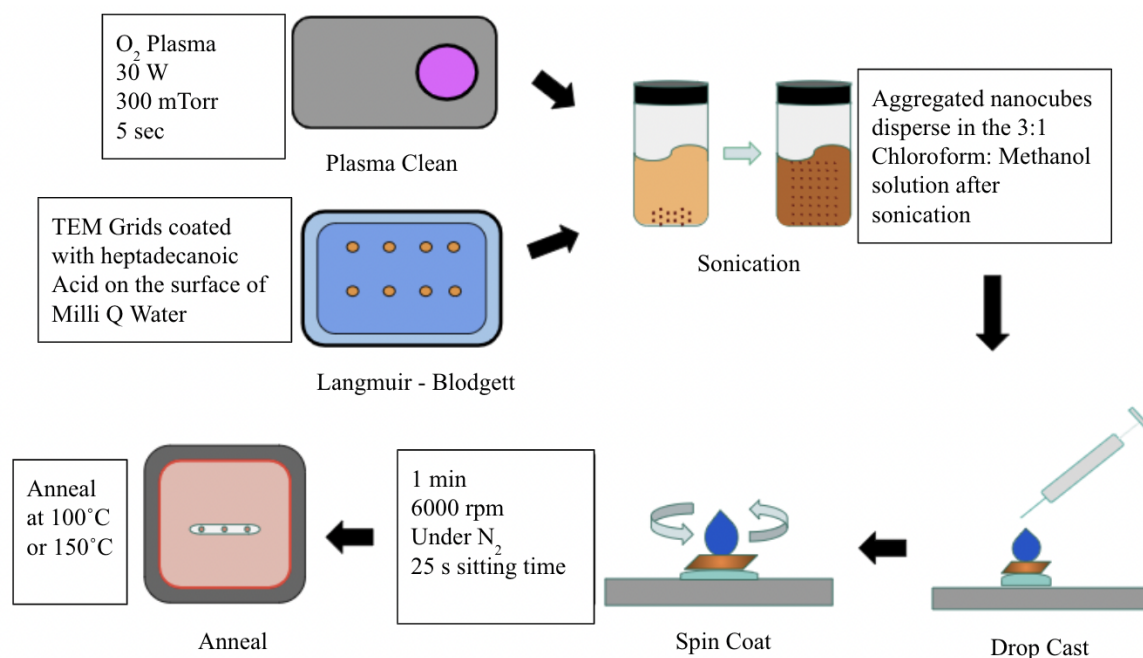


Figure 6: Schematic representation of the variables used in this experiment

2.1.1 Plasma Cleaning

In this project, a plasma cleaner is used for both removing organic contaminants on the TEM grid, and for hydrophilizing the surface. Plasma cleaning can be applied to an array of materials along with surfaces with complex geometries. A plasma cleaning system allows the efficient cleaning of a surface without harming other properties of the surface.

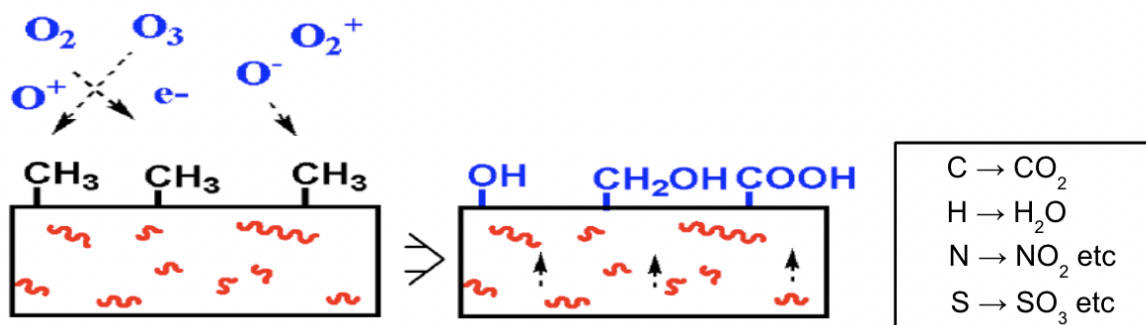


Figure 7: Schematic representation of surface oxidation, post plasma cleaning

The three known states of matter are solid, liquid, and gas. We can move between the states by adding or removing energy (e.g. heating/cooling). If we continue to add enough energy, gas molecules will become ionized (lose one or more electrons) and so carry a net positive charge. If enough molecules are ionized to affect the overall electrical characteristics of the gas the result is called plasma. A plasma contains positive ions, electrons, neutral gas atoms or molecules, UV light, and also excited gas atoms and molecules, which can carry a large amount of internal energy. Plasmas glow because the light is emitted as these excited neutral particles relax to a lower energy state (Figure 8). All of these components can interact with the surface during plasma treatment. By choosing the gas mixture, power, pressure, etc. we can quite precisely tune, or specify, the effects of the plasma treatment.⁴²

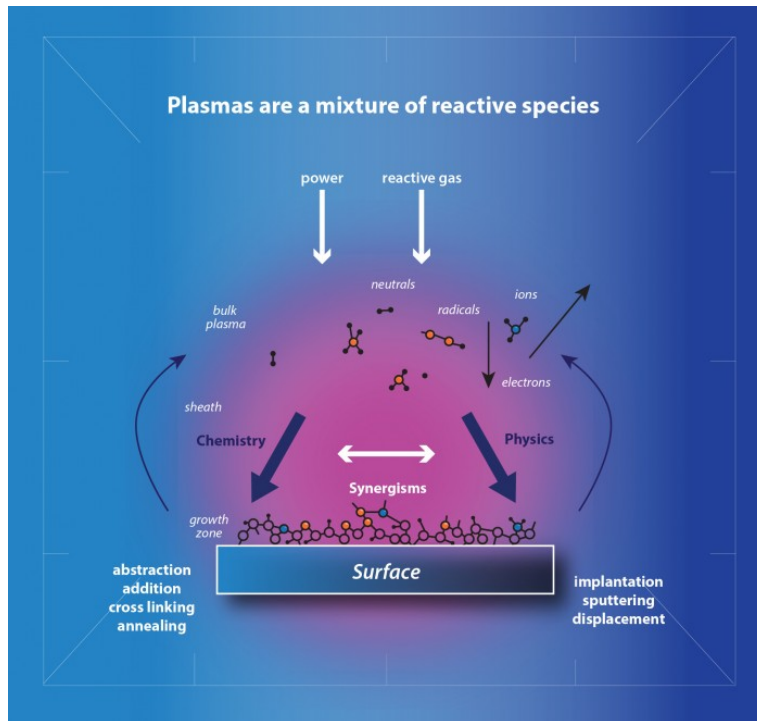


Figure 8: Plasma cleaning a contaminated substrate.⁴²

Plasma treatment can be performed in an evacuated enclosure or chamber. The air is pumped out and gas is allowed to flow in at low pressure before the energy in the form of electrical power is applied. It's important to note that the plasma treatment is a low-temperature process, meaning that heat-sensitive materials can be processed quite readily. This system also works with chemical functional groups, such as, carboxyl, carbonyl, and hydroxyl on the surface, which renders most surfaces hydrophilic. For this experiment, an oxygen plasma was used to clean the substrate using a pressure of 300 mmHg for 5 seconds. The oxygen plasma treatment increases the presence of OH groups which enables more hydrogen bonding. This in turn increases the surface hydrophilicity. Hence, there is a decrease in the water contact angle and an increase in wettability to enhance the bonding or adhesion to other surfaces.⁴²

2.1.2 The Langmuir Trough

We have seen that plasma cleaning can be utilized to remove contaminants on the substrate and increase the hydrophilicity of the substrate. In contrast, the Langmuir trough technique is utilized to coat the substrate with a heptadecanoic acid (HDA) layer, in an attempt to increase its hydrophobicity. The Langmuir trough method consists of two different deposition techniques: the Langmuir-Blodgett (LB) and the Langmuir-Schaefer (LS) techniques. For either of these techniques to be successful, it has to be ensured that the Langmuir trough is very clean. Otherwise, dust particles can hinder the formation of a smooth HDA monolayer. For this purpose, ethanol can be used to clean down the trough. The trough is then filled with Milli Q water. Using a microsyringe, small volumes of the HDA solution can be spread all over the water surface in the trough at the air-water interface. The layer is left to stabilize for a few minutes and to allow the evaporation of the solvent.

An external force is applied to those floating surfactant molecules using the barriers in the Langmuir trough. The barriers are used to compress the HDA molecules together to ensure the packing of the molecules for even dispersion. The Wilhelmy plate suspended over the water surface measures the surface pressure and if the compression of the barriers is sufficient, a solid film will be created in the trough. The HDA films can be successfully studied if they reach a solid-state. Langmuir trough deposition is traditionally carried out in the solid phase where the surface pressure is high enough to ensure sufficient cohesion in the monolayer. This means that attraction between the molecules in the monolayer is sufficient to prevent the monolayer from falling apart during transfer to the solid substrate and ensures the buildup of homogeneous multilayers. At the solid-state, the monolayers can form highly self-assembled arrays with uniform arrangement and spacing. On the other hand, at the liquid and gaseous states, the

molecules have uneven packing with large spacing. Even though it should be ensured that there is enough compression to allow the formation of a solid monolayer, care should be taken to not allow extreme compression of the solid-state. This may cause the uniform packing of the HDA molecules to break and eventually lead to the formation of multilayers of molecules as shown by the dip in the isotherm. A good isotherm can be typically used to identify the changes in the different states.

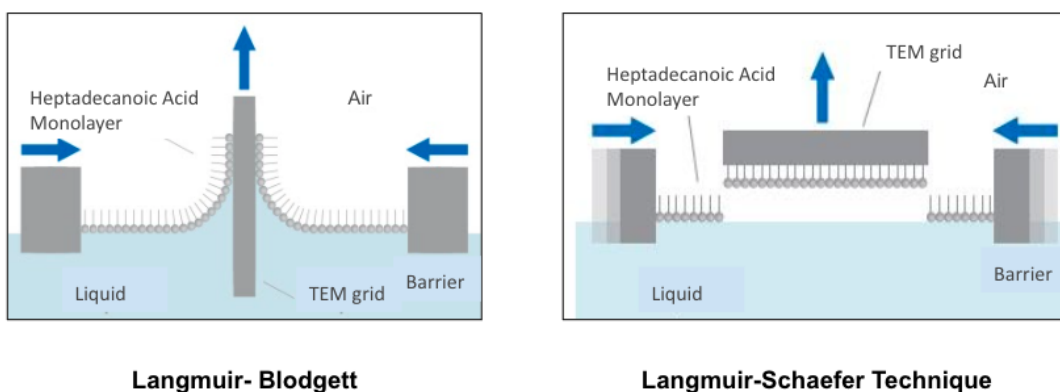


Figure 9: Langmuir Trough methods - Langmuir Blodgett and Langmuir Schaefer deposition techniques.⁴³

2.1.2.1 Langmuir-Blodgett Technique

Both the Langmuir-Blodgett (LB) and Langmuir-Schaefer (LS) techniques are useful in the formation of controlled thin films at the air-water interface. The main difference between the two techniques is the direction of deposition of the substrate on the water surface. The LB technique utilizes the vertical dipping of TEM grids under the water surface. The TEM grid is gradually immersed into the water surface. After the deposition and stabilization of the HDA solution on

the water surface, the grid is gradually extracted vertically from the water (Figure 9). This leaves a layer of the HDA as a thin film of molecules on the TEM grid substrate surface.

2.1.2.2 Langmuir-Schaefer Technique

The Langmuir-Schaefer technique involves the horizontal deposition of the HDA on the grid (Figure 9). In this method, after the compression and stabilization of heptadecanoic molecules on the water surface, the TEM grids are carefully released on the dispersed HDA surface to allow the transfer of the particles onto the substrate. The grids are allowed to stabilize for 25 seconds and are then extracted horizontally from the surface.

2.2 Preparation and Application of Nanocube Monolayer Films

Nanocube thin films can be prepared using many different methods. The main technique used to prepare nanocube films in this experiment is spin coating. Here, the substrate of choice is a carbon-coated TEM grid. Manipulating the surface chemistry of the substrate in an attempt to prepare stable, homogenous, and well-packed particles in a monolayer is essential in the application of nanocubes. The two manipulation techniques involved in this study include Langmuir trough and plasma cleaning. Post application of the nanoparticles to the substrate of choice, the iron oxide nanocubes are annealed to further enable the smooth formation of a monolayer.

2.2.1 Sonicating

The purpose of sonication is to apply ultrasound waves with a frequency of 20 kHz to agitate particles in a sample so that they are evenly distributed in the solution and not remain aggregated at the bottom of the vial. This in turn will allow the particles to spread more when spin-cast onto a TEM grid.⁴⁴

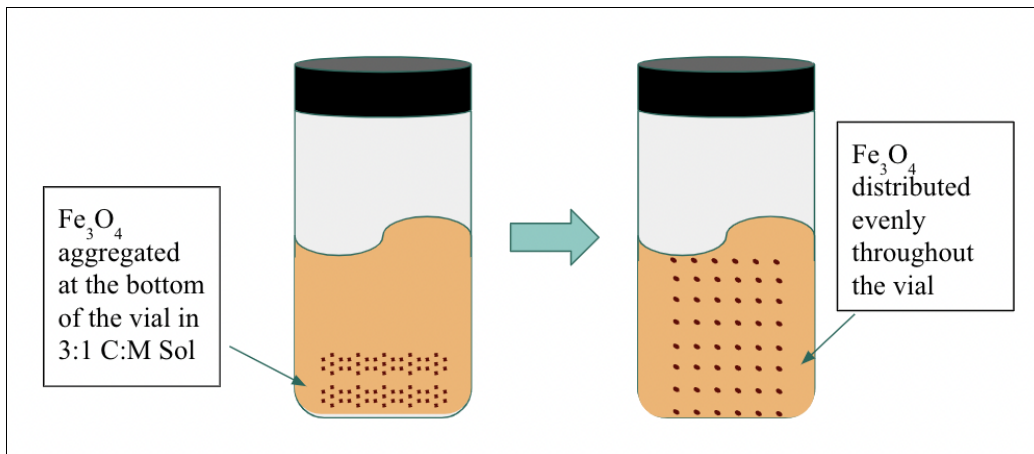


Figure 10: Before, and after sonication of the iron oxide nanoparticles suspended in a 3:1 Chloroform: Methanol dispersing agent

2.2.2 Spin Coating

Spin coating is a transient process of flow and mass transfer. Coating thickness and uniformity depend on the competition between centrifugally driven drainage of the liquid film and concentration-driven evaporation of solvents. Volatile solvents are transported in the film by convection and diffusion, and on reaching the free surface can vaporize and depart by diffusion and convection inflowing gas.⁴⁵

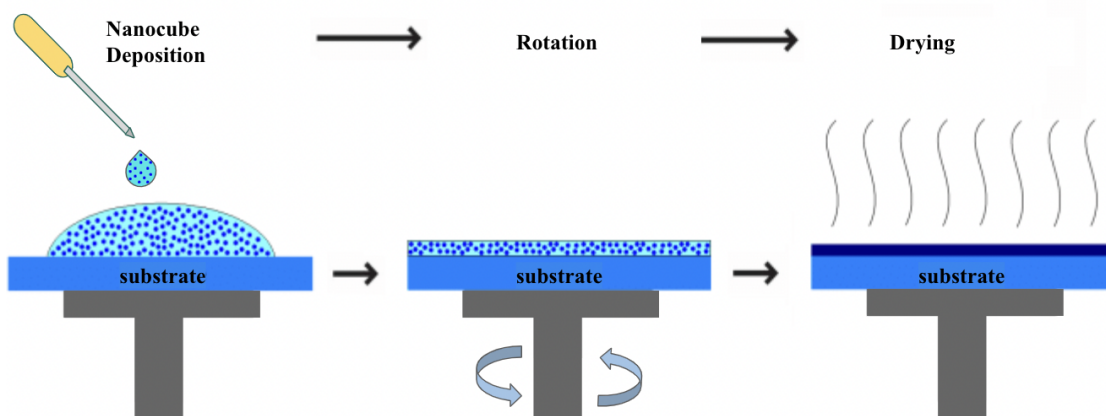


Figure 11: Schematic representation of the principle of the spin coating process for assembly of nanocube films.⁴⁶

In spin coating, the nanocube solution is deposited on a rotating substrate. In this method, a small piece of the silicon wafer is placed on the spin coater, and a vacuum is switched on to keep the wafer in place. A substrate of choice, usually a carbon TEM grid is placed on the wafer. Before placing the grid, a small drop of water is pipetted on the surface to allow adhesion of the grid on the wafer surface. 10 μL of nanocubes, suspended in a 3:1 chloroform: methanol dispersing agent solution, is pipetted using a micropipette on the TEM grid. The solution is allowed to sit for 25 seconds to control evaporation. The wafer with the adhered TEM grid is spun at 600 rpm for 1 minute under nitrogen. The centrifugal force resulting from the rotation of the spin coater causes the solution to spread and form a thin layer on the substrate as the solvent evaporates. The formation of nanocubes film depends on properties such as speed of spinning, temperature, nature of solvent and substrate, etc.

2.3 Post Assembly manipulation

2.3.1 Annealing

Annealing is a heat treatment process that changes the physical and sometimes also the chemical properties of a material. Simulated annealing in the context of molecular dynamics refers to the controlled heating and cooling of a system to overcome energetic barriers and find energetically favorable minima much faster. This process can be repeated multiple times throughout the simulation.⁴⁷ Yuxue C.⁴⁸ discusses the effect of annealing on the conductivity of monolayers of CoPt nanoparticles. Upon annealing, it was noticed that the conductivity of several orders of magnitude increased with rising annealing temperature until a maximum at about 400 °C was reached. In this study, the nanocubes were annealed in a sealed oven at different temperatures for different periods.

2.4 Characterization of Iron (III) Oxide (Fe₃O₄) Nanocubes

2.4.1 Fourier Transform Infra-Red (FTIR) Spectroscopy

Fourier transform infrared spectroscopy (FTIR) analysis can be used to gain more insight into the formation and dissociation of certain bonds and functional groups. FTIR samples can be extracted from the reaction mixture at different instances of time. In traditional IR spectrometry, a sample is exposed to different frequencies of IR radiation. The spectra obtained tells us about the detected frequencies that can pass through the sample. FTIR on the other hand can collect electromagnetic spectral data in a wide range as it exposes the sample with many different frequencies simultaneously in a single light beam. By using a mathematical operation called the ‘Fourier Transform’, FTIR converts the raw data collected by the spectroscope into the desired spectrum to determine the frequencies that passed through the sample. From this, a spectrum of Transmittance (%) against Wavenumber (cm⁻¹) is generated.

The FTIR at different reaction times can be analyzed to study peaks corresponding to the vibrational transitions characteristic of different bonds. Bonds such as C=O, C-H, and O-H bonds which are present in the surfactant, decanoic acid, show characteristic peaks. The appearance and disappearance of such peaks correspond to bond formations and dissociations as the reaction progresses. Therefore, by looking at the peaks on the spectra and their relative frequencies absorbed by each bond, FTIR spectroscopy can be used to determine the presence of decanoic acid on the synthesized Fe₃O₄ nanocubes.⁴⁹

2.4.2 Ultra Violet Spectroscopy Spectroscopy

Spectroscopy is the interaction between waves that originated in the electromagnetic spectrum and molecules present in the sample matrix under analysis. The development and implementation of these spectroscopy methods in different fields are based on the interactions between matter and light that resulted in absorption, emission, and scattering events characteristic of the sample.⁵⁰

UV-vis spectroscopy is an inexpensive, simple, flexible, non-destructive, analytical method appropriate for a wide class of organic compounds and inorganic species.⁵¹ It is a sensitive method in molecular spectroscopy that uses ultraviolet and visible light in the wavelength range between 200 and 780 nm. As stated above, this spectroscopic method is based on the absorption, scattering, diffraction, refraction, and reflection properties of the sample analyzed. The absorption of UV and Vis light is restricted to certain molecular functional groups called chromophores, in which electrons are excited at different frequencies.⁵²

As in many spectroscopic applications, the Beer-Lambert law describes the correlation between light absorption by the molecule, the light path length of the sample, and the concentration of the absorbing molecules in the liquid medium. Therefore, based on the

absorption measurement, the presence and concentration of analytes in the food matrix as a consequence of its chemical and physical properties can be determined and quantified.⁵³

2.4.3 Dynamic Light Scattering (DLS)

The detection of light scattering from matter is a useful technique with applications in numerous scientific disciplines where, depending on the light source and detector, specific properties of molecules can be studied. In a typical light-scattering experiment, a sample is exposed to a monochromatic wave of light, and an appropriate detector detects the signal.

In this study, dynamic light scattering (DLS) is used to calculate the mean size of the iron oxide nanocubes. DLS, also known as photon correlation spectroscopy or quasi-elastic light scattering, is a technique that primarily measures the Brownian motion of macromolecules in a solution that arises due to bombardment from solvent molecules, and relates this motion to the size of particles. Such motion of macromolecules depends on their size, temperature, and solvent viscosity. This is done by directing a photon beam through the given solution and quantifying the dynamic fluctuations in the scattered light. When looking at a graph, one can infer the average diameter of the suspended particles, depending on where the maximum light intensity is recorded.⁵⁴

2.4.4 Transmission Electron Microscopy (TEM)

The prepared thin films of iron oxide nanocubes on TEM grids can be analyzed using a transmission electron microscope (TEM). Electron beams are shot through the instrument onto the surface of the grid from the electron gun as a filament heats up. As the electron beam traverses, it passes through a series of lenses that scatter or diffract leading to the formation of an

image. Contrasts in the image are produced by differences in electron beam scattering or diffraction formed between various elements of the microstructure or defect. As a result, the surface morphology and assembly of particles on the substrate can be observed. After passing through a series of lenses, the electron beam interacts with the sample, and a resulting beam is transmitted. The scattering of electrons due to structural details on the grid surface can be projected on a fluorescent screen which can then be imaged to study the size and spacing of the particles using the software.⁴⁹

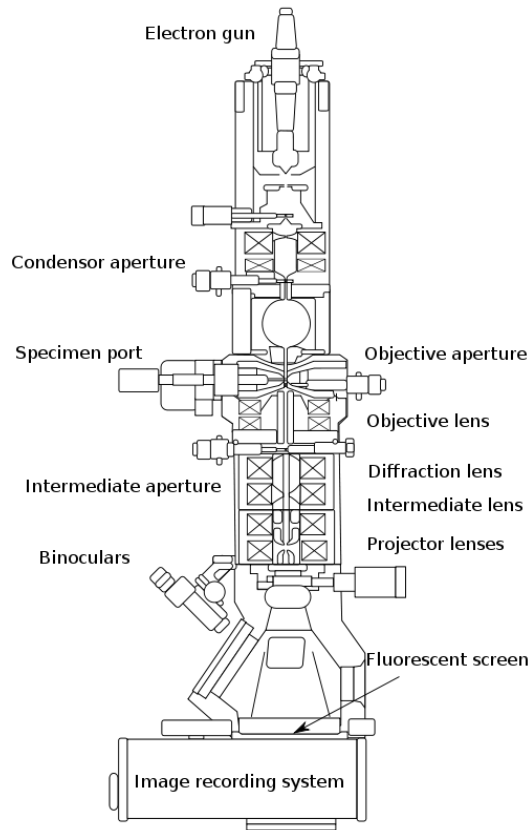


Figure 12: Layout of optical components in a basic TEM.⁵⁵

Transmission electron microscopy is a vital characterization tool for directly imaging nanomaterials as it can be used to achieve and study the behavior of materials at very large magnifications. This is essential to obtain quantitative measures of particle size, size distribution,

morphology, and also the behavior of the nanomaterials. Analysis of TEM images can be performed to measure the size of the nanocubes to obtain quantitative results about their size distribution.⁴⁹

When using TEM analysis to measure nanomaterials, there are possibilities for errors in the measurement. This is because, when measuring size distributions, only a very small sampling size is observed. A typical magnetic nanocube suspension is composed of 10^{10} to 10^{15} particles/mL. However, measurements of samples are done only for a few hundred (10^2) to 1000 (10^3) particles. Hence the sampling size is several magnitudes smaller than the actual amount of particles present in the solution. This subsequently gives us a very small sample pool to draw statistically conclusive remarks.

3. EXPERIMENTAL METHODS

3.1 An Overview of Synthesis Procedure of Crystalline, Monodisperse Fe₃O₄ Nanocubes

The synthesis procedure for the Fe₃O₄ nanocubes involving decanoic acid (surfactant and reducing agent), dibenzyl ether (solvent), and the metal-containing bulk material, iron acetylacetonate, (Fe(acac)₃) was carried out through thermal decomposition in collaboration with a previous student in our research project, Jennifer Tasneem.⁵⁶ The reactants were obtained from Sigma Aldrich and used without further purification. Heated in a sand bath, the reactants were added and mixed in the reaction vessel. Figure 13 shows the structures of chemical reagents, while Figure 14 gives an overview of the synthesis apparatus.⁵⁶

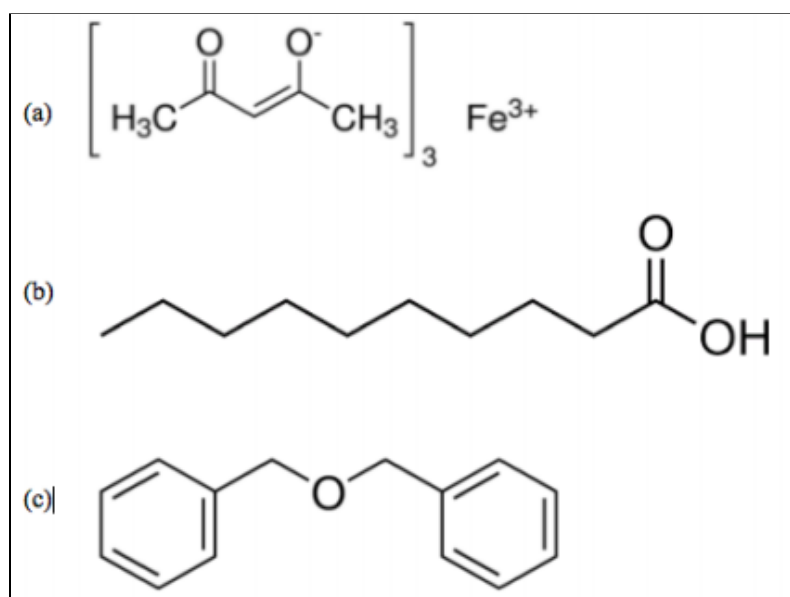


Figure 13: Chemical structures of the reagents used in the synthesis of Fe₃O₄ nanocubes: (a) iron acetylacetonate (b) decanoic acid (c) dibenzyl ether.⁵⁶

Constant nitrogen gas flow was maintained into the vessel to keep the synthesis environment inert.⁵⁶

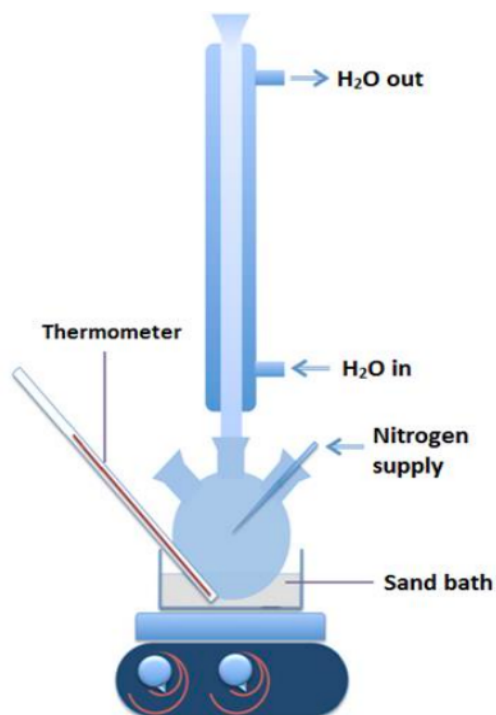


Figure 14: Setup of the reaction vessel for the synthesis of nanocubes.⁵⁶

A thermometer was used to measure the temperature of the sand bath. In a three-neck reaction vessel with a reflux condenser, the dry components, 0.5188 g decanoic acid (3 mmol) and 0.3529 g iron (III) acetylacetonate (1 mmol) were added and mixed (Figure 14). Lastly, 25 mL of the organic solvent, dibenzyl ether was added. The reaction mixture was heated to 200 °C at a steady heating rate of 5-6 °C/min and agitated with a magnetic stir bar.⁵⁶

Throughout the reaction, the initial clear orange color of the solution gradually changed to a deep red. The solution was maintained at 200 °C \pm 10 °C for 2 hours. It was then heated at a rate of 5-6 °C/min until it reached approximately 300 °C at reflux until a brownish-black color resulted.

3.2 Confirmation of Magnetic Fe₃O₄ Nanocubes

A sample of the reaction mixture was removed to check the IR spectrum, 10 minutes after the start of the synthesis. Next, a sample of the Fe₃O₄ nanocube solution was taken at the end of the reaction. IR spectra of the surfactant decanoic acid and the solvent dibenzyl ether were taken as well. All samples were taken using a Bruker-Alpha FTIR instrument. To obtain accurate data, 32 scans of each sample were conducted in the range of 750 cm⁻¹ to 4000 cm⁻¹. Spectra produced were collected for further analysis to understand and study the dissociation and formation of bonds in the reaction mixture during the reaction.

FTIR samples were taken 10 minutes after the reaction began. Following reflux, the sand bath was removed and the reaction mixture cooled overnight to room temperature.⁵⁶ The nanocubes were then washed using hexane: acetone (1:1) to remove any residual materials. After washing, they were centrifuged a total of four times at 8000 rpm/min for 5 min, dried again overnight, and dispersed into a 3:1 ratio of chloroform: methanol dispersing agent.

Along with FTIR, an UltraViolet Visible (UV-Vis) sample was prepared and analyzed. A prepared 1 cm cuvette containing the iron oxide nanocubes was placed into a Cary 100 – UV Visible spectrometer. The range is set from 300 to 800 nm. First, a low-resolution absorption spectrum was measured using a scan rate of 120 nm per minute followed by the measurement of a high-resolution spectrum at a scan rate of 12nm per minute.

Finally, a dynamic light scattering (DLS) sample was prepared. The iron oxide nanocubes dispersed in a 3:1 dispersing agent were first sonicated, before taking the DLS sample. The nanocubes were then allowed to sit for 24 hours before the second DLS sample was taken.

3.3 Transmission Electron Microscopy Grid Surface Manipulation

For this study, three different substrate modifications were utilized. The substrate of choice was a carbon-based TEM grid that was already hydrophobic. The first substrate modification was plasma cleaning, which was used to increase the hydrophilicity of the TEM grid. Second, the TEM grid was left without any modifications. Lastly, the substrate was coated with a heptadecanoic acid using Langmuir Blodgett techniques to further increase the hydrophobicity.

3.3.1 Plasma Treatment

In this study, plasma treatment was performed to remove any organic contaminants from the surface of the TEM grids and to increase the hydrophilicity of the grids. Before plasma cleaning, the plasma cleaner and cold trap were set up (Figure 16). The TEM grids were placed in a clean petri dish with the copper side facing up. The two oxygen pumps were switched on, and the petri dish was placed inside the vacuum chamber. The chamber was then evacuated using a vacuum to remove all the air. Once the pressure dropped to around 100 mmHg. The chamber was then filled with oxygen till the pressure was around 300 mmHg. The oxygen was allowed to sit for 30 seconds before it was evacuated from the chamber. This process was repeated two more times to ensure that the chamber was filled with oxygen before the plasma treatment.

The chamber was once again filled with oxygen until the pressure reached around 300 mmHg. The power switch was turned to the highest setting, and the plasma was turned on. Once the plasma chamber turned purple, the treatment was run for 5 seconds, before switching off the plasma treatment. Finally, the chamber was opened, the petri dish covered, and the TEM grids allowed to equilibrate in the chamber for 15 minutes before being removed.

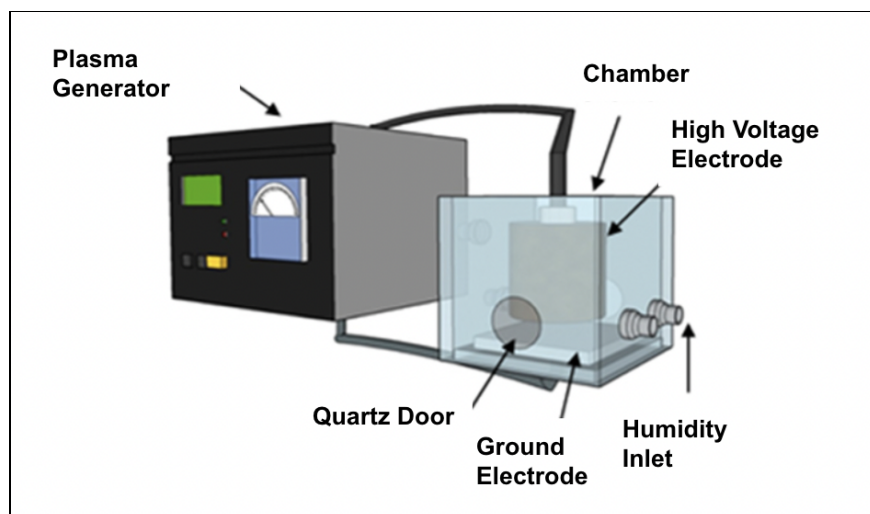


Figure 15: Schematic representation of plasma treatment set up.⁵⁷

3.3.2 Cleaning of Langmuir Trough

In an attempt to increase the hydrophobicity of the substrate, the TEM grid was coated with a heptadecanoic acid (HDA) coating using the Langmuir-Blodgett (LB) deposition technique. As mentioned in the previous section, the success of the LB technique relies considerably upon the cleanliness of the trough before any solution is loaded. Dust particles can interfere with the formation of uniform monolayers at the air-water interface of the Langmuir trough so the initial step involved extensive cleaning. Several times before any HDA solution was prepared, the trough was wiped down using deionized (DI) water followed by chloroform. The Langmuir trough was then vacuumed using a suction vacuum pen, after which it was filled with Milli-Q water. The Wilhelmy plate, which hangs above the water, was placed on the electro balance to measure the surface pressure of water in the trough and monitored using the NIMA software. An increase in surface pressure indicated the presence of dust or other unwanted particles on the water surface.

Vacuum suctioning using a vacuum pen was once again performed to clean the trough and skim the water surface. The barrier compression speed on the NIMA software program, attached to the LB trough, was set to 25 cm² /min. After calibrating the pressure to zero, the barriers were allowed to compress. The compression of the barriers generated the surface pressure vs. area isotherm graph. If the pressure, as monitored through the isotherm, was seen to drop below -0.1 mN/m, the barriers were stopped and the vacuum was applied to clean the surface of the water again. The lowest surface area the Langmuir trough barriers can compress to is 78 cm². In this area, the vacuum set-up was used one last time to clean the surface of the water.

3.3.3 Coating TEM Grid with HDA using the Langmuir Blodgett Technique

After cleaning the Langmuir trough, the compression barriers were opened to around 230 cm². The TEM grid substrate, which was attached to the instrument, was then slowly deposited into the trough, perpendicular to the surface of the water using the NIMA software controls. 10 μ L of a 1:1 ratio of Heptadecanoic Acid (HDA) in hexane, was spread across the water surface using a microsyringe at room temperature. The HDA particles were allowed to stabilize as the solvent evaporated for approximately 5 minutes. The barriers were then allowed to compress with a very slow compression rate of 20 cm² /min and a target pressure of 60 bar (Figure 18). The compression generated an isotherm which can be analyzed to study the two-dimensional phase changes. Isotherms generated from HDA were studied for an estimation of when the particles packed into the solid phase. The target pressure for HDA (P_s) was 30 bar in this case. Figure 16 shows the correlation between the isotherms generated and the HDA phase on the water surface.

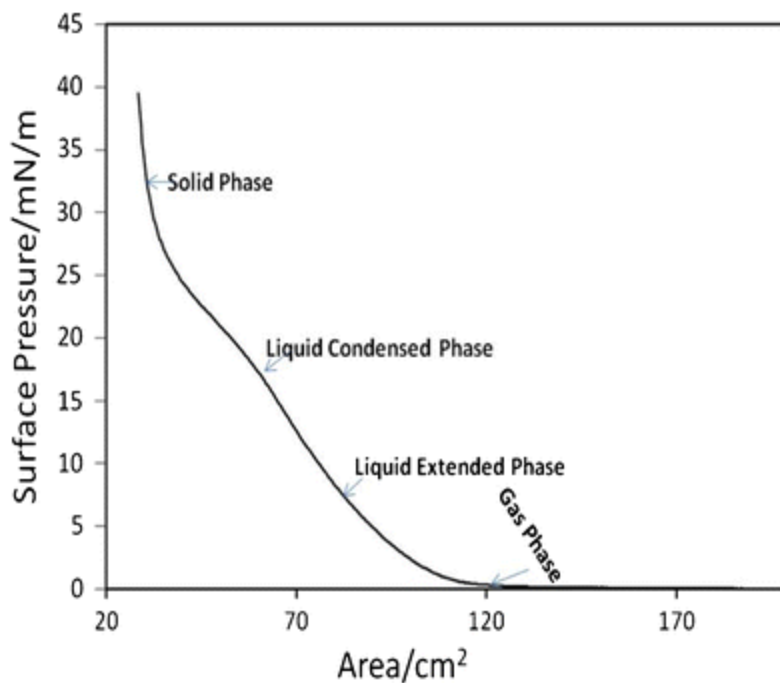


Figure 16: Relationship between isotherm generated and phases of the packed HDA particles.⁵⁸

As the barriers are compressed, the nanocubes are allowed to come close to each other, leading to the packing of the particles into a thin film. After compression, the particles were again allowed to stabilize before being transferred onto the substrate.

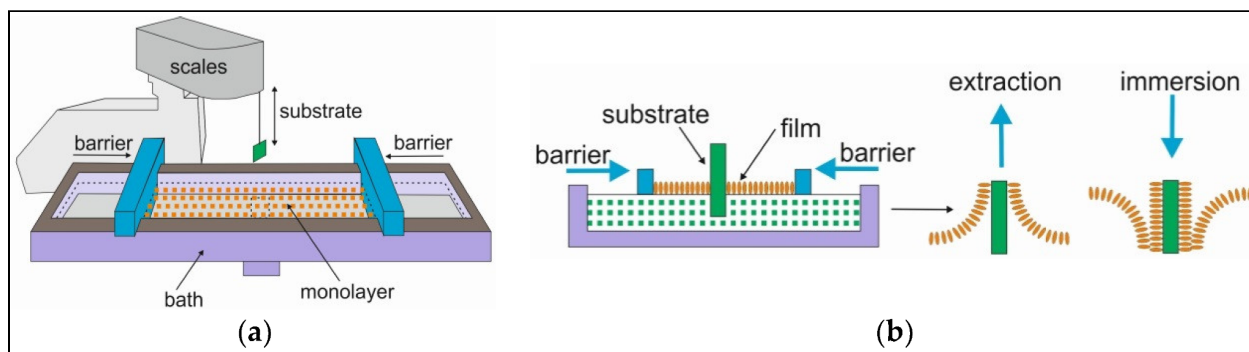


Figure 17: Schematic diagram of compression barriers packing nanocubes into a solid layer for assembly using Langmuir-Blodgett technique.⁵⁹

Figure 17 (a) depicts a graph of the Langmuir-Blodgett technique. Figure 17 (b) shows the gas phase of particles on the trough can be seen above, while the solid packed phase of the particles is seen below.⁵⁹

The packed HDA layer was transferred onto a carbon TEM grid using the vertical extraction technique (LB). After letting the packed HDA layer sit for 5 minutes, the TEM grid was carefully extracted from the surface of the water in a vertical motion, again using the NIMA software at a speed of 5 mm/min. The grid was then allowed to air dry so that when all solvent completely evaporated, a thin film of the HDA was left behind on the surface.

3.3.4 Coating TEM Grid with Heptadecanoic Acid using Langmuir Schaefer Technique

After cleaning of the Langmuir trough, the compression barriers were fully opened, and 10 μL of a 1:1 ratio of Heptadecanoic Acid (HDA) in hexane, was spread across the water surface using a microsyringe at room temperature. The same procedure used in LB is used for the formation of a tightly packed solid HDA layer. Once the layer is complete, 6 TEM grids are placed on the HDA layer, shiny side down, and allowed to sit for 5 minutes. They were then removed using a tweezer and placed in a petri dish to dry for 5 minutes before storing.

3.4 Film Preparation

3.4.1 Sonication

Sonication refers to the process of applying sound energy to agitate particles or discontinuous fibers in a liquid. Ultrasonic frequencies (>20 kHz) are usually used, so the process is also known as ultrasonication. Sonication can be conducted using either an ultrasonic bath or an ultrasonic probe (sonicator).⁶⁰

The Iron Oxide nanocubes suspended in a 3: 1 Chloroform: Methanol dispersing agent were sonicated for 5 minutes every time before they were spin-cast. The sample was placed in the sonicator and manually held in place. The vial was half-submerged in the water to enable proper sonication and distribution of the particles.

3.4.2 Spin Coating

A previously cut silicon wafer was cleaned three times using chloroform and a Kim-wipe. It was left in the hood for excess chloroform to evaporate. A drop of Milli-Q water was drop-cast onto the silicon wafer using a pipette. Next, a clean TEM grid was placed on the surface of the wafer using the drop of Milli-Q water for adhesion. The wafer, water, and TEM grid were left to partially dry for 2 minutes. Then, 10 μ L of nanocubes, suspended in a 3:1 chloroform: methanol dispersing agent solution was micro pipetted onto the center of the TEM grid. The nanocubes were allowed to sit for 25 seconds on the silicon wafer to account for solvent evaporation. The silicon wafer was placed on the spin coater and held in place using a vacuum. The nanocubes were then spin-cast at 6000 rpm for 1 minute under nitrogen.

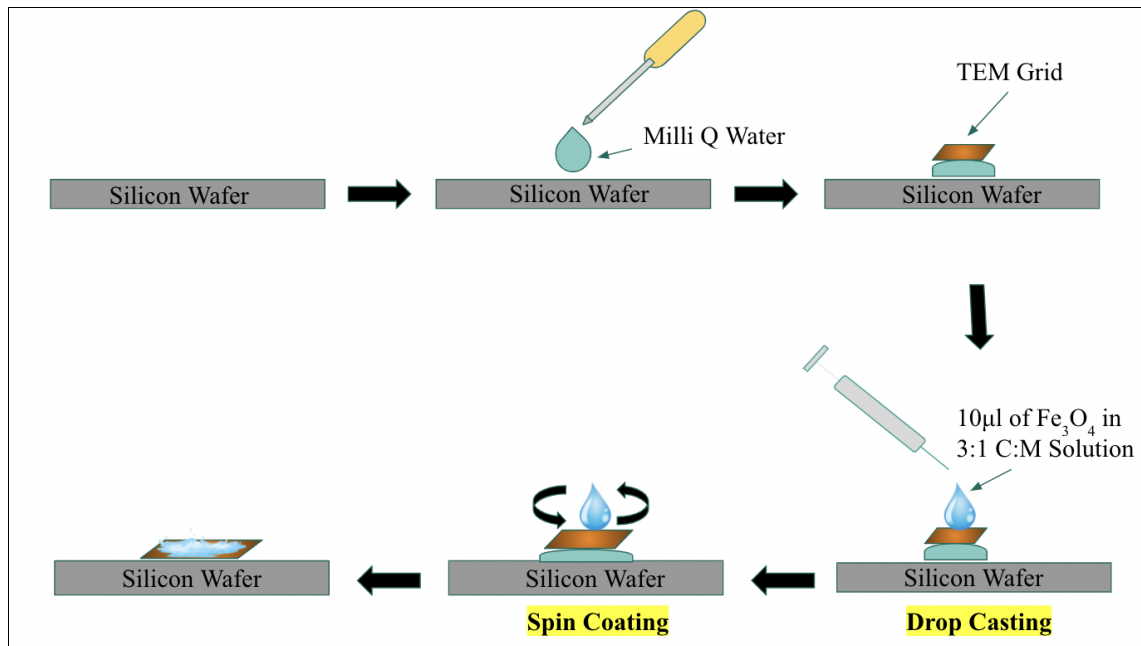


Figure 18: Schematic representation of drop-casting, and spin coating 10 µl of Fe₃O₄ in 3:1 C: M solution onto a carbon TEM grid

The samples, all prepared on TEM grids, were stored for further analysis using the transmission electron microscope.

3.4.3 Annealing Procedure

In addition to spin coating the nanocubes, the additional post-annealing procedure was performed using an oven. After the nanocubes suspended in a 3:1 chloroform: methanol solvent ratio was spin-coated, the sample was left to dry for 1 minute, then placed in the oven for either 0.5, 1, 1.5, 2, 6, 12, 18, or 24 hours in a sealed oven at different temperatures of 100 °C, 125 °C and 150 °C. In total, 8 samples were prepared for each substrate modification (plasma cleaning, and without substrate modification), at each of the different temperatures (100 °C, 125 °C, and 150 °C).

3.5 Characterization Using TEM to Measure the Nanocube Size Distribution

All samples obtained using the spin coating deposition technique with a 3:1 chloroform:methanol dispersing agent was characterized using a TEM.⁵⁶ Afterward, using the Java-based image processing program software, ImageJ, the size of the iron oxide nanocubes suspended in a 3:1 chloroform:methanol solution was analyzed to obtain size distribution using a sample size of 750 nanocubes. A graphical representation of the size of the iron oxide nanocubes coated with decanoic acid surfactant coating can be seen in figure 19.

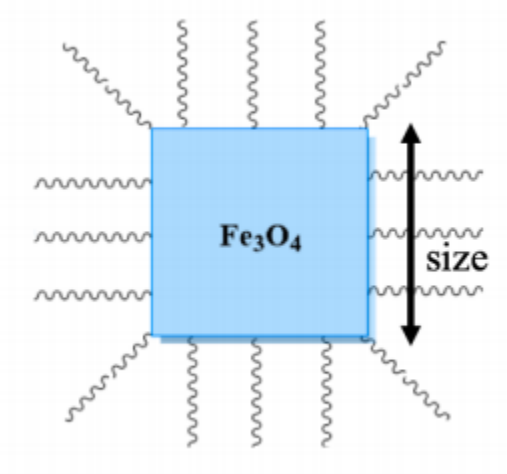


Figure 19: Measuring the diameter size of a Fe_3O_4 nanocube.⁵⁶

Following the size characterization of the nanocubes, the percentage of surface area covered by the nanocubes was also calculated using the Java-based program ImageJ, and plotted with respect to the annealing times for each substrate modification (plasma cleaning, and no substrate modification), at each of the different temperatures (100 °C, 125 °C, and 150 °C).

4. RESULTS AND DISCUSSION

4.1 Magnetic Fe₃O₄ nanocubes, and their characteristics

This study analyses the formation of magnetic nanocubes into a monolayer using surface modification, and post-assembly manipulation techniques. The particles of interest, in this case, are magnetic Iron (III) Oxide (Fe₃O₄) nanocubes coated with a decanoic acid surfactant and suspended in a 3:1 Chloroform: Methanol (C: M) dispersing agent. These particles were synthesized by Jennifer Tasneem in 2017.⁵⁶

To confirm the magnetic property, and stability of the Fe₃O₄ nanocubes, IR spectroscopy and a neodymium magnet were used. To confirm the magnetism, when a small neodymium magnet was placed near a solution of iron oxide nanocubes, the particles were seen to be attracted towards the neodymium. This behavior confirms their magnetic nature (Figure 20).⁵⁶

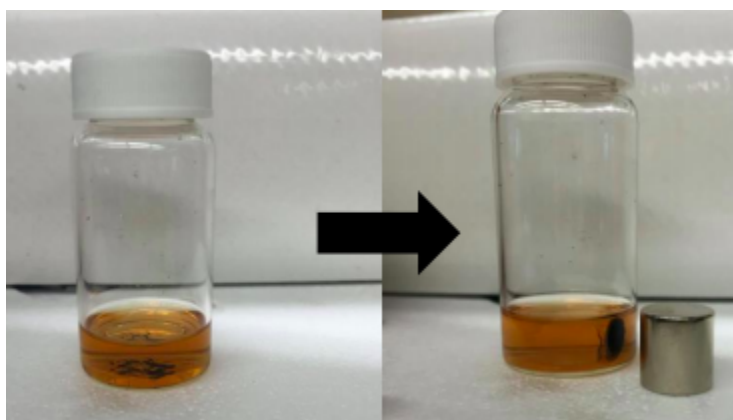


Figure 20: Fe₃O₄ nanocubes attraction to a neodymium magnet through a vial.⁵⁶

4.1.1 Decanoic acid surfactant coating

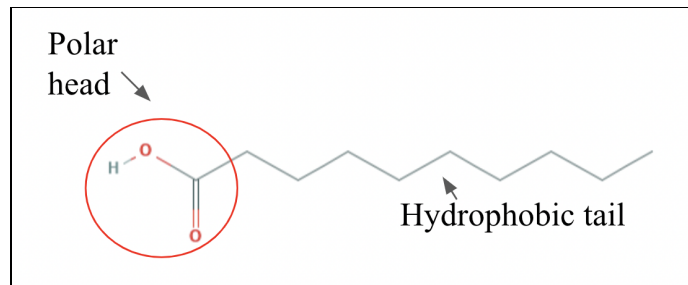


Figure 21: Chemical structure of the decanoic acid used as the Fe_3O_4 nanocube surfactant coating

As mentioned before, when synthesized, the Fe_3O_4 nanocubes were coated with a decanoic acid surfactant coating to curb further growth during nucleation. The decanoic acid molecule is amphiphilic. This means that it is both hydrophobic, and hydrophilic. When coating the Fe_3O_4 nanocubes, the hydrophilic, or polar head is attached to the surface of the molecule while the hydrophobic carbon tail is exposed to the environment. This results in an overall hydrophobic Fe_3O_4 molecule.

4.1.2 Size and shape analysis

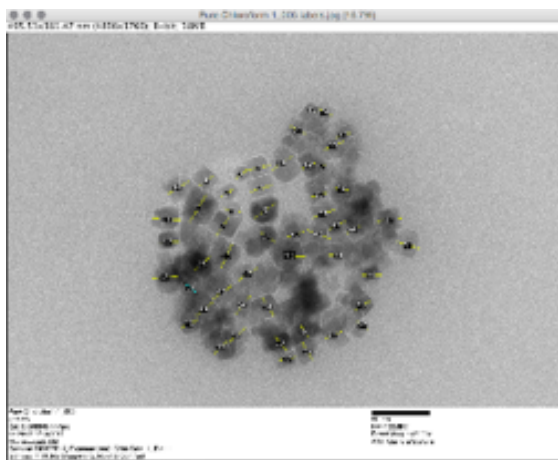


Figure 22: Highly magnified (73,000 X) image of magnetic Fe_3O_4 nanocubes as seen in Image J

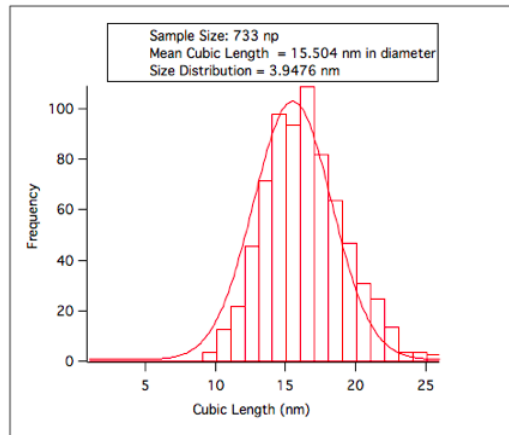


Figure 23: Size distribution histogram of magnetic Fe₃O₄ nanocubes with a mean size of 15.50 ± 3.95 nm

Given that the particles were synthesized in 2017, it was important to analyze the nanocubes to ensure that they were stable and had not degraded over time. To ensure that the particles were stable, and had retained their size and shape, the Fe₃O₄ nanocubes were imaged using TEM and analyzed using a java-based program ImageJ (Figure 22). The length of 733 nanocubes was measured, and the values were plotted on a histogram. It was found that the nanocubes had a mean size of around 15.50 nm with a standard deviation of 3.95 nm (Figure 23).

4.1.3 Dynamic Light Scattering (DLS)

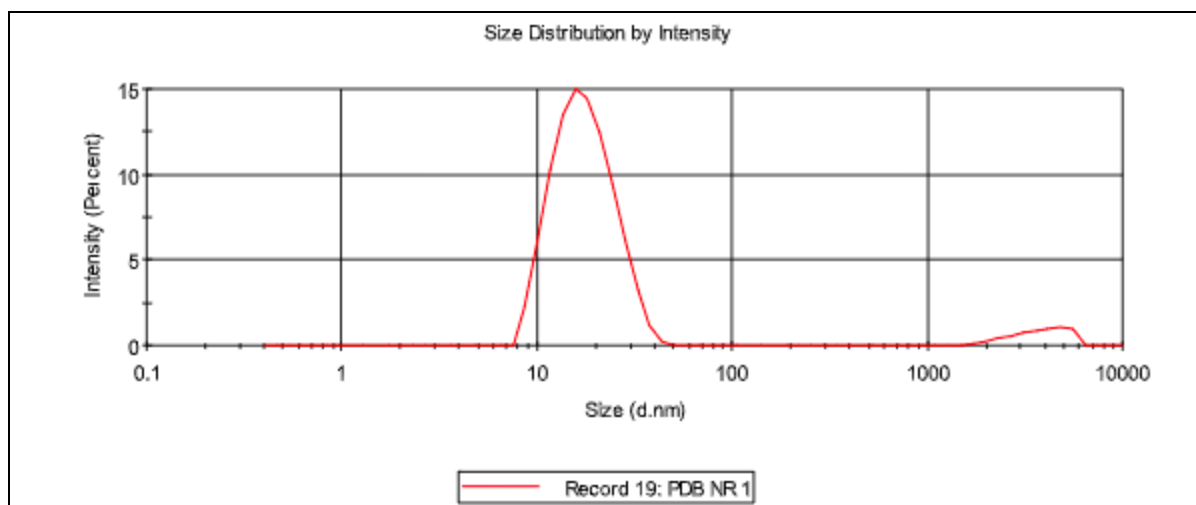


Figure 24: DLS graph of magnetic Fe_3O_4 nanocubes suspended in a 3:1 C: M dispersing agent with a mean diameter of 18.10 ± 6.30 nm

As mentioned before, dynamic light scattering not only measures the diameter of particles in a solution, but also the solvent sphere encapsulating the particle of interest. The first time DLS was run the nanocubes suspended in 3:1 solution were sonicated. It was observed that the particles had an average diameter of 1230 nm. The purpose of sonication is to disperse the aggregated nanocubes at the base of the vial into solution. However, this can also result in the introduction of larger aggregated particles coated with a solvent coating suspended in solution. This subsequently gives a larger diameter.

In contrast, after the magnetic iron oxide nanocubes were allowed to sit in the cuvette for 24 hours, and then run through DLS, it was found that the average diameter was 18.10 nm with a standard deviation of 6.30 nm. Allowing the nanocubes to sit for 24 hours gave the aggregated particles time to settle at the bottom of the cuvette, while the lone particles remained in solution allowing us to accurately measure the diameter. Manually measuring the nanocubes yielded an average size of 15.50 nm, while DLS gave a diameter of 18.10 nm (Figure 24). The increase in particle size found when running DLS, was due to the solvent sphere surrounding the nanocubes.

4.1.4 UV Visible Spectra

The purpose of UV visible spectra is to use ultraviolet light to see the reflection spectroscopy of the magnetic iron oxide nanoparticles suspended in a 3:1 C: M solution to understand the chemical structure of the compound.

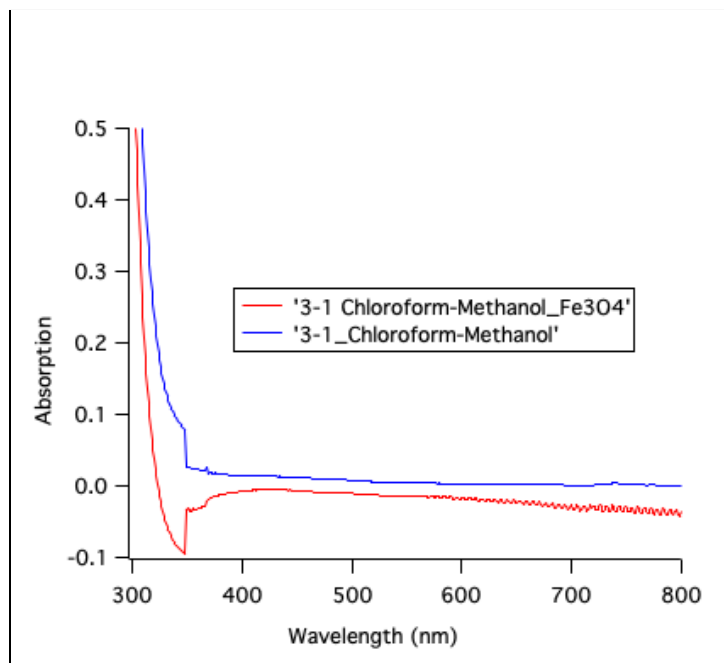


Figure 25: UV Vis Spectra of pure 3:1 C: M solution, against Magnetic Fe₃O₄ Nanocubes, suspended in a 3:1 C: M Dispersing Agent

The Fe₃O₄ suspended in a 3:1 C: M dispersing agent, graphed next to the pure 3:1 C: M dispersing agent (Figure 25). The Magnetic Fe₃O₄ Nanocubes suspended in a 3:1 C: M dispersing agent spectra showed a peak at 420 nm, similar to Yew, Yen Pin, et al. (2016).⁶¹ This absorption line can not be seen in the pure 3:1 C: M solution, indicating the presence of magnetic iron oxide nanocubes. It is important to note that the difference in height of the two spectra was due to an instrumental error, and the spectrum below 400 nm is not analysed as it indicates the transition between ultraviolet, and visible light.

4.1.5 Fourier Transform Infrared Spectroscopy (FTIR)

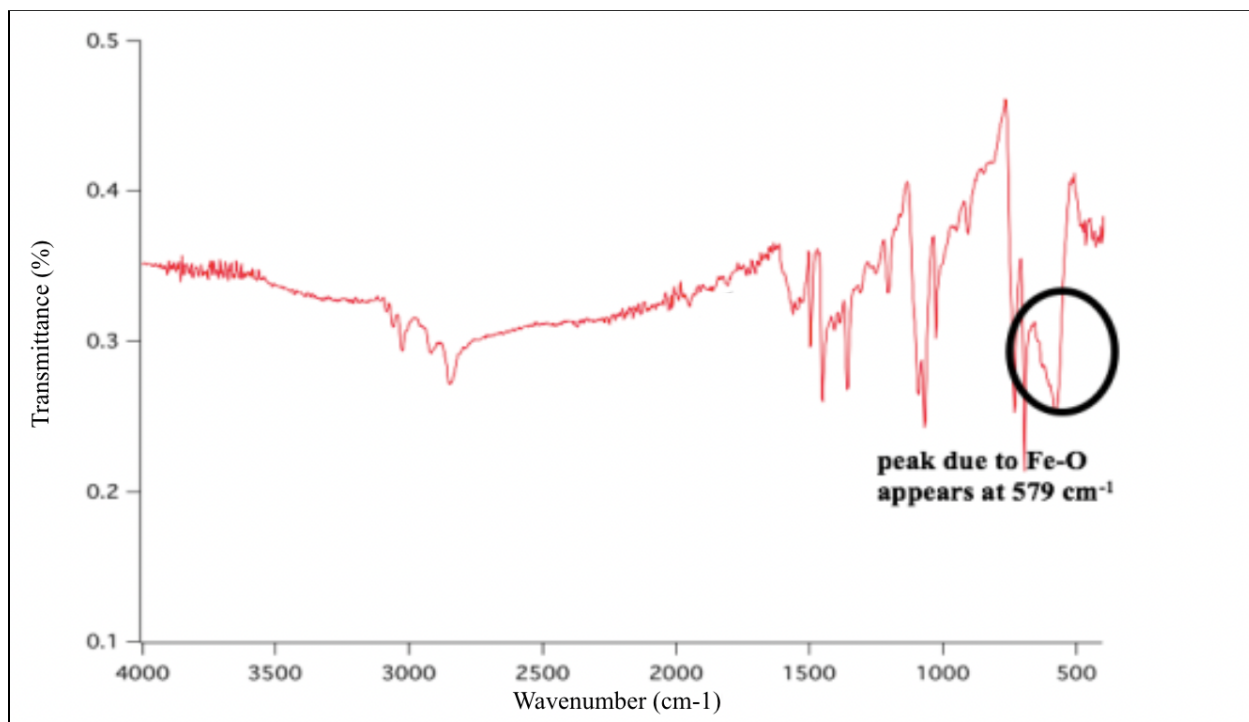


Figure 26: FTIR of the magnetic Fe₃O₄ nanocubes with a peak at 579 cm⁻¹ showing the presence of Fe₃O₄⁴⁷

When analyzing a Fe₃O₄ FTIR spectrum, the appearance of two well-defined peaks at 577 and 631 cm⁻¹ are due to the presence of iron–oxygen (Fe O) which indicates that the synthesized nanoparticles are iron oxide as validated by the literature values (Figure 26).⁶² The FTIR seen in figure 26 shows a peak at 579 cm⁻¹. This confirms the iron-oxygen bond formation in the FTIR spectrum, further verifying the presence of the magnetic Fe₃O₄ nanocubes seen in the UV-Vis Spectra mentioned above.

4.2 Assembly of Magnetic Fe₃O₄ Nanocubes, and modifications

The following section discusses the results found using different surface modification techniques such as plasma cleaning and Langmuir-Blodgett techniques on the TEM grids substrate, followed by post-deposition manipulation using annealing of the magnetic Fe_3O_4 nanocubes.

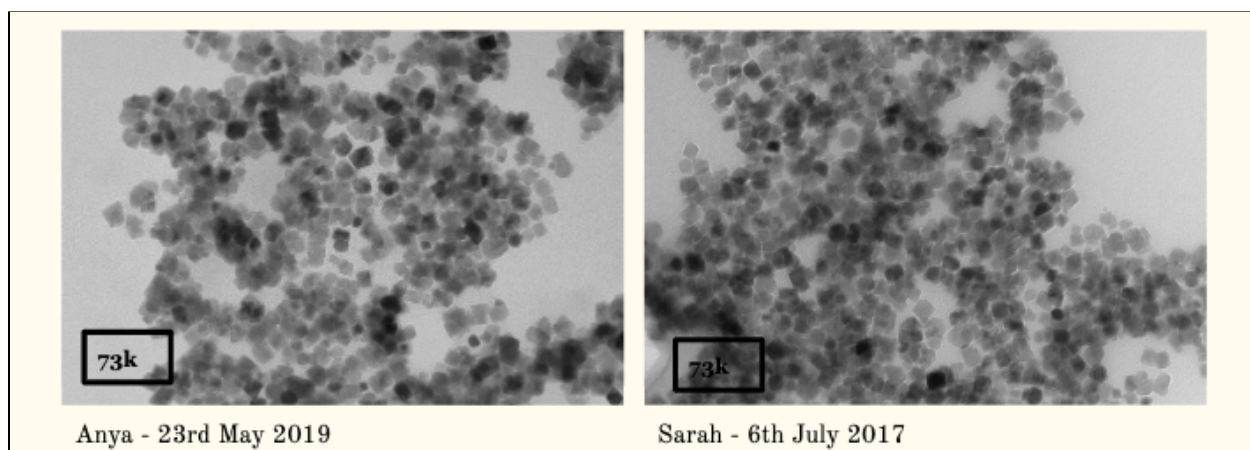


Figure 27: Highly magnified TEM image of iron oxide nanocubes suspended in a 3:1 C: M solution is taken on July 6th, 2017, and May 23rd, 2019 spin-cast on a carbon TEM grid with no surface modification

A TEM image taken at 73,000x magnification by Sarah Andoh of the iron oxide nanocubes suspended in a 3:1 C: M solution spin-cast at 6000 rpm for 1 minute on 6th July 2017, was compared with an image I took of the same particles under the same conditions on 23rd May 2019 (Figure 27). Here, it can be seen that the size and shape of the particles look the same, as highlighted in figure 23. However, the nanocubes do not show a visible formation of a smooth monolayer, compelling us to investigate the effect of substrate modification on the evolution of a monodisperse layer.

4.2.1 Modifications of the substrate, and nanoparticles

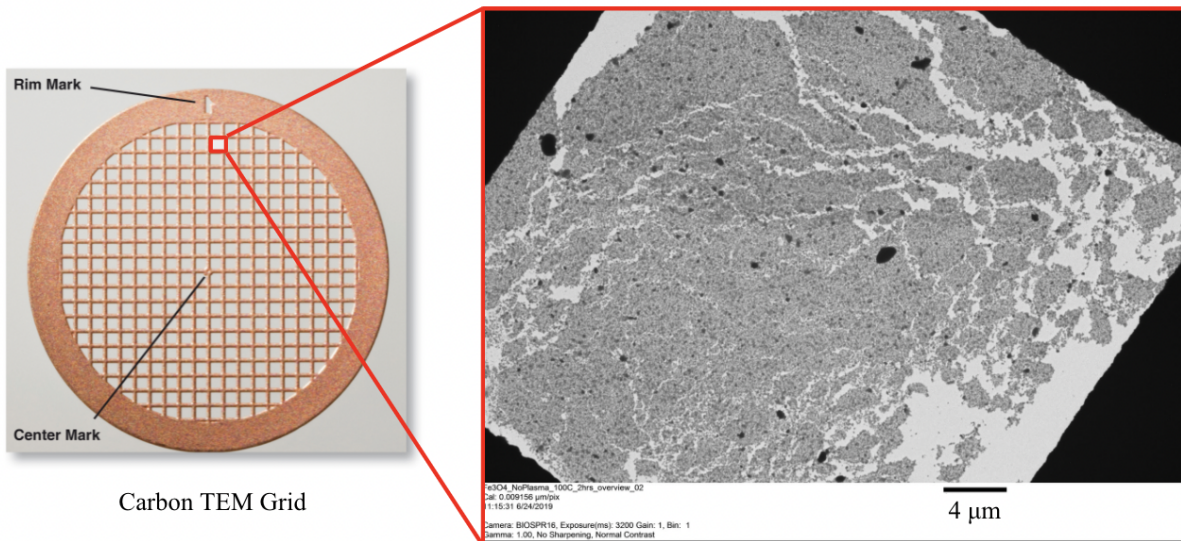


Figure 28: Carbon coated TEM grid, and an image of one square as viewed under Transmission Electron Microscopy

The substrate of choice in this study is a carbon-coated TEM grid seen in figure 28, which is known to be hydrophobic. When analyzing the TEM image, the light gray shows the carbon TEM substrate, the dark grey indicates the presence of the iron oxide nanocubes and the black spots indicate aggregated particles. A TEM image of the Fe_3O_4 nanocubes at 52,000x magnification that has been spin-cast onto a substrate with no modification and no annealing (Figure 29). This image indicates the lack of an even monolayer. In an attempt to aid the monolayer formation, the surface chemistry of the substrate is modified, followed by the post assembly manipulation of the Fe_3O_4 nanocubes.

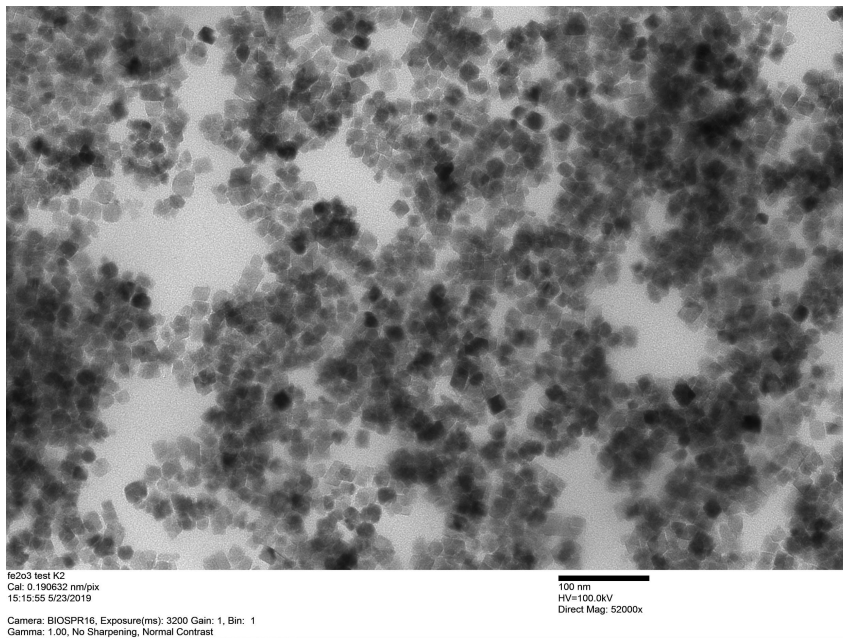


Figure 29: TEM image of Fe₃O₄ nanocubes spin-cast onto a TEM grid with no surface modification, and no annealing at a magnification of 52,000x

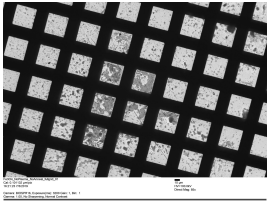
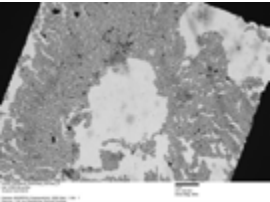
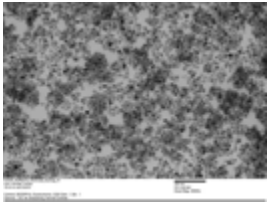
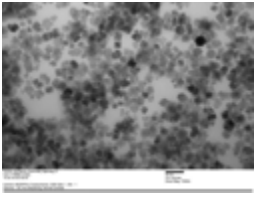
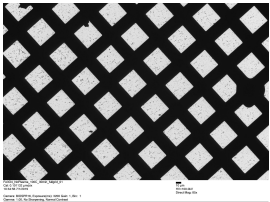
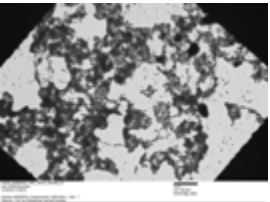
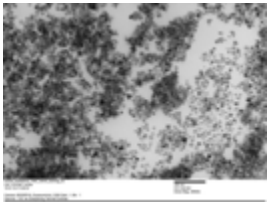
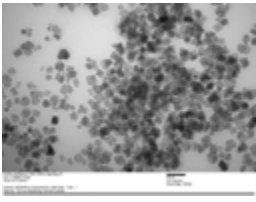
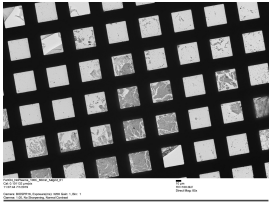
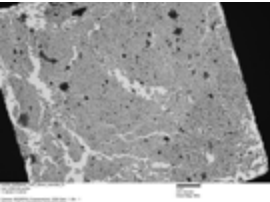
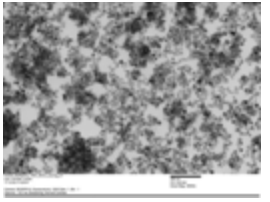
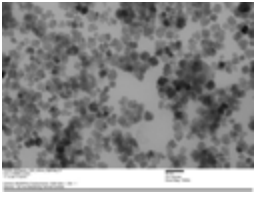
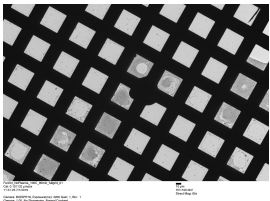
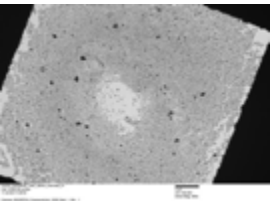
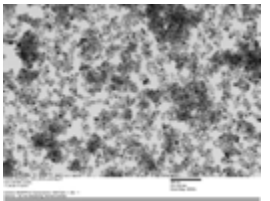
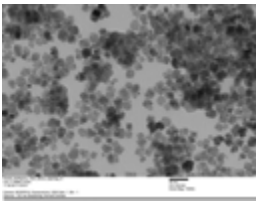
The substrate was modified to increase hydrophobicity by coating the grids with a hydrophobic HDA molecule using LB, increase hydrophilicity using oxygen plasma cleaning, or was not modified at all (no substrate modification). The Fe₃O₄ nanocubes were then spin-cast onto the substrate at 6000 rpm for 1 minute under nitrogen. Finally, the particles that were annealed at 100 °C, 125 °C, 150 °C, or not annealed, were viewed under TEM at different magnifications of 900x, 27.5kx, and 72kx. The images were then compiled into tables depending on the substrate modification technique, and on the temperature, they were annealed.

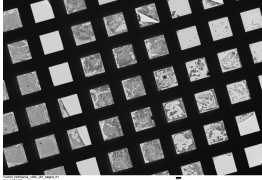
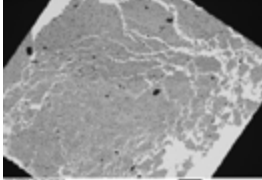
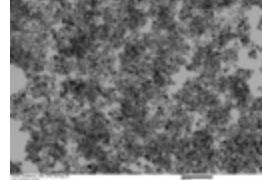
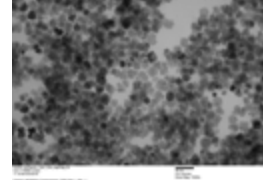
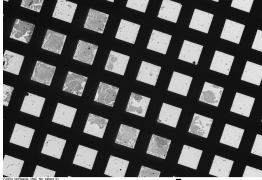
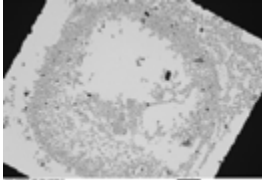
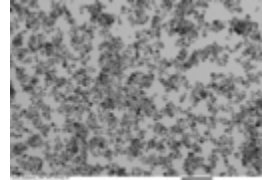
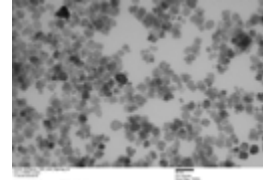
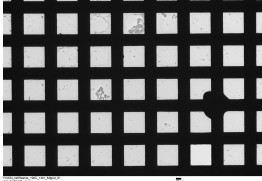
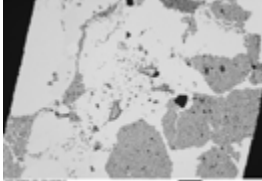
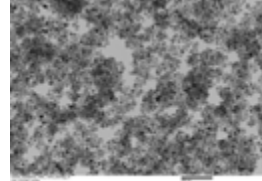
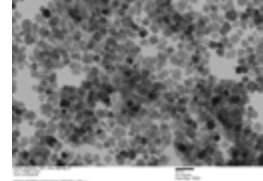
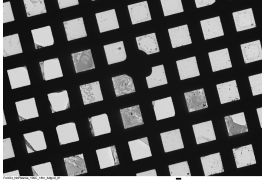
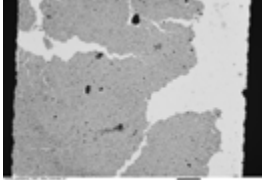
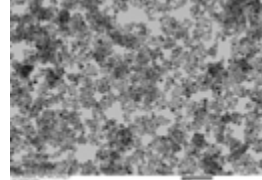
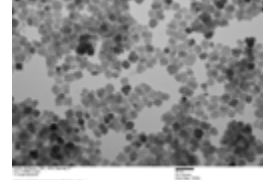
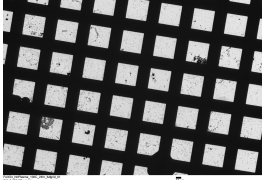
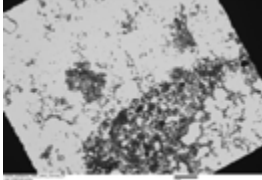
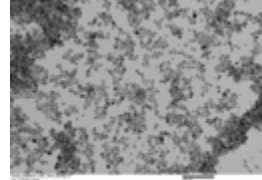
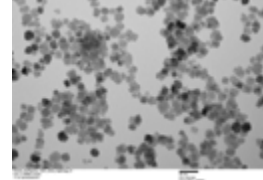
4.2.1.1 Particles Annealed at 100° C.

The following table shows the magnetic iron oxide nanocubes spin-cast on a TEM grid with no surface modification, followed by annealing at 100 °C for different time intervals. The table shows a full grid TEM image at 150x magnification, an overview of one grid at 900x

magnification, a low magnification image at 27,500 x magnification, spin-cast, and a highly magnified image at 73,000 x magnification.

Table 1: Fe₃O₄ nanocubes spin-cast, on TEM Grids, with no surface modification, annealed at 100 °C

Time (hr)	Full Grid (150x)	Overview (900x)	Low Mag (27.5kx)	High Mag (73kx)
0				
0.5				
1				
1.5				

2	 <p>SEM image showing a grid-like structure, likely a membrane or scaffold, with a regular pattern of square openings.</p>	 <p>SEM image showing a porous, interconnected network structure, possibly a bio-scaffold or membrane.</p>	 <p>SEM image showing a porous, interconnected network structure, similar to the previous image.</p>	 <p>SEM image showing a porous, interconnected network structure, similar to the previous images.</p>
6	 <p>SEM image showing a grid-like structure, similar to the first row.</p>	 <p>SEM image showing a porous, interconnected network structure.</p>	 <p>SEM image showing a porous, interconnected network structure.</p>	 <p>SEM image showing a porous, interconnected network structure.</p>
12	 <p>SEM image showing a grid-like structure.</p>	 <p>SEM image showing a porous, interconnected network structure.</p>	 <p>SEM image showing a porous, interconnected network structure.</p>	 <p>SEM image showing a porous, interconnected network structure.</p>
18	 <p>SEM image showing a grid-like structure.</p>	 <p>SEM image showing a porous, interconnected network structure.</p>	 <p>SEM image showing a porous, interconnected network structure.</p>	 <p>SEM image showing a porous, interconnected network structure.</p>
24	 <p>SEM image showing a grid-like structure.</p>	 <p>SEM image showing a porous, interconnected network structure.</p>	 <p>SEM image showing a porous, interconnected network structure.</p>	 <p>SEM image showing a porous, interconnected network structure.</p>

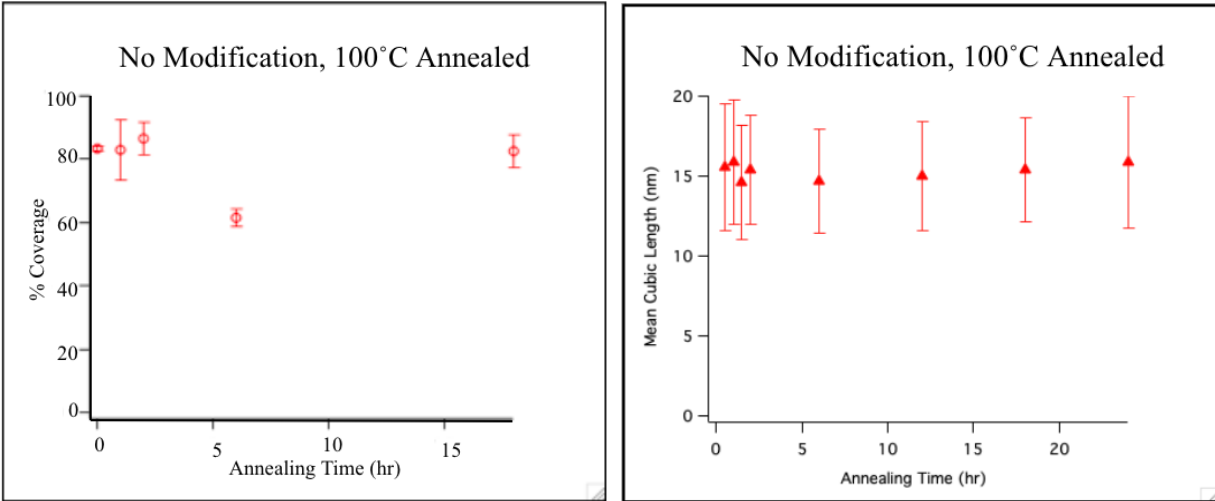
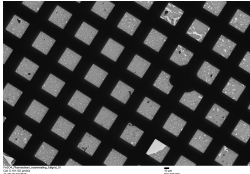
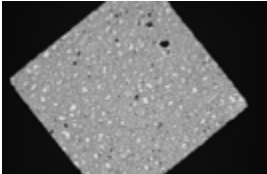
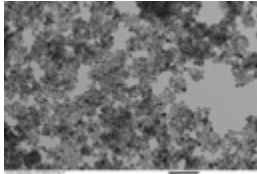
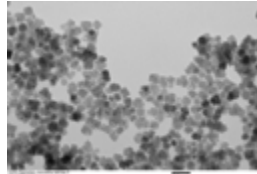
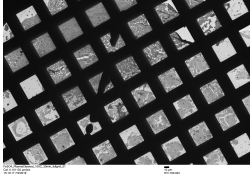
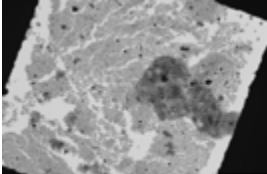
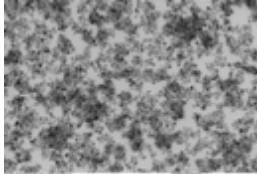
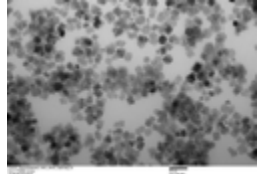
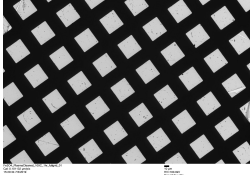
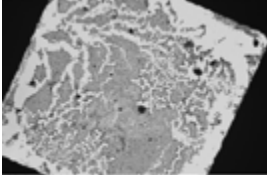
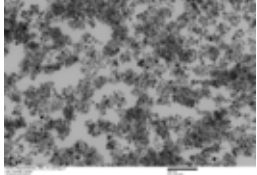
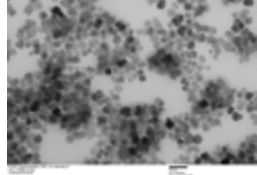
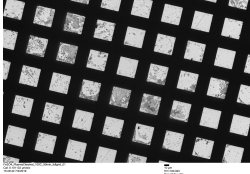
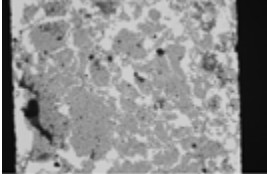
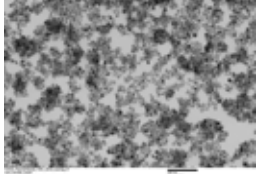
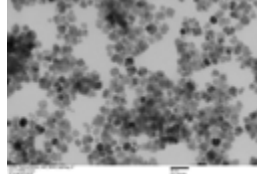
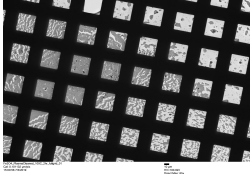
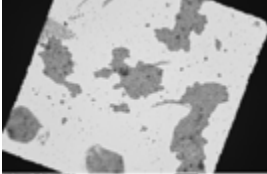
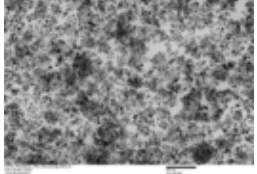
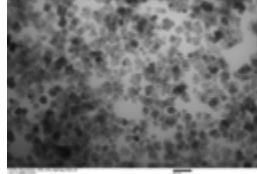


Figure 30: (a) Nanocube percentage coverage of TEM grid with no surface modification annealed at 100°C against time with an average of 79.2 ± 4.7 % (b) Mean nanocube size for nanocubes against annealing time with a mean length of 15.2 ± 3.4 nm

In table 1, it is seen that the TEM grids with no surface modification, showed the most surface coverage at an annealing temperature of 100°C for the 1 hour, 1.5 hours and 2 hour time periods. After the 2 hour time period, the surface coverage gradually decreased. Under magnification, the full coverage at the specified annealing times can be observed. Annealing at this temperature showed no change to the particle shape and size.

On measuring the percentage coverage of the magnetic iron oxide nanocubes, it was found that the average percentage coverage was around 79.2 ± 4.7 % (n=5) for the nanocubes spin-cast on the TEM grid with no surface modification, followed by annealing at 100°C (Figure 30 (a)). Particle size distribution was similar to the nanocube size in figure 23, with a mean of 15.2 ± 3.4 nm (n=9),(Figure 30 (b)).

Table 2: Fe₃O₄ nanoparticles spin-cast on plasma cleaned TEM Grids, annealed at 100°C.

Time (hr)	Full Grid (150x)	Overview (900x)	Low Mag (27.5kx)	High Mag (73kx)
0				
0.5				
1				
1.5				
2				

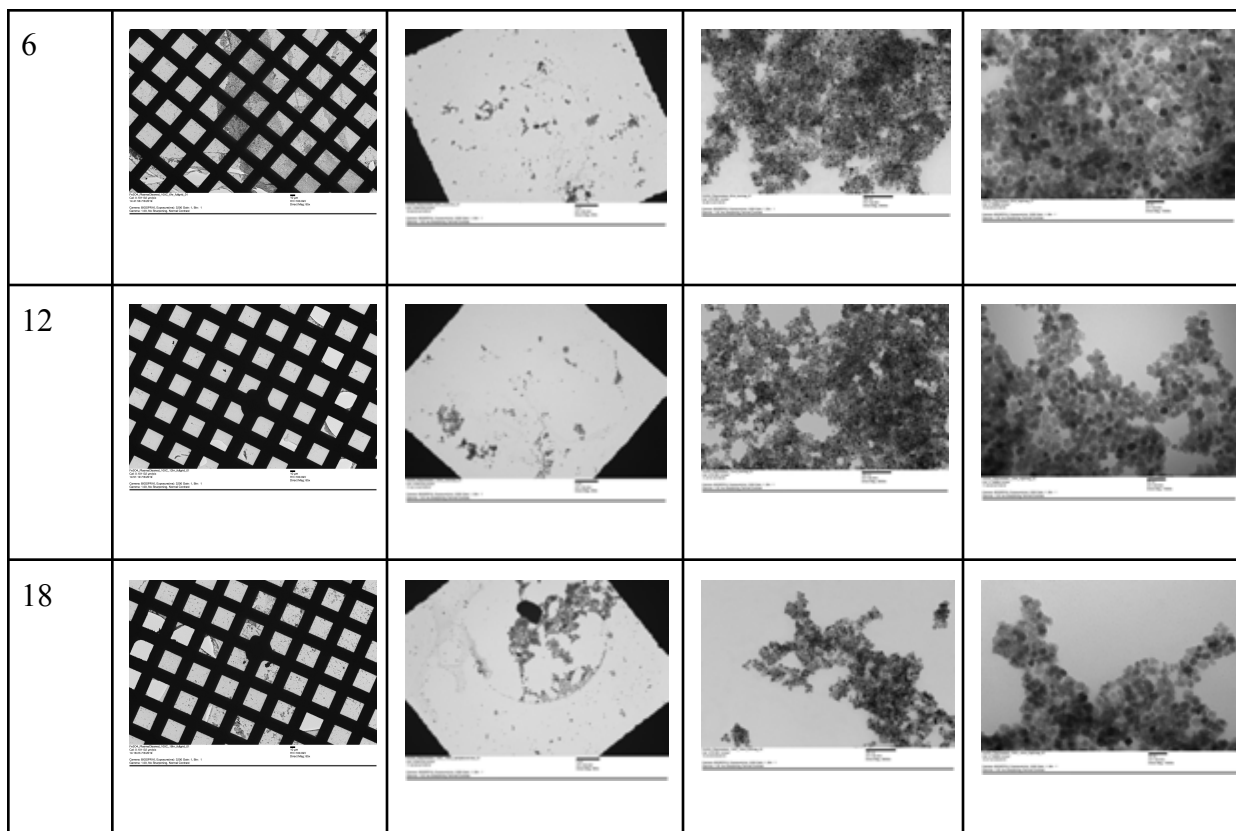


Table 2 shows the magnetic iron oxide nanocubes spin-cast on a plasma cleaned TEM grid, followed by annealing at 100 °C for different time intervals. The table shows a full grid TEM image at 150x magnification, an overview of one grid at 900x magnification, a low magnification image at 27,500 x magnification, and a highly magnified image at 73,000 x magnification.

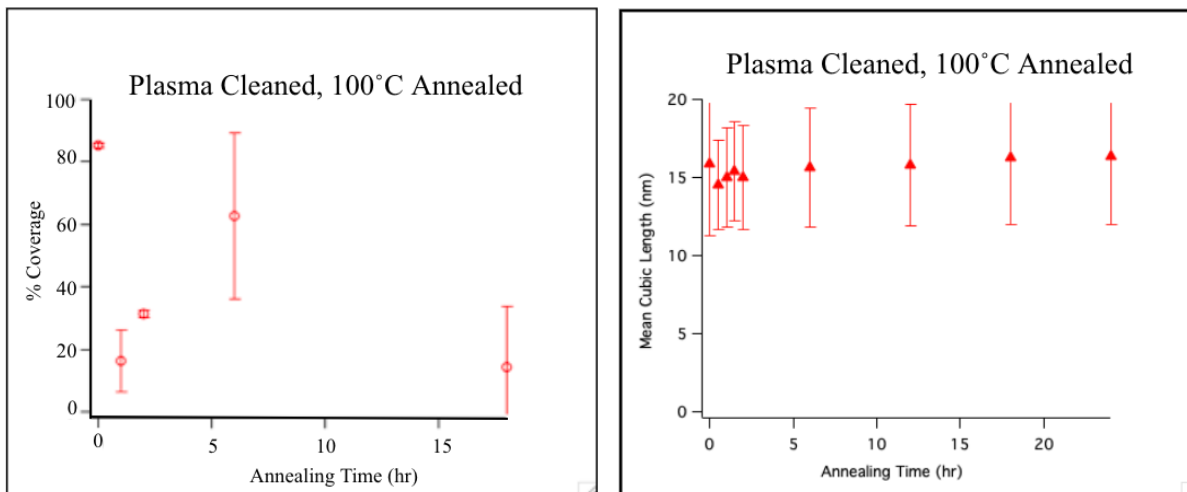


Figure 31: (a) Nanocube percentage coverage of plasma cleaned TEM grid annealed at 100°C against time with an average of 42.0 ± 11.7 % (b) Mean nanocube size for nanocubes against annealing time with a mean length of 15.5 ± 3.7 nm

On measuring the percentage coverage of the magnetic iron oxide nanocubes, it was found that the average percentage coverage was around 42.0 ± 11.7 % (n=5) for the nanocubes spin-cast on the plasma cleaned TEM grid, followed by annealing at 100°C (Figure 31 (a)). Particle size distribution was similar to the nanocube size in figure 23 with a mean of 15.5 ± 3.7 nm (n=9) (Figure 31 (b)).

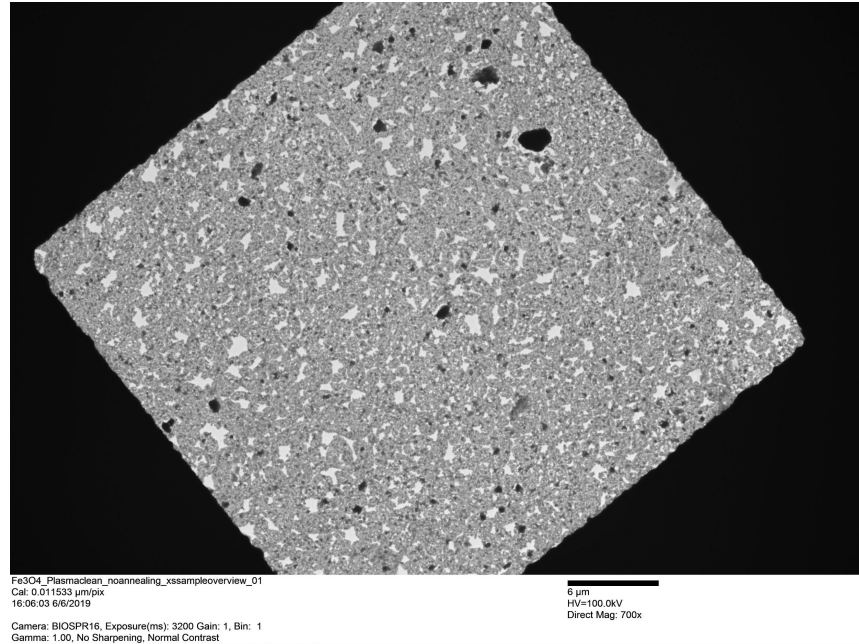
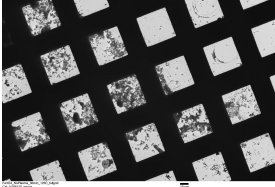
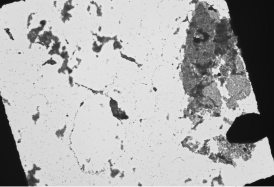
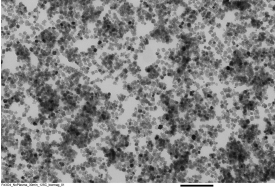
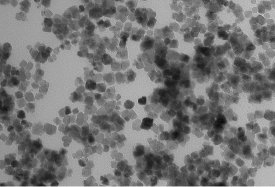
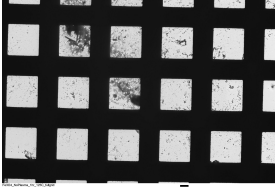
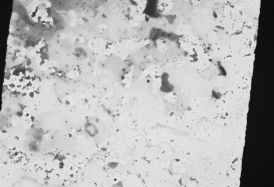
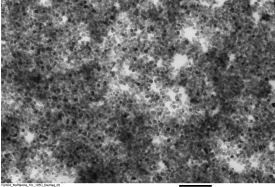
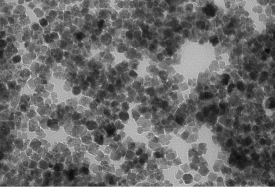
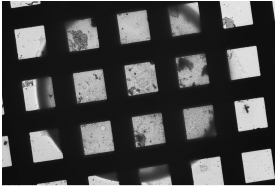
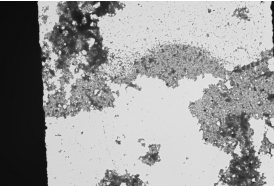
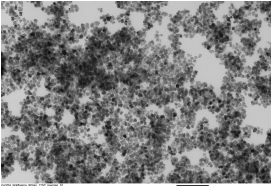
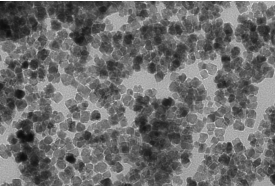
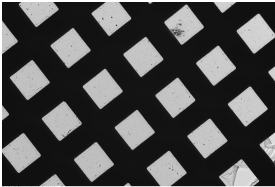
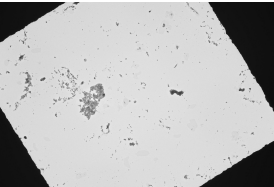
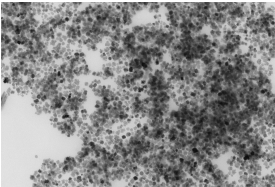
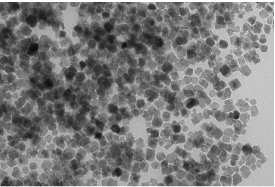
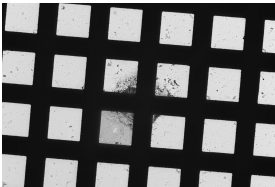
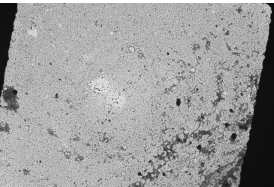
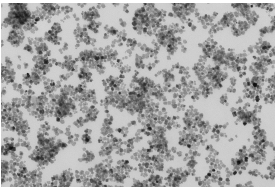
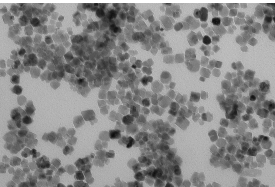


Figure 32: 900x magnified TEM image of magnetic iron oxide nanoparticles spin-cast on Carbon Coated TEM grid for 1 minute at 6000 rpm under Nitrogen

For the plasma cleaned TEM grids annealed at 100 °C, almost 100% surface coverage is observed with some small holes before annealing as seen in figure 32. With an increase in annealing time, the holes become cracks and eventually show the formation of closely packed islands of nanocubes as seen in table 2. This could be because the annealing increased the kinetic energy of the nanocubes deposited on the substrate. This in turn promoted the aggregation of the nanocubes as a result of unfavorable interactions with the plasma cleaned hydrophilic substrate.

4.2.1.2 Particles Annealed at 125 °C

Table 3: Fe₃O₄ nanoparticles spin-cast on TEM Grids, with no surface modification, annealed at 125 °C

Time (hr)	Full Grid (150x)	Overview (900x)	Low Mag (27.5kx)	High Mag (73kx)
0.5				
1				
1.5				
2				
6				

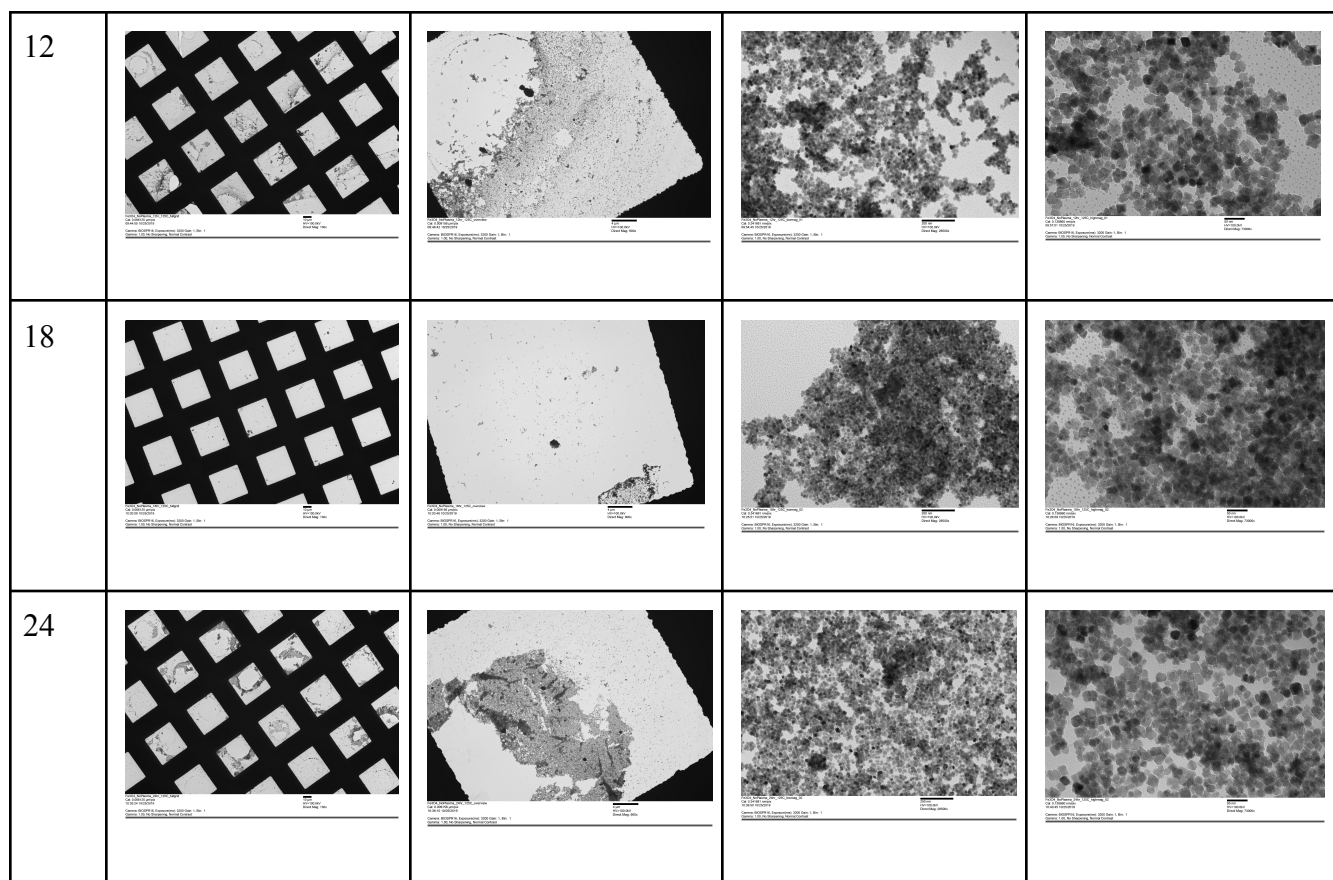


Table 3 shows the magnetic iron oxide nanocubes spin cast on a TEM grid with no surface modification, followed by annealing at 125 °C for different time intervals. The table shows a full grid TEM image at 150x magnification, an overview of one grid at 900x magnification, a low magnification image at 27,500 x magnification, and a highly magnified image at 73,000 x magnification.

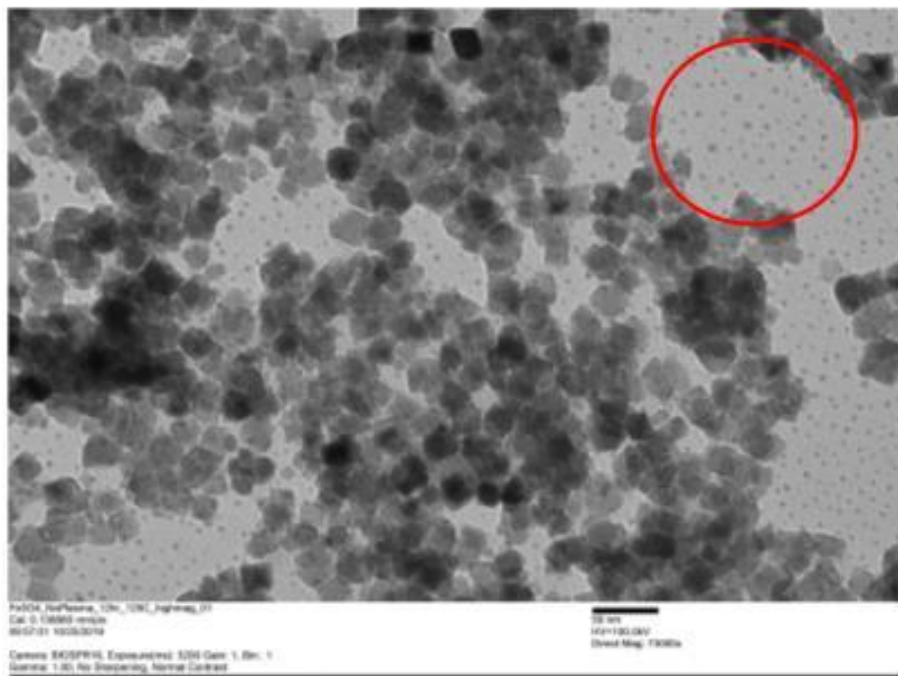


Figure 33: Appearance of spherical particles on the TEM grid with no surface modification after annealing at 125 °C for 6 hours as seen in the red circle.

For the TEM grids with no surface modification, annealed at 125 °C, the most surface coverage is seen at an annealing time of 6 hours, as seen in table 3. No other grids showed signs of a smooth distribution. In the highly magnified images, particle size and shape remain the same, however, particle aggregation can be noticed. Spherical-shaped particles begin to appear after annealing for 6 hours, and the carbon coating becomes unstable (Figure 33).

Fe_3O_4 nanocubes are not very stable under ambient conditions and are easily oxidized to Fe_2O_3 or dissolved in an acidic medium. To avoid the possible oxidation in the air, the synthesis of Fe_3O_4 nanocubes must be done in anaerobic conditions. Based on this point, Fe_3O_4 nanocubes can also be utilized to prepare the spherical Fe_2O_3 nanoparticles by oxidation or anneal treatment under an oxygen atmosphere. Given the particles were annealed for a prolonged period of time under aerobic conditions, the spherical particles could be the oxidation of Fe_3O_4 nanocubes to Fe_2O_3 nanoparticles.⁶³

Table 4: Fe₃O₄ nanoparticles spin-cast on Plasma cleaned TEM Grids annealed at 125 °C

Time (hr)	Full Grid (150x)	Overview (900x)	Low Mag (27.5kx)	High Mag (73kx)
0.5				
1				
1.5				
2				

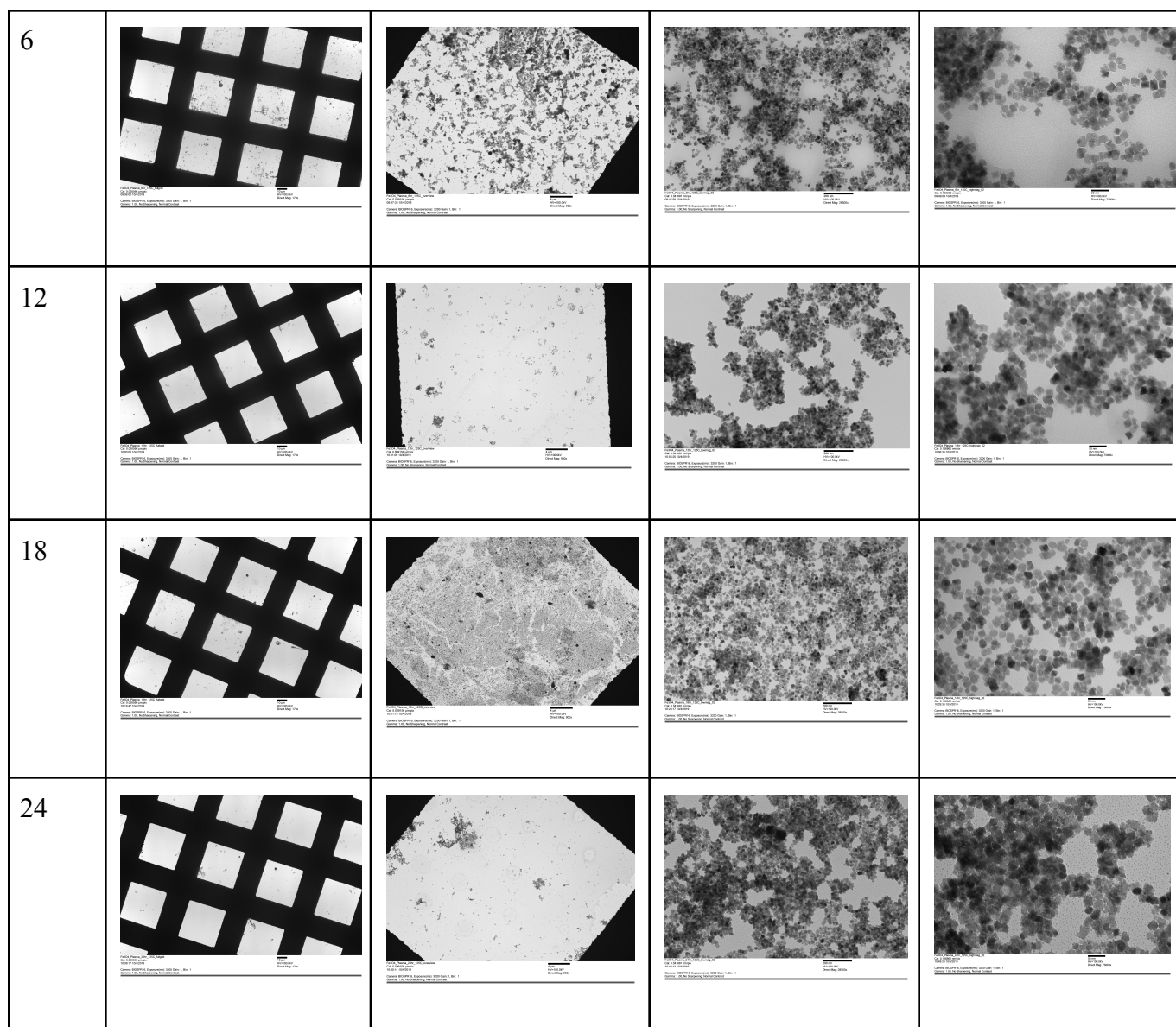
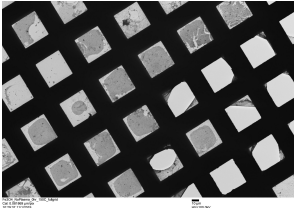
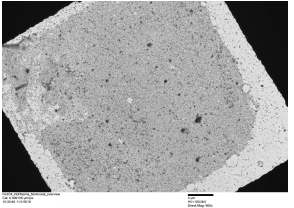
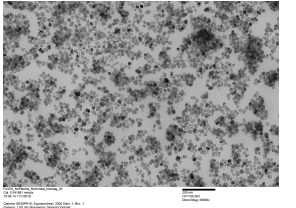
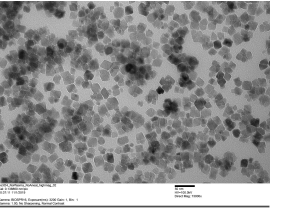
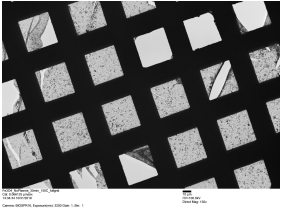
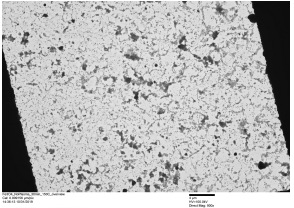
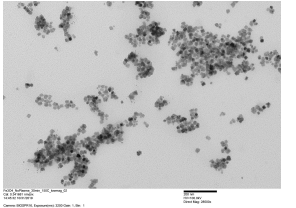
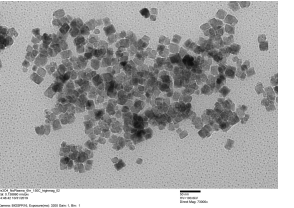
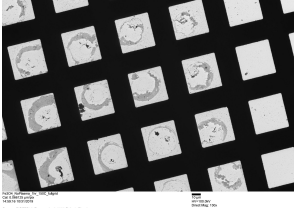
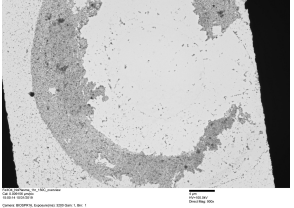
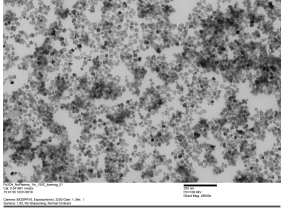
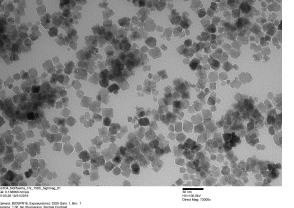


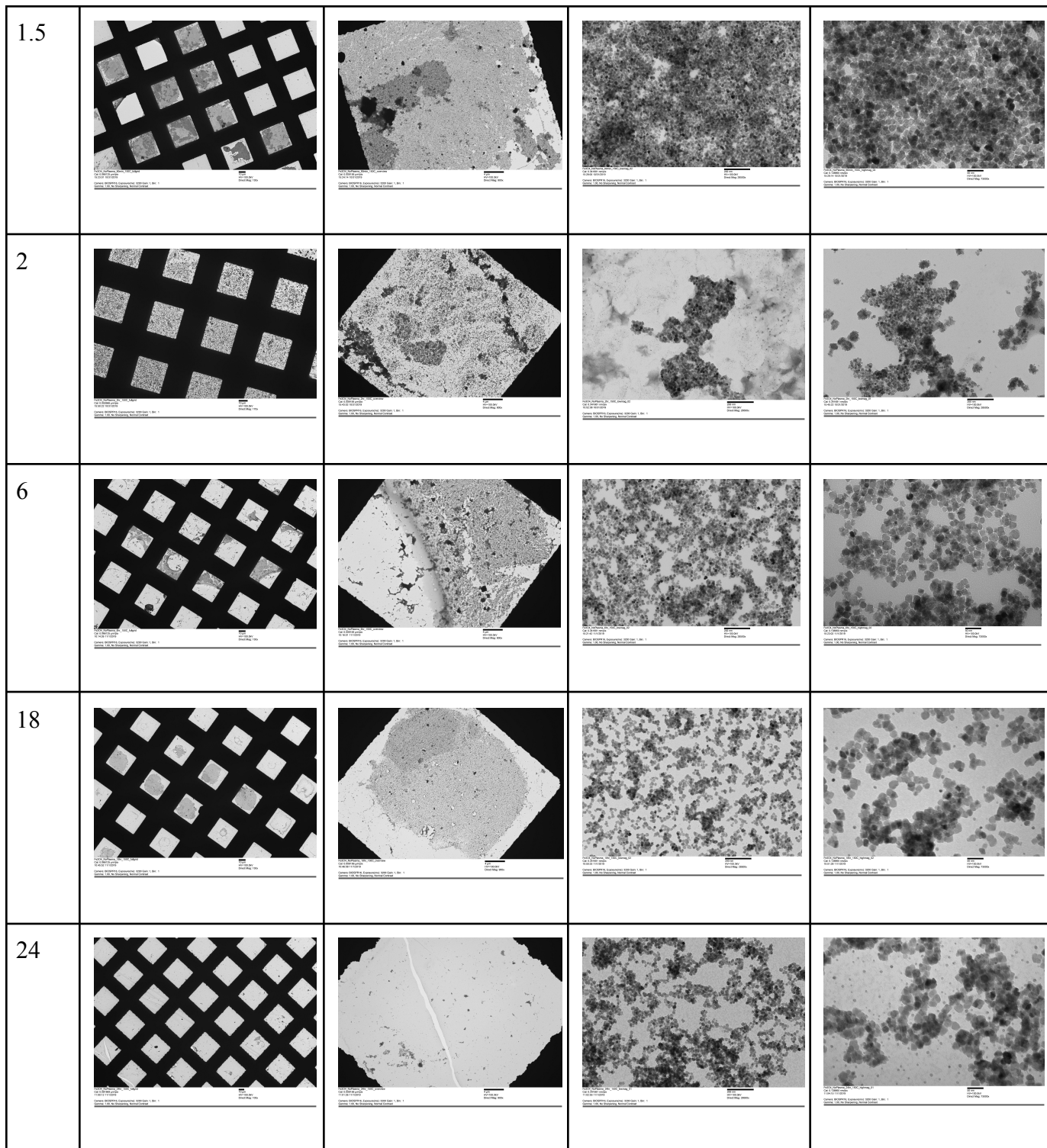
Table 4 shows the magnetic iron oxide nanocubes spin cast on a plasma cleaned TEM, followed by annealing at 125 °C for different time intervals. For the plasma cleaned TEM grids, annealed at 125 °C, the most surface coverage is seen at an annealing time of 2 hours, and 18 hours. Particles seemed to be aggregated. Once again, no other grids showed signs of a smooth distribution.

4.2.1.3 Particles Annealed at 150 °C

Table 5 shows the magnetic iron oxide nanocubes spin-cast on a TEM grid with no surface modification, followed by annealing at 150 °C for different time intervals. The table shows a full grid TEM image at 150x magnification, an overview of one grid at 900x magnification, a low magnification image at 27,500 x magnification, and a highly magnified image at 73,000 x magnification.

Table 5: Fe₃O₄ nanocubes spin-cast on TEM Grids with no surface modification, annealed at 150 °C

Time (hr)	Full Grid (150x)	Overview (900x)	Low Mag (27.5kx)	High Mag (73kx)
0				
0.5				
1				



For the TEM grids with no surface modification that were annealed at 150°C, the most surface coverage is seen when the grids were not annealed (Annealing time of 0 hours). There is

also significant surface coverage on TEM grids annealed for 1.5 and 18 hours. After 6 hours of annealing at 150°C, spherical-shaped particles begin to appear on the TEM grids.

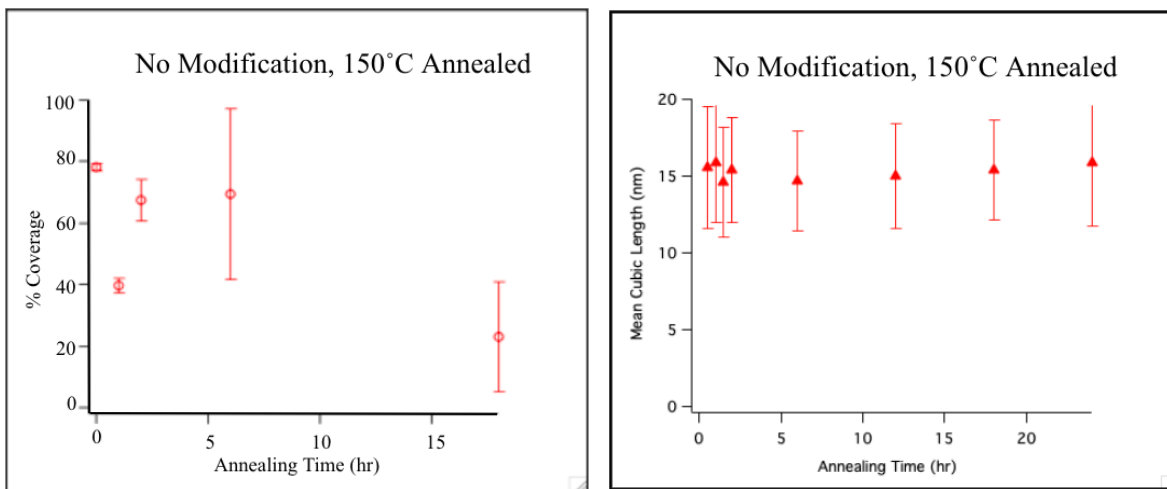


Figure 34: (a) Nanocube percentage coverage of TEM grid with no surface modification annealed at 150°C against time with an average of 55.5 ± 11.2 % (b) Mean nanocube size for nanocubes against annealing time with a mean length of 15.3 ± 3.62 nm

On measuring the percentage coverage of the magnetic iron oxide nanocubes, it was found that the average percentage coverage was around 55.5 ± 11.2 % ($n=5$) for the nanocubes spin-cast on the plasma cleaned TEM grid, followed by annealing at 150°C (Figure 34 (a)). Particle size distribution was similar to the nanocube size in figure 23 with a mean of 15.3 ± 3.62 nm ($n=8$) (Figure 34 (b)).

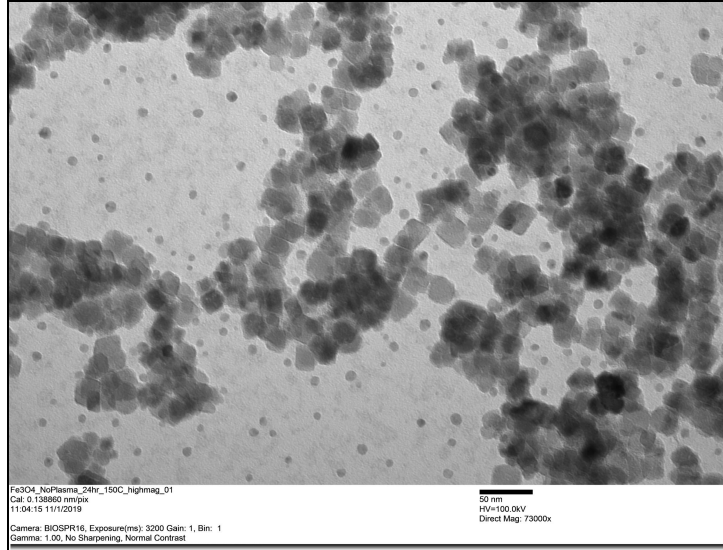
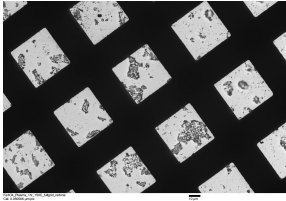
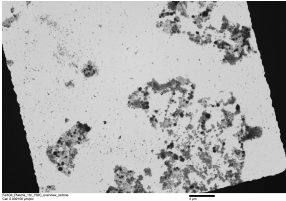
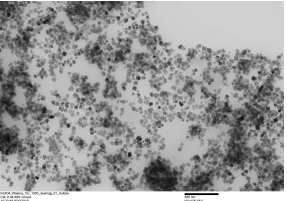
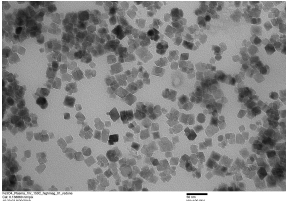
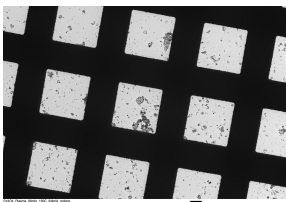
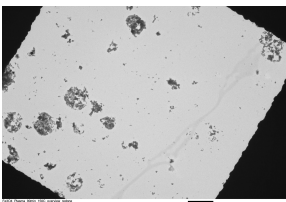
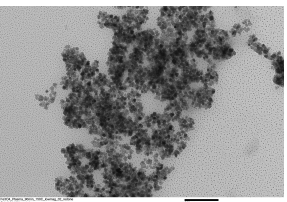
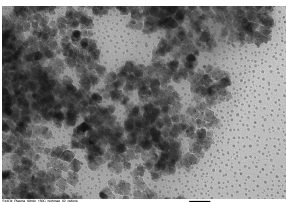
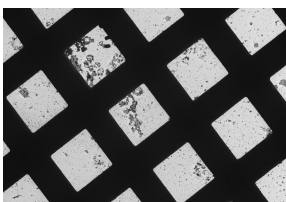
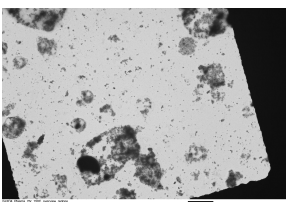
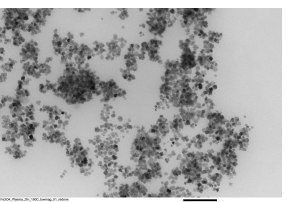
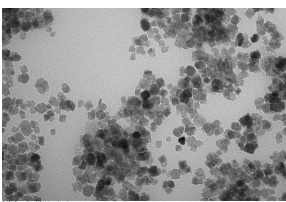
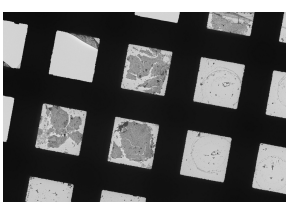
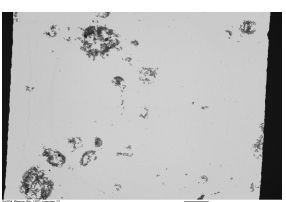
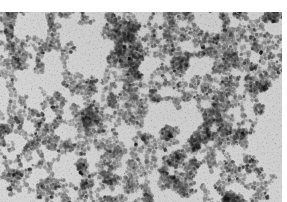
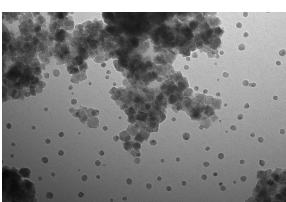
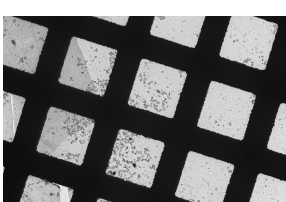
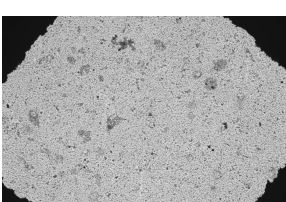
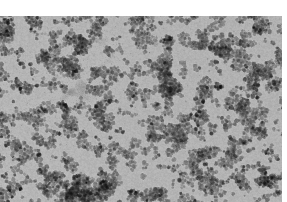
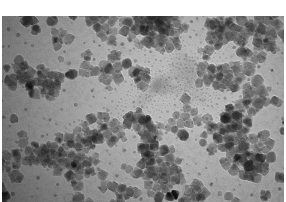


Figure 35: Highly magnified TEM image of spherical nanoparticles that was observed after annealing the TEM sample with no surface modification at 150 °C for 24 hours

As seen in figure 35, spherical-shaped particles were observed on the TEM grid with no surface modification after 24 hours of annealing.

Table 6: Fe₃O₄ nanoparticles spin-cast on Plasma cleaned TEM Grids annealed at 150 °C

Time (hr)	Full Grid (150x)	Overview (900x)	Low Mag (27.5kx)	High Mag (73kx)
0.5				

1	 <p>Micrograph showing a grid pattern with sparse particles.</p>	 <p>Micrograph showing a grid pattern with sparse particles.</p>	 <p>Micrograph showing a grid pattern with sparse particles.</p>	 <p>Micrograph showing a grid pattern with sparse particles.</p>
1.5	 <p>Micrograph showing a grid pattern with sparse particles.</p>	 <p>Micrograph showing a grid pattern with sparse particles.</p>	 <p>Micrograph showing a grid pattern with sparse particles.</p>	 <p>Micrograph showing a grid pattern with sparse particles.</p>
2	 <p>Micrograph showing a grid pattern with sparse particles.</p>	 <p>Micrograph showing a grid pattern with sparse particles.</p>	 <p>Micrograph showing a grid pattern with sparse particles.</p>	 <p>Micrograph showing a grid pattern with sparse particles.</p>
6	 <p>Micrograph showing a grid pattern with sparse particles.</p>	 <p>Micrograph showing a grid pattern with sparse particles.</p>	 <p>Micrograph showing a grid pattern with sparse particles.</p>	 <p>Micrograph showing a grid pattern with sparse particles.</p>
12	 <p>Micrograph showing a grid pattern with sparse particles.</p>	 <p>Micrograph showing a grid pattern with sparse particles.</p>	 <p>Micrograph showing a grid pattern with sparse particles.</p>	 <p>Micrograph showing a grid pattern with sparse particles.</p>

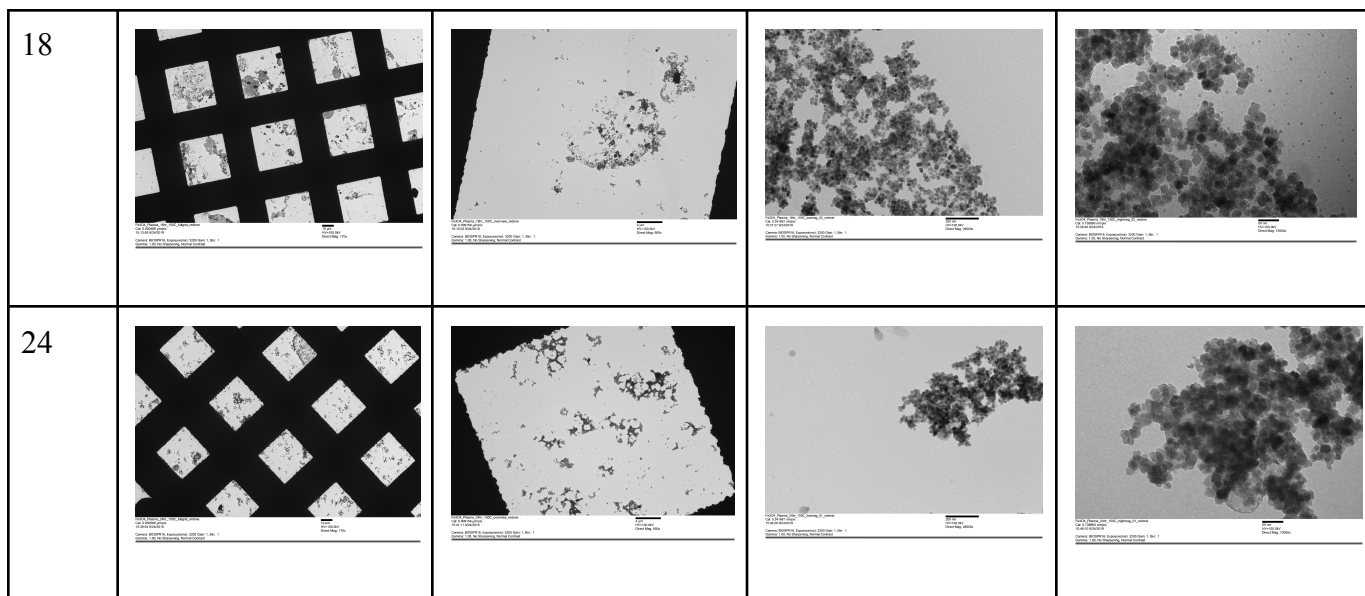


Table 6 shows the magnetic iron oxide nanocubes spin cast on a plasma cleaned TEM grid, followed by annealing at 150°C for different time intervals. The TEM grids that were plasma cleaned and annealed at 150°C, show very little surface coverage overall as seen in table 6. Once again we see the appearance of spherical-shaped particles on the TEM grids after 1.5 hours of annealing at this temperature (Figure 35).

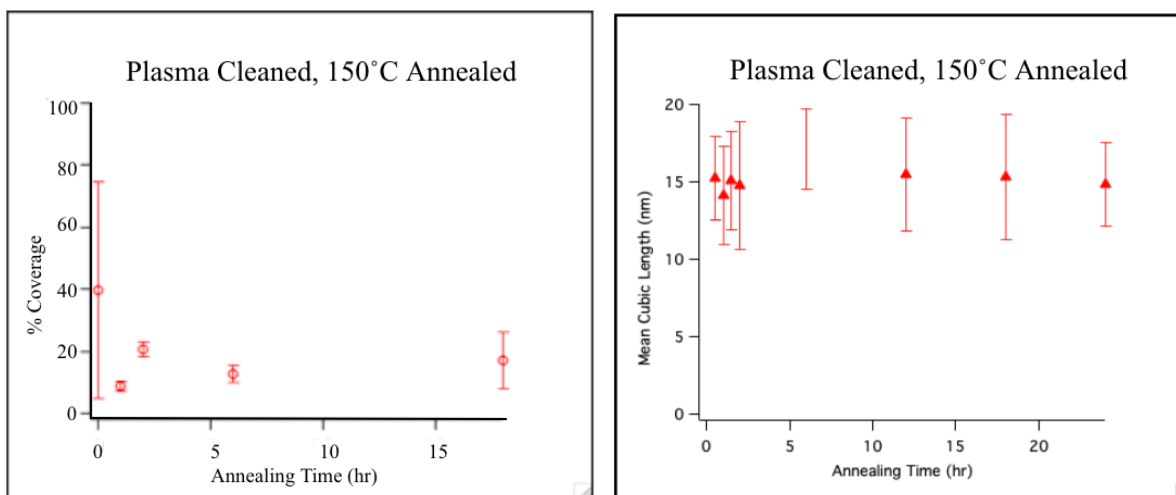


Figure 36: (a) Nanocube percentage coverage of plasma cleaned TEM grid annealed at 150 °C against time with an average of 19.7 ± 10.1 % (b) Mean nanocube size for nanocubes against annealing time with a mean length of 15.6 ± 3.62 nm

On measuring the percentage coverage of the magnetic iron oxide nanocubes, it was found that the average percentage coverage was around 19.7 ± 10.1 % (n=5) for the nanocubes spin-cast on the plasma cleaned TEM grid, followed by annealing at 150 °C (Figure 36 (a)). Particle size distribution was similar to the nanocube size in figure 23 with a mean of 15.6 ± 3.62 nm (n=8) (Figure 36 (b)).

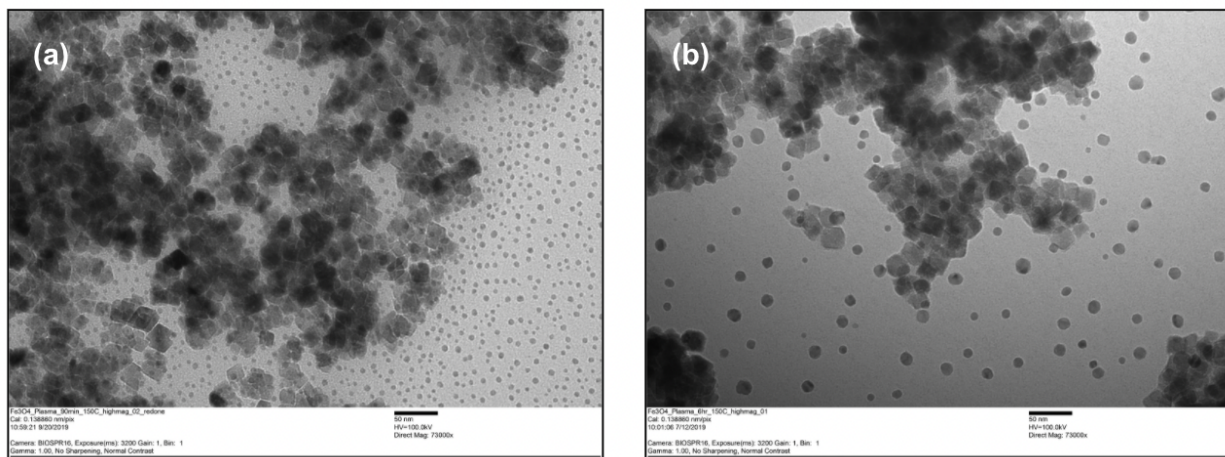


Figure 37: Highly magnified TEM image of spherical nanoparticles that was observed after annealing the plasma cleaned TEM sample at 150 °C for (a) 1.5 hours (b) 6 hours.

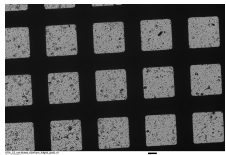
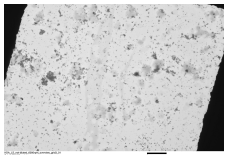
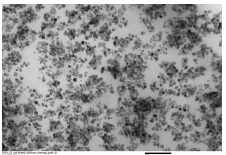
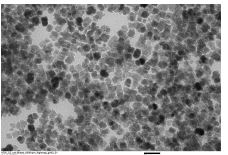
Spherical-shaped particles were observed on the plasma cleaned TEM grid after 1.5, and 6 hours of annealing (figure 37). At 1.5 hours, the spherical particles are fairly small. With an increase in annealing time to 6 hours, the size of the particles increased. This pattern is similar to what was observed for the TEM grids with no surface modification, annealed for 24 hours at 150 °C as seen in figure 34. It is found that synthesized Fe_3O_4 nanocube assemblies can be transformed easily into $\gamma\text{-Fe}_2\text{O}_3$ nanoparticles by annealing at high temperature (250 °C) and

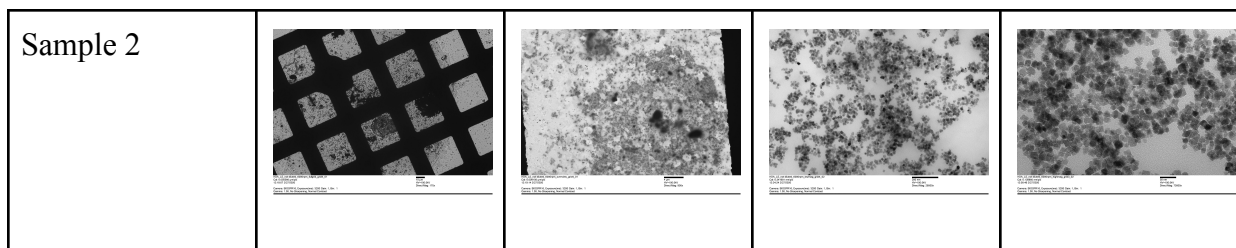
oxygen for 2 hours.⁶³ γ -Fe₂O₃ are spherical nanoparticles. Although the Fe₃O₄ nanocubes were heated at a lower temperature of 150°C, the emergence of smaller spherical particles after 1.5 hours, that subsequently led to larger particles when annealed for a longer interval of 6 hours on an oxygen plasma cleaned substrate, could be due to the formation of spherical γ -Fe₂O₃ nanoparticles.

4.2.2 Particles spin-cast onto TEM grids coated with HDA

In an attempt to increase the hydrophobic nature of the carbon-coated TEM grids, LB and LS techniques were used to coat the TEM grids with a hydrophobic HDA layer. The reason for an increase in the hydrophobicity of the substrate is due to the hydrophobic nature of the decanoic acid coating of the Fe₃O₄ nanocubes. Given that - like interact, the hope is that an increase in the hydrophobic interactions will facilitate the smooth, and even formation of a monolayer.

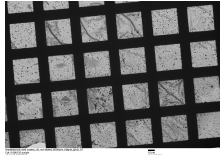
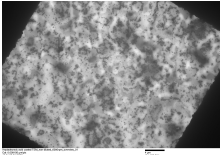
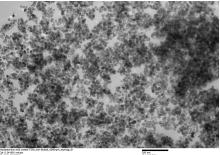
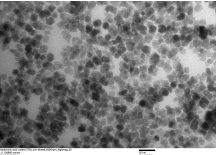
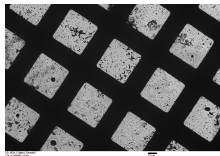
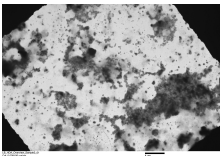
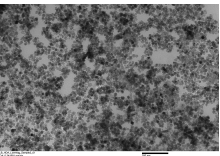
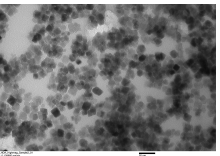
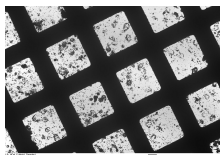
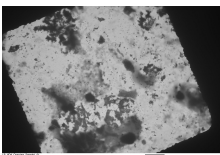
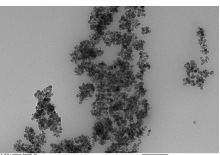
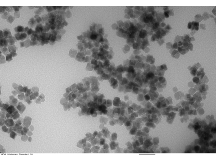
Table 7: Fe₃O₄ nanocubes deposited on HDA Coated TEM grids using the LS technique at different magnifications

Sample #	Grid View (170x)	Overview (900x)	Low Mag (27,500x)	High Mag (73,000x)
Sample 1				



The TEM Grids coated with HDA using the LS technique have fairly full coverage of Fe_3O_4 nanocubes. Little aggregation can be observed, however, the overall surface coverage seen is promising.

Table 8: Fe_3O_4 nanocubes deposited on HDA Coated TEM grids using the LB technique at different magnifications

Sample #	Grid View (170x)	Overview (900x)	Low Mag (27,500x)	High Mag (73,000x)
Sample 1				
Sample 2				
Sample 3				

The TEM Grids coated with HDA using the LB technique have fairly full coverage of

Fe_3O_4 nanocubes similar to the LS coated TEM grids. However, the smooth monolayer can not be observed, and instead, severe aggregation of the nanocubes is noticed. The difference in particle distribution based on HDA coating using LS, or LB is yet to be understood.

As mentioned before, LB and LS are great techniques that can be utilized to manipulate the surface chemistry of the substrate of choice. Currently, not much work has been done to analyze the effect of drop-casting HDA onto the TEM grid to assist the monolayer formation of Fe_3O_4 nanocubes (Table 7). However, in the future, we hope to pursue the effect of hydrophobic interactions as an effective way of monolayer formation.

CONCLUSION AND FUTURE PLANS

From the study, one can conclude that the magnetic iron oxide nanocubes that were synthesized over three years ago were stable, and had the same size and shape distribution when compared to the histogram used by Sarah Andoh.⁴⁹ The average length of these nanocubes was measured by analyzing a sample size of 733 nanocubes, and was found to be 15.50 ± 3.95 nm. Using DLS, it was found that the nanocubes had a diameter of 18.10 ± 6.30 nm. The increase in size was due to the spherical solvent cap around the nanocube.

When measuring the UV-visible spectra of the Fe_3O_4 nanocubes in a 3:1 C: M dispersing solution, the presence of a peak at 420 nm on the absorption of light indicated that the nanocubes were iron (III) oxide.⁶¹ The information found using FTIR spectra is further supported by the presence of a peak at 579 cm^{-1} indicating the presence of an iron-oxygen bond seen in literature values.⁶²

It was seen that with an increase in temperature, the particle shape and size started to change. For the most part, the Fe_3O_4 nanocubes are stable up to 150°C . However, when the nanocubes were annealed for 6 hours at 125°C , the formation of spherical particles was observed on the TEM grid with no surface modifications. The same trend was seen on the TEM grid with no surface modification after 24 hours of annealing at 150°C , and once again on the plasma cleaned TEM grid after 1.5, and 6 hours annealed at 150°C . At 1.5 hours, the spherical particles were fairly small. With an increase in annealing time to 6 hours, the size of the particles increased.

Through this study, it was seen that the TEM grids, known to be slightly hydrophobic, have the most even distribution of nanocubes when no substrate modification was performed. The TEM grids with no surface modification, annealed at 100°C show the highest surface

coverage of $79.2 \pm 4.70\%$ ($n=5$) with a more evenly distributed nanocubes layer.

With an increase in the hydrophilicity of the substrate, due to plasma cleaning, the even distribution of Fe_3O_4 nanocubes decreases. Annealing on hydrophilic substrate results in island formations which could be due to unfavorable interactions between the nanocubes and the substrate. The TEM Grids coated with HDA using the LS technique had fairly full coverage of Fe_3O_4 nanocubes, and less aggregation was observed. In contrast, the TEM Grids coated with HDA using the LB technique had fairly full coverage of Fe_3O_4 nanocubes similar to the LS coated TEM grids, but a smooth monolayer could not be observed, and instead, severe aggregation of the nanocubes is noticed. The difference in particle distribution based on HDA coating using LS, or LB is yet to be understood.

It has been hypothesized that the hydrophobic carbon tails on the heptadecanoic acid attract the hydrophobic carbon tails of the decanoic acid-coated nanocubes allowing for most even dispersion of nanocubes. However, little work has been done to see the effect of HDA coated TEM grids on the monolayer formation, and more research is needed.

In the future, more work needs to focus on the effect of increased substrate hydrophobicity on the formation of a monolayer, as well as to understand how LS and LB might alter the final product. Along with that, an examination of the contact angle can also be used to measure the extent of hydrophobicity of the TEM grids coated with heptadecanoic acid. Finally, a study of the growth mechanism during the synthesis of nanocubes, as well as magnetism as a property that is affected by the size and shape of the nanoparticles is necessary.

REFERENCES

1. National Nanotechnology Initiative (NNI). National Science and Technology Council. Committee on Technology, Subcommittee on Nanoscale Science, National Technology Initiative Strategic Plan, www.nano.gov (2011, accessed 25 August 2015).
2. Hulla. J.E., et. al; Nanotechnology: History and future. *Division of Toxicology*, (2015) 34:12: 1318-1321.
3. Darr J. A, et.al; Continuous Hydrothermal Synthesis of Inorganic Nanoparticles: Applications and Future Directions. *Chemical Reviews*, (2021) 22:39:27
4. Xu Z. et.al; Inorganic nanoparticles as carriers for efficient cellular delivery. *Chemical Engineering Science* (2006) 61.; 1027-1040
5. “Properties and Applications of Magnetic Nanoparticles.” *Properties and Applications of Magnetic Nanoparticles - CD Bioparticles*, www.cd-bioparticles.com/t/Properties-and-Applications-of-Magnetic-Nanoparticles_55.html.
6. Prathna T.C., et. al; Biomimetic Synthesis of Nanoparticles: Science, Technology & Applicability, Biomimetics Learning from Nature, *IntechOpen* (2010)
7. Modena, M., et. al; Nanoparticle characterization: What to measure? *Advanced Materials* (2019), 31:32
8. Grancharov S.G., et. al; “Bio-Functionalization of Monodisperse Magnetic Nanoparticles and Their Use as Biomolecular Labels in a Magnetic Tunnel Junction Based Sensor.” *J. Phys. Chem. B*, (2005) 109, 26, 13030–13035
9. Peng, X., Manna, L., Yang, W. et al. Shape control of CdSe nanocrystals. *Nature.*, (2000), 404, 59–61. <https://doi.org/10.1038/35003535>

10. In I., Jun Y., Kim J., and Kim S. Y., Spontaneous one dimensional arrangement of spherical Au nanoparticles with liquid crystal ligands *Chem. Commun.*, (2005), 800-801
11. Akbarzadeh, A., Samiei, M. & Davaran, S. Magnetic nanoparticles: preparation, physical properties, and applications in biomedicine. *Nanoscale Res Lett* (2002) 7, 144.
<https://doi.org/10.1186/1556-276X-7-144>
12. Suzuki, K.; Kijima, K. Phase transformation of BaTiO₃ nanoparticles synthesized by RF-plasma CVD. *J. Alloys Compd.* (2006) 419, 234–242
13. Schlabach, D. V. S. S. Microwave Plasma Synthesis of Materials - From Physics and Chemistry to Nanoparticles: A Materials Scientist's Viewpoint. *Inorganics*, (2014) 2, 468–50.
14. Yokel, R. A.; MacPhail, R. C. Engineered nanomaterials: exposures, hazards, and risk prevention. *J. Occup. Med. Toxicol.*, (2011) 6:7, 1–27.
15. Dimitriev Y., Ivanova Y., Iordanova. R.; History of Sol-Gel Science and Technology. *Journal of the University of Chemical Technology and Metallurgy*, (2008) 43, 2: 181-192
16. Trejos T., Flores A., Almirall J. R.; Micro-spectrochemical analysis of document paper and gel inks by laser ablation inductively coupled plasma mass spectrometry and laser-induced breakdown spectroscopy. *Atomic Spectroscopy*, (2010) 65:11. 884-895
17. Benelmekki M., Vernieres J., Kim J., et. al.; The formation of ternary metallic-dielectric multicore-shell nanoparticles by inert-gas condensation method. *Materials Chemistry and Physics*, (2015) 151: 275-281
18. Xu Y., et. al; Solvothermal Synthesis and Ultrafast Photonics of Black Phosphorus Quantum Dots. *Advanced Optical Material*, (2016) 4:8, 1223-1229

19. Stankovich S., et. al; Synthesis of graphene-based nanosheets via chemical reduction of exfoliated graphite oxide, *Chem. Commun.*(2007), 45: 7, 1558-1565
20. Polte J.; Fundamental growth principles of colloidal metal nanoparticles – a new perspective *CrystEngComm*, (2015) 17, 6809-683
21. Jun Y., et.al; Nanoscale Size Effect of Magnetic Nanocrystals and Their Utilization for Cancer Diagnosis via Magnetic Resonance Imaging. *J. Am. Chem. Soc.*, (2005) 127, 16, 5732–5733
22. Ling D., Lee N., and Hyeon T.: Chemical Synthesis and Assembly of Uniformly Sized Iron Oxide Nanoparticles for Medical Applications *Accounts of Chemical Research.*, (2015) 48 (5), 1276-1285 DOI: 10.1021/acs.accounts.5b00038
23. Bu A.; Iron Oxide Nanoparticles, Characteristics, and Applications. *Partner and Operations Manager, Ocean NanoTech LLC* (2021)
24. Roco M. C.: Nanoparticles and nanotechnology research. *Journals of nanoparticle research*, (1999) 1: 1-6
25. Sanguansri P., Augustin M. A.; Nanoscale material development - a food industry perspective. *Trends Food Sci. Technology*, (2006) 17: 547-556
26. Liu W.; Nanoparticles and their biological and environmental applications. *Journal of Bioscience and Bioengineering*, (2006) 102:1, 1-7
27. Taton T.A., Mirkin C.A., Letsinger R.L.; Scanometric DNA array detection with nanoparticle probes. *Science*. (2000) 289: 1757-1760
28. Pathak S., Choi S.K., Arnheim N., Thompson M.E.; Hydroxylated quantum dots as luminescent probes for in situ hybridization. *J. Am. Chem. Soc.*,(2001) 123: 4103-4104

29. Wu X., Liu H., Liu J., Haley K.N., Treadway J.A., Larson J.P., Ge N., Peale F., Bruchez M.P.; Immunofluorescent labeling of cancer marker Her2 and other cellular targets with semiconductor quantum dots. *Nat. Biotechnol.*, (2002) 21: 41-46
30. Kloepfer J.A., Mielke R.E., Wong M.S., Neelson K.H., Stucky G., Nadeau J.L.; Quantum dots as strain- and metabolism-specific microbiological labels. *Appl. Environ. Microbiol.*, (2003) 69: 4205-4213
31. Zhang Q., Zhu L., Feng H.H., Ang S., Chau F.S., Liu W.-T.; Microbial detection in microfluidic devices through dual staining of quantum dots-labeled immunoassay and RNA hybridization. *Anal. Chim. Acta*, (2005) 556: 171-177
32. Zhao X.J., Hilliard L.R., Mechery S.J., Wang Y.P., Bagwe R.P., Jin S.G., Tan W.H.; A rapid bioassay for single bacterial cell quantitation using bioconjugated nanoparticles. *Proc. Nat. Acad. Sci. USA*, (2004) 101: 15027-15032
33. Nurmi J.T., Tratnyek P.G., Sarathy V., Baer D.R., Amonette J.E., Pecher K., Wang C., Linehan J.C., Matson D.W., Penn R.L., Driessen M.D.; Characterization and properties of metallic iron nanoparticles: spectroscopy, electrochemistry, and kinetics. *Environ. Sci. Technol.*, (2005) 39: 1221-1230
34. Tahmasebi T., and Piramanayagam S. N.; Nanoscience and Nanotechnology for Memory and Data Storage. *World Scientific*. (2011) 07:01. 25-30
35. Nuncic M.; How nanotechnology could change data storage in the future. (n.d.). November (2018), from <https://www.ontrack.com/en-us/blog/how-nanotechnology-changes-data-storage-in-the-future>
36. Belkind A. & Gershman S.; Plasma cleaning of surfaces. *Vac. Technol. Coat*, (2008) 1-11.

37. Petty M. C.; Langmuir Blodgett Films - An Introduction. *Cambridge University Press*, (1996)
38. KSV NIMA; Fabrication Highly Organized Nanoparticle Thin Films. *Biolin Scientific*. (2017)
39. Sui, M., Li, M. Y., Kunwar, S., Pandey, P., Zhang, Q., & Lee, J.; Effects of annealing temperature and duration on the morphological and optical evolution of self-assembled Pt nanostructures on c-plane sapphire. *PloS one*, (2017) 12(5)
40. Tan ST, Sun XW, Zhang XH, Chua SJ, Chen BJ, Teo CC. (2006). Cluster coarsening in zinc oxide thin films by post growth annealing. *Journal of applied physics*, 100(3), 033502.
41. Ruffino F, Grimaldi MG (2010). Atomic force microscopy study of the growth mechanisms of nanostructured sputtered Au film on Si (111): evolution with film thickness and annealing time. *Journal of Applied Physics*,107(10), 104321.
42. Princeton Scientific Corporation - Plasma Treatment Equipment
43. Sponsored by Biolin Scientific Oct 6 2014. "The Deposition and Characterization of Single Sheet Graphene Films." *AZoM.com*, (2018)
www.azom.com/article.aspx?ArticleID=11433.
44. Pradhan S., Hedberg J., Blomberg E. et al. Effect of sonication on particle dispersion, administered dose and metal release of non-functionalized, non-inert metal nanoparticles. *J Nanopart Res*, (2016) 18: 285
45. Bornside D. E., Macosko C. W., Scriven L. E.; Modeling of Spin Coating. *Chemical Engineering and Materials Science*. 1987. 4, 13: 122 - 130

46. Gao T., Jelle B.; Nano Electrochromics for Smart Windows: Materials and Methodologies. (2016)
47. PharmAI; Running Molecular Dynamics with Simulated Annealing in OpenMM. April 29, (2021)
<https://www.pharm.ai/2020/10/09/running-molecular-dynamics-with-simulated-annealing>
48. Yuxue C., Wolfkühler D., Myalitsin A., Perlich J., Meyer A., and Klinke C.. "Tunable Electrical Transport through Annealed Monolayers of Monodisperse Cobalt–Platinum Nanoparticles." *ACS Nano*. (2010) 5.1: 67-72.
49. Andoh, Sarah E: Synthesis, Characterization, and Assembly of Decanoic Acid - Coated Magnetic Iron (III) Oxide (Fe₃O₄) Nanocubes into Monolayer Films. (2019)
50. Schmid, F.X. Biological macromolecules: UV-visible spectrophotometry. In *Encyclopedia of Life Sciences*; Robinson, S., Ayres, E., Eds.; Macmillan Publishers: London, UK, (2001); pp. 1–4.
51. Rocha F. S., Gomes A.J., Lunardi C. N., Kaliaguine S., Patience G.S.; Experimental Methods in Chemical Engineering: Ultra Violet Spectroscopy - UV-Vis, *Canadian Society for Chemical Engineering*, (2018) 12: 2512-2517
52. Claßen, J.; Aupert, F.; Reardon, K.F.; Solle, D.; Scheper, T. Spectroscopic sensors for in-line bioprocess monitoring in research and pharmaceutical industrial application. *Anal. Bioanal. Chem.* (2017) 409, 651–666.
53. Cozzolino, D.; Cynkar, W.U.; Shah, N.; Smith, P. Multivariate data analysis applied to spectroscopy: Potential application to juice and fruit quality. *Food Res. Int.* (2011) 44, 1888–1896

54. Harding S. E., Jumel K., Coligan J. E., Dunn B. M., Ploegh H. L., Speicher D. W., Wingfield P. T.; Light scattering. Current protocols in protein science. *John Wiley & Sons, Inc.*, (1998)
55. "Transmission Electron Microscopy." *Wikipedia*, Wikimedia Foundation, 22 Apr. 2021, en.wikipedia.org/wiki/Transmission_electron_microscopy.
56. Tasneem Jennifer, *Synthesis And Characterization Of Decanoic Acid Coated Magnetic Iron (Iii) Oxide Nanocubes For The Preparation Of Uniform Nanocube Monolayers*, (2017)
57. Feizollahi, E.; Iqdiam, B.; Vasanthan, T.; Thilakarathna, M.S.; Roopesh, M.S. Effects of Atmospheric-Pressure Cold Plasma Treatment on Deoxynivalenol Degradation, Quality Parameters, and Germination of Barley Grains. *Appl. Sci.* (2020) *10*, 3530. <https://doi.org/10.3390/app10103530>
58. Ahamad N., Ianoul A., & Amin, A.; Fabrication of 2D and 3D Architectures with Silver Nanostructures Building Blocks and Studying Their Refractive Index Sensitivity. *Plasmonics*. (2018)13. 10.1007/s11468-016-0487-8.
59. Nowak, P.; Maziarz, W.; Rydosz, A.; Kowalski, K.; Ziabka, M.; Zakrzewska, K. SnO₂/TiO₂ Thin Film n-n Heterostructures of Improved Sensitivity to NO₂. *Sensors* (2020) *20*, 6830. <https://doi.org/10.3390/s20236830>
60. Chung D. D. L; 6 - Cement-Matrix Composites. *Science Direct*. (2017) *2*: 333-386
61. Yew, Yen Pin, et al. "Green Synthesis of Magnetite (Fe₃O₄) Nanoparticles Using Seaweed (*Kappaphycus Alvarezii*) Extract." *Nanoscale Research Letters*, (2016) www.ncbi.nlm.nih.gov/pmc/articles/PMC4889538/.

62. Hwang S., Umar A., Dar G., Kim S., Badran R.; Synthesis and Characterization of Iron Oxide Nanoparticles for Phenyl Hydrazine Sensor Applications. *Sensor Letters*, (2014) 12: 1–5
63. Wu W., He Q. & Jiang C. Magnetic Iron Oxide Nanoparticles: Synthesis and Surface Functionalization Strategies. *Nanoscale Res Lett*, (2008), 3, 397
<https://doi.org/10.1007/s11671-008-9174-9>

APPENDIX

Table 1: Surface Coverage (%) of TEM grids with no surface modification annealed at 100°C

No Surface modification annealed at 100°C		
Time (hr)	Surface Coverage (%)	Standard Deviation (%)
0.0	83.2	0.91
1.0	82.8	9.47
2.0	86.4	5.28
6.0	61.5	2.66
18	82.4	5.16
Average	79.2	4.70

Table 2: Surface Coverage (%) of plasma cleaned TEM grids annealed at 100°C

Plasma cleaned, annealed at 100°C		
Time (hr)	Surface Coverage (%)	Standard Deviation (%)
0.0	85.5	0.93
1.0	16.1	10.0
2.0	31.3	1.40
6.0	62.7	26.5
18	14.2	19.6
Average	42.0	11.7

Table 3: Surface Coverage (%) of TEM grids with no surface modification annealed at 150°C

No Surface modification annealed at 150°C		
---	--	--

Time (hr)	Surface Coverage (%)	Standard Deviation (%)
0.0	78.0	1.40
1.0	39.7	2.56
2.0	67.4	6.77
6.0	69.6	27.7
18	23.0	17.8
Average	55.5	11.3

Table 4: Surface Coverage (%) of plasma cleaned TEM grids annealed at 150°C

Plasma cleaned, annealed at 150°C		
Time (hr)	Surface Coverage (%)	Standard Deviation (%)
0.0	39.5	34.8
1.0	8.92	1.61
2.0	20.7	2.21
6.0	12.6	3.00
18	17.0	9.13
Average	19.7	10.1

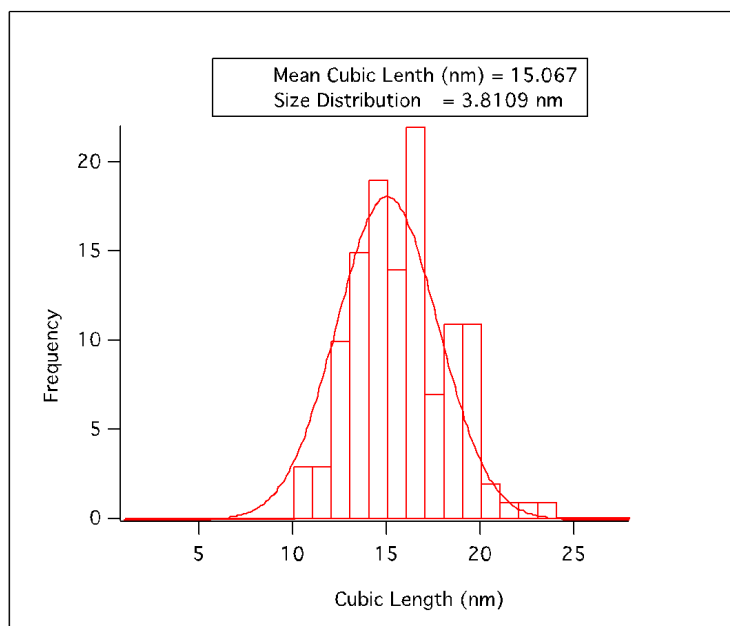


Figure 1: Nanocubes spin cast onto a TEM grid with no surface modification, and no annealing

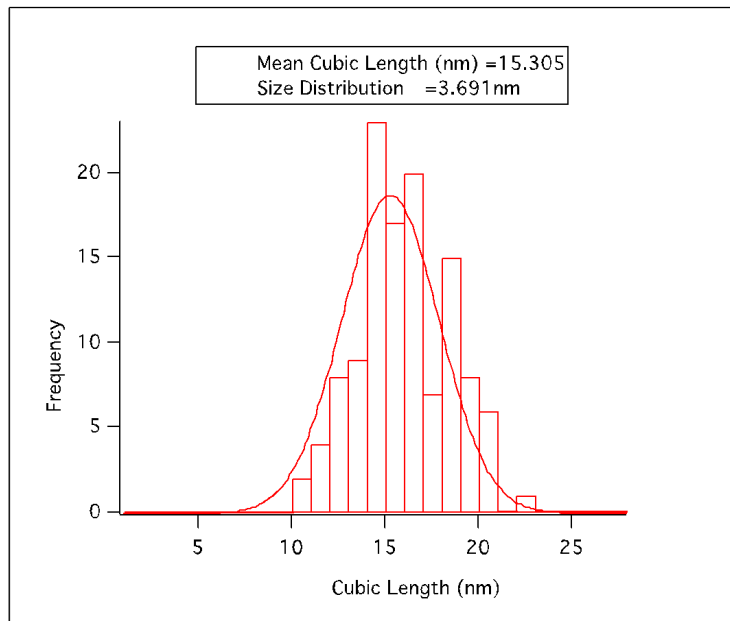


Figure 2: Nanocubes spin cast onto a TEM grid with no surface modification, annealed at 100°C for 0.5hr

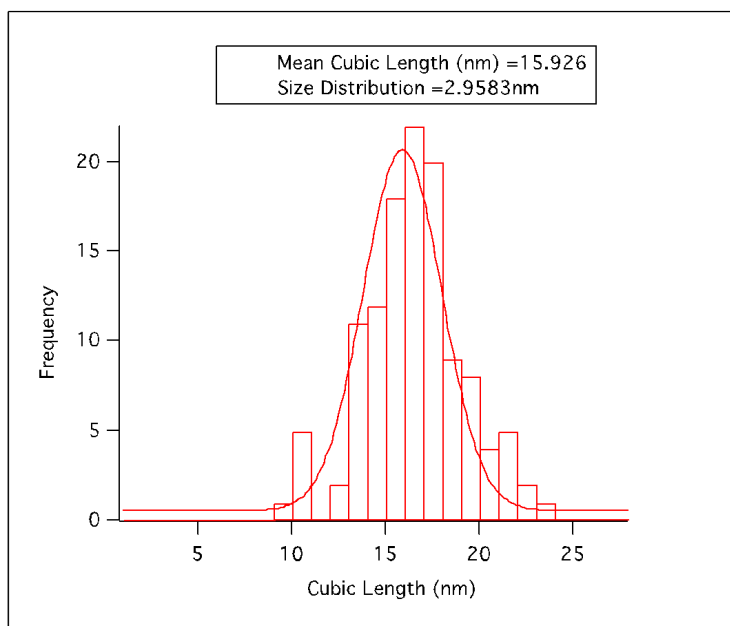


Figure 3: Nanocubes spin cast onto a TEM grid with no surface modification, annealed at 100°C for 1.0 hr

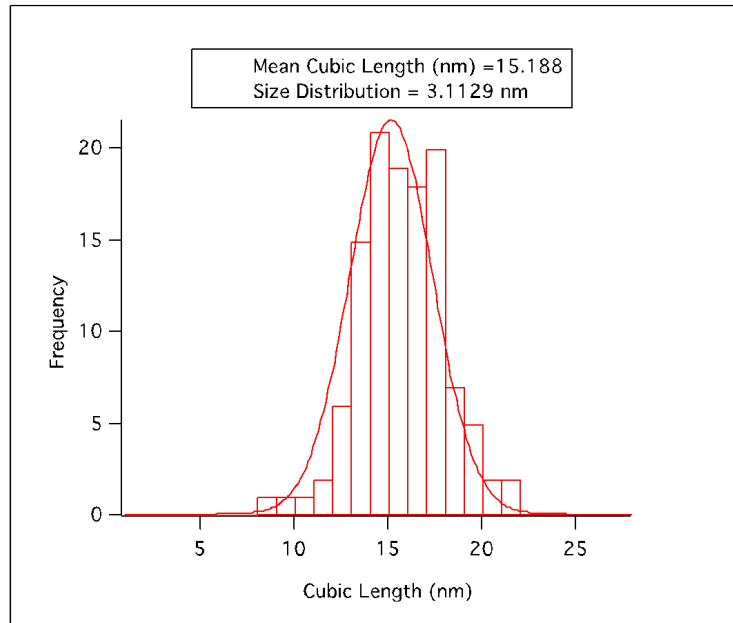


Figure 4: Nanocubes spin cast onto a TEM grid with no surface modification, annealed at 100°C for 1.5hr

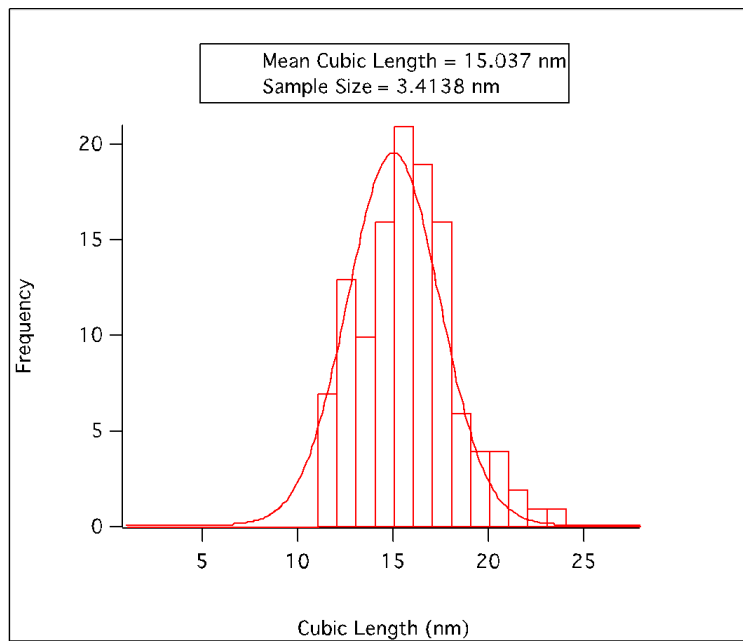


Figure 5: Nanocubes spin cast onto a TEM grid with no surface modification, annealed at 100°C for 2.0 hr

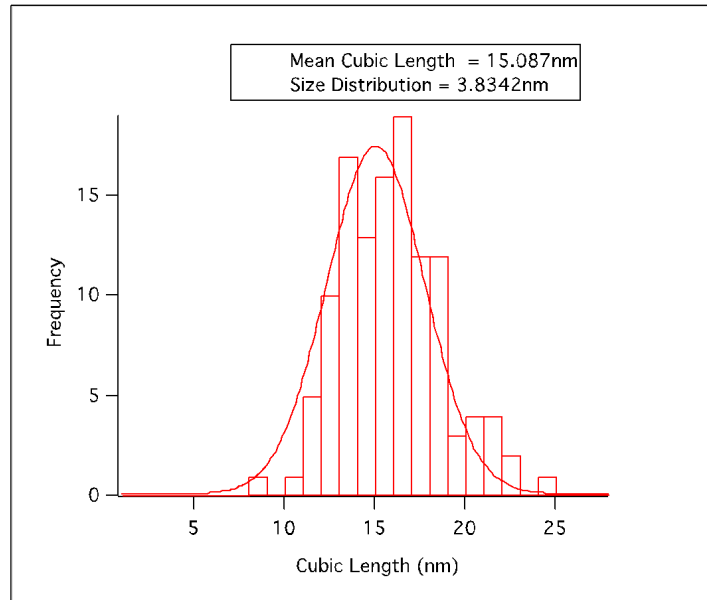


Figure 6: Nanocubes spin cast onto a TEM grid with no surface modification, annealed at 100°C for 6 hr.

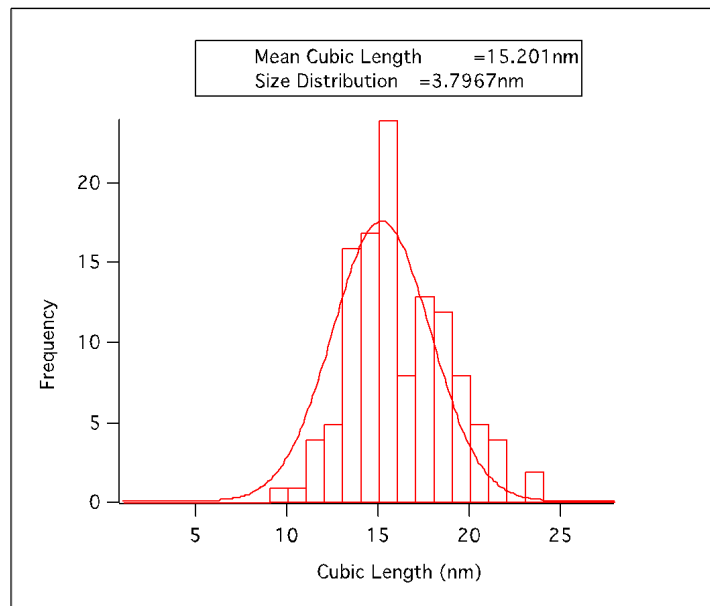


Figure 7: Nanocubes spin cast onto a TEM grid with no surface modification, annealed at 100°C for 12 hr

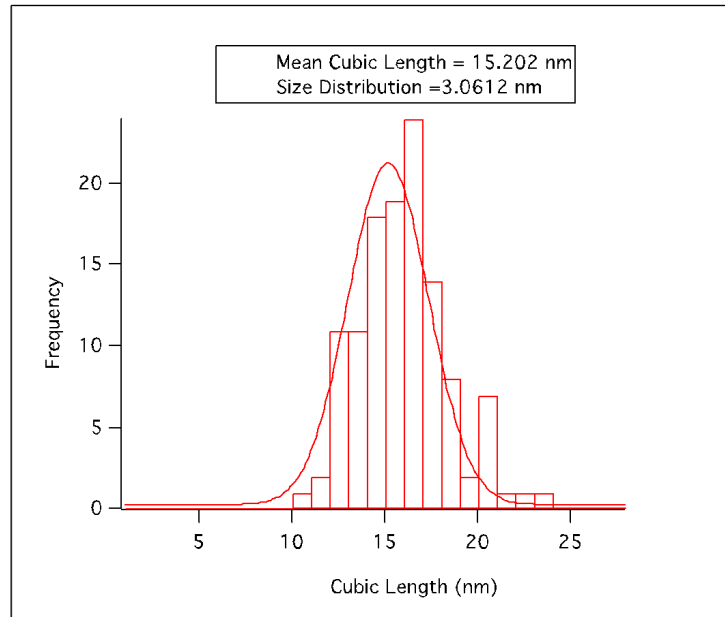


Figure 8: Nanocubes spin cast onto a TEM grid with no surface modification, annealed at 100°C for 18 hr

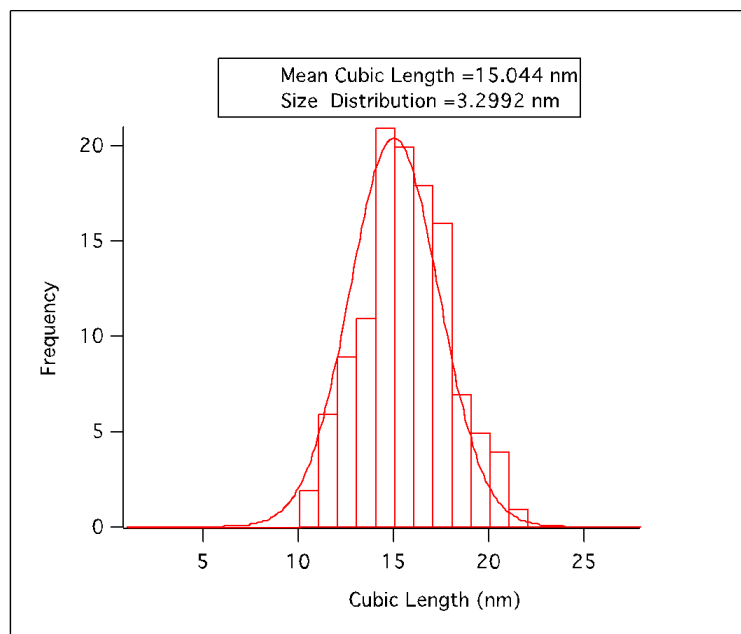


Figure 9: Nanocubes spin cast onto a TEM grid with no surface modification, annealed at 100°C for 24 hr

Table 5: Mean length of nanocubes spincast on TEM grids with no surface modification, and annealed at 100°C

No Surface Modification, Annealed at 100°C		
Annealing Time	Mean Length (nm)	Standard Deviation (nm)
0.0	15.1	3.81

0.5	15.3	3.70
1.0	16.0	3.00
1.5	15.2	3.11
2.0	15.0	3.41
6.0	15.1	3.83
12	15.2	3.80
18	15.2	3.06
24	15.0	3.30
Average	15.2	3.44

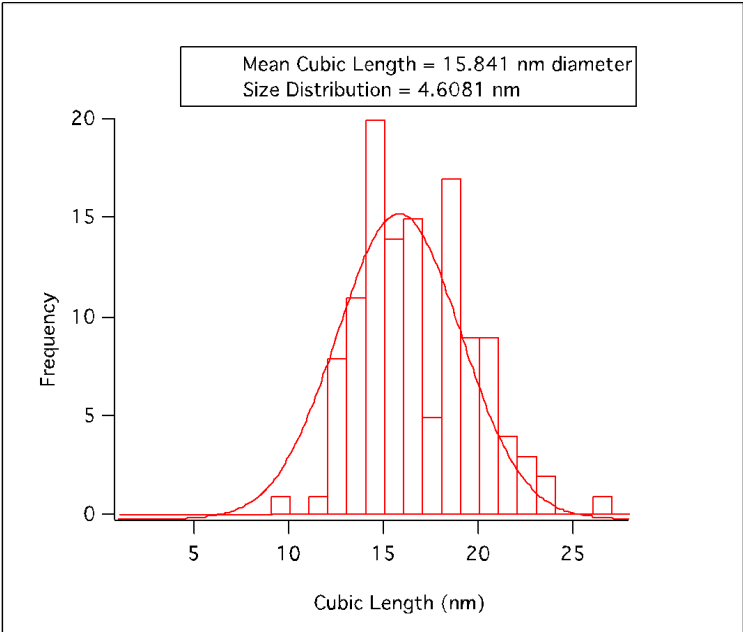


Figure 10: Nanocubes spin cast onto a plasma TEM grid with no surface modification, and no annealing

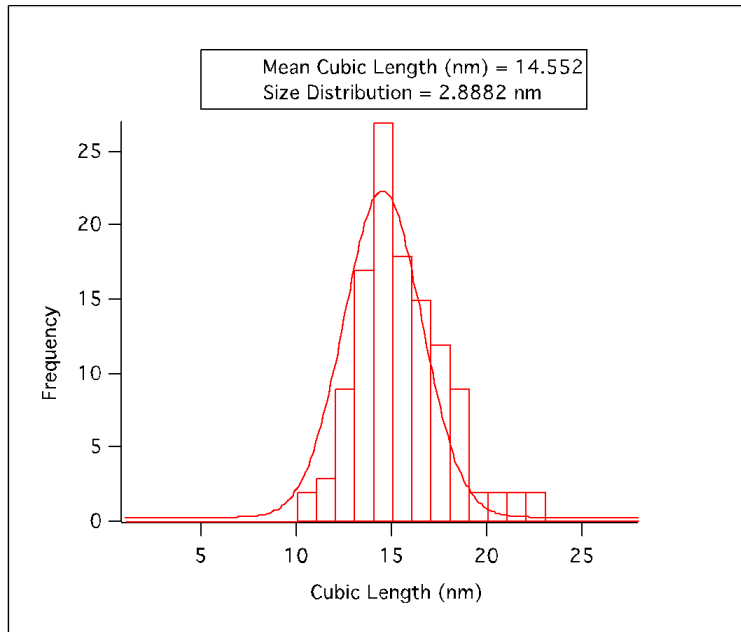


Figure 11: Nanocubes spin cast onto a plasma cleaned TEM grid, annealed at 100°C for 0.5 hr

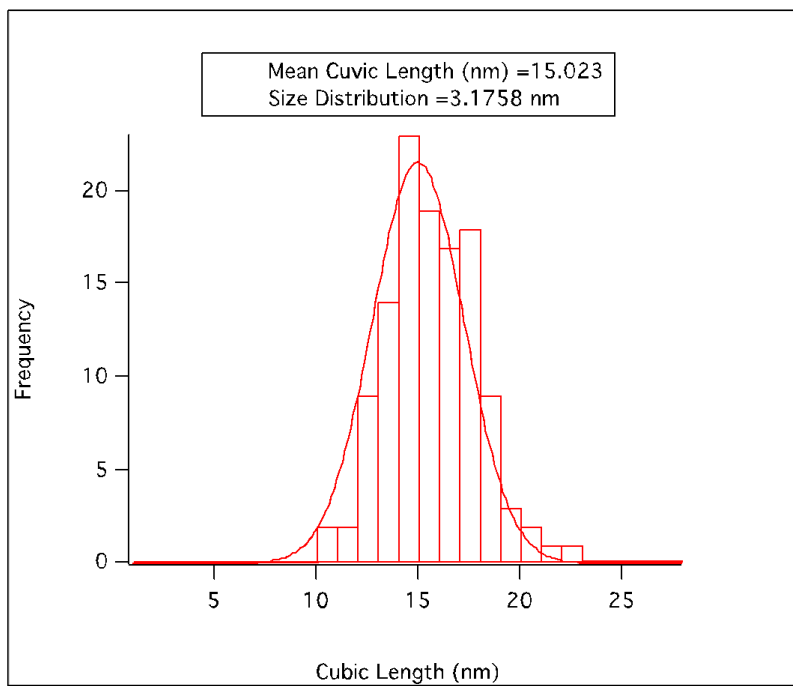


Figure 12: Nanocubes spin cast onto a plasma cleaned TEM grid, annealed at 100°C for 1.0 hr

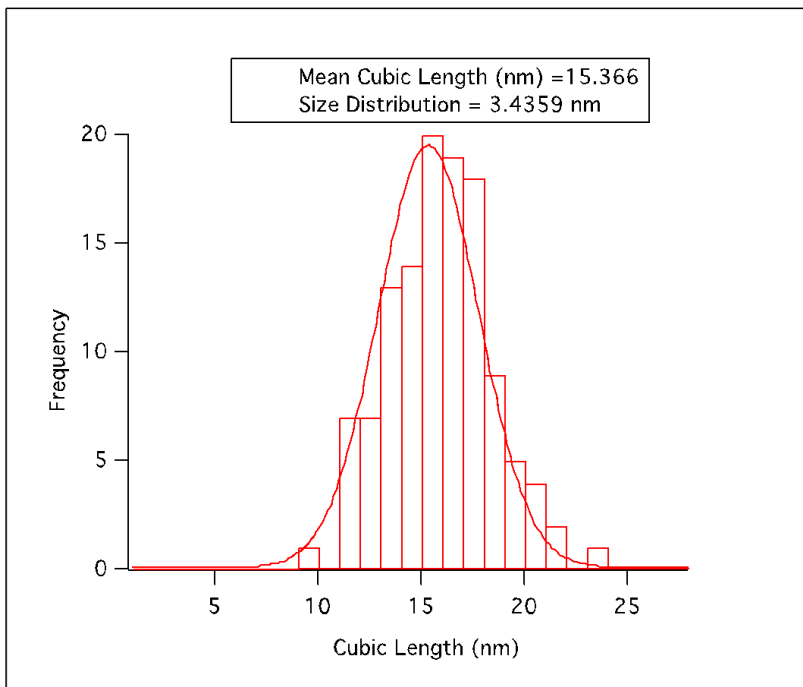


Figure 13: Nanocubes spin cast onto a plasma cleaned TEM grid, annealed at 100°C for 1.5 hr

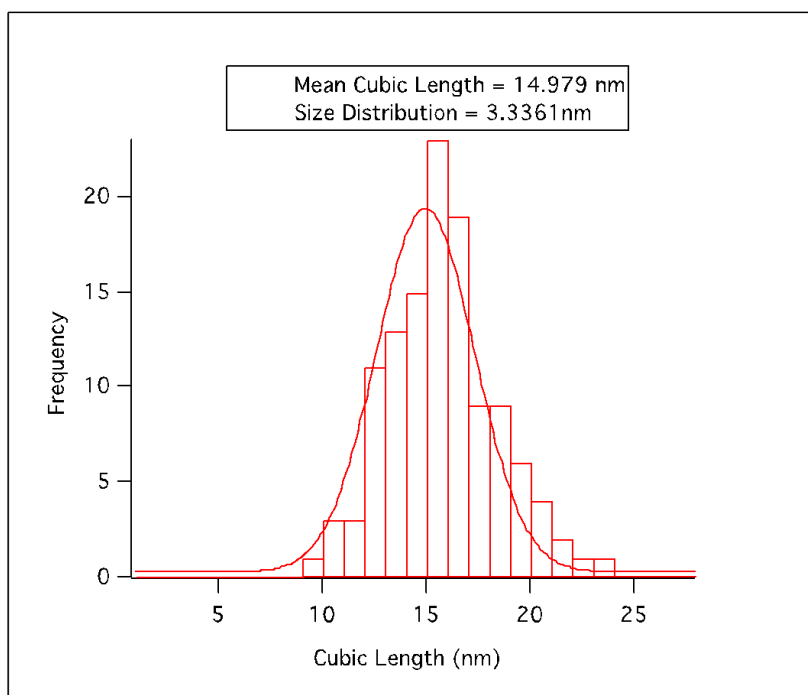


Figure 14: Nanocubes spin cast onto a plasma cleaned TEM grid, annealed at 100°C for 2.0 hr

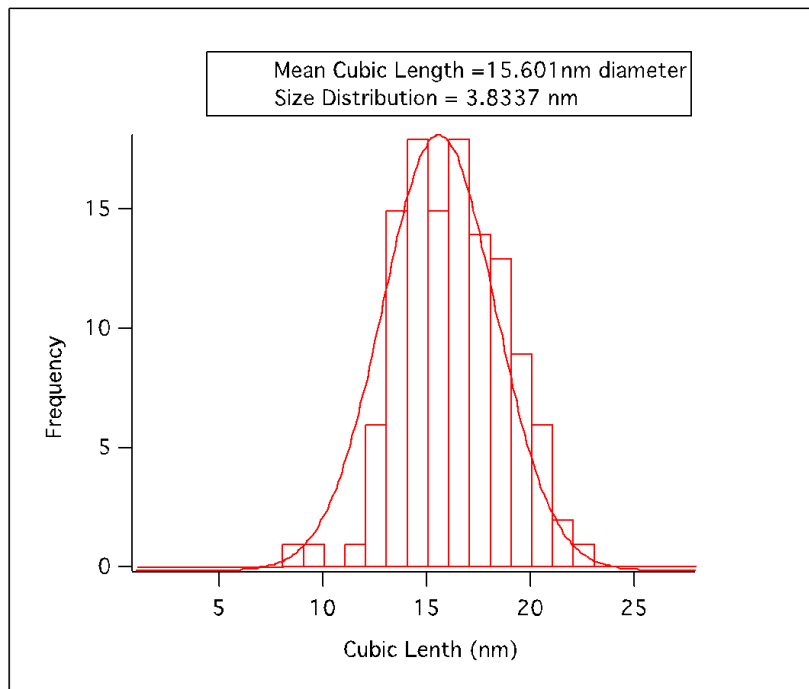


Figure 15: Nanocubes spin cast onto a plasma cleaned TEM grid, annealed at 100°C for 6.0 hr

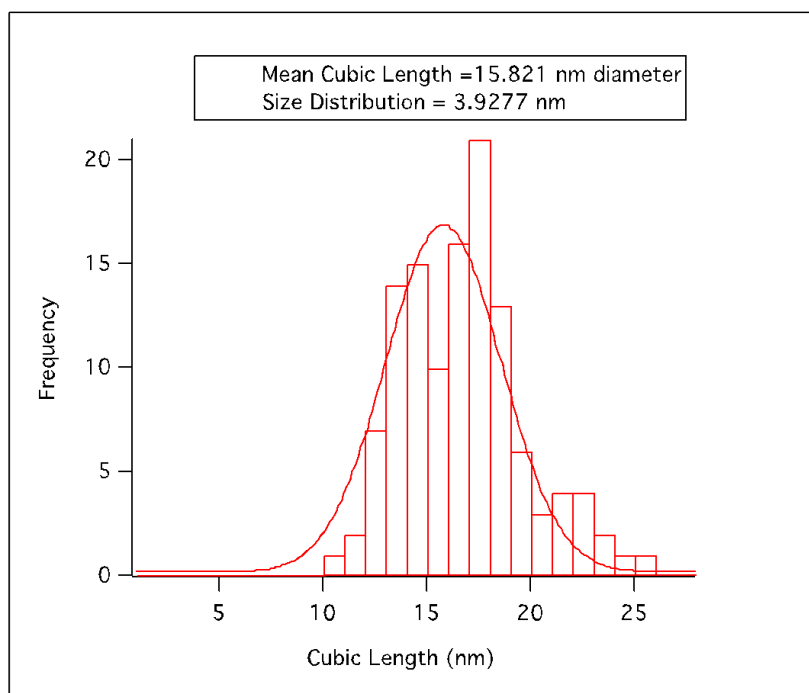


Figure 16: Nanocubes spin cast onto a plasma cleaned TEM grid, annealed at 100°C for 12.0 hr

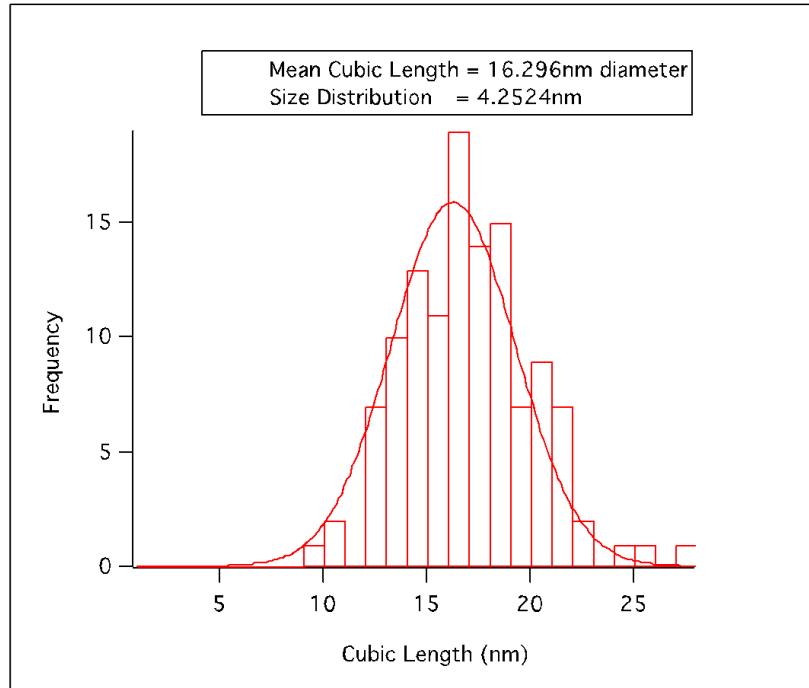


Figure 17: Nanocubes spin cast onto a plasma cleaned TEM grid, annealed at 100°C for 18.0 hr

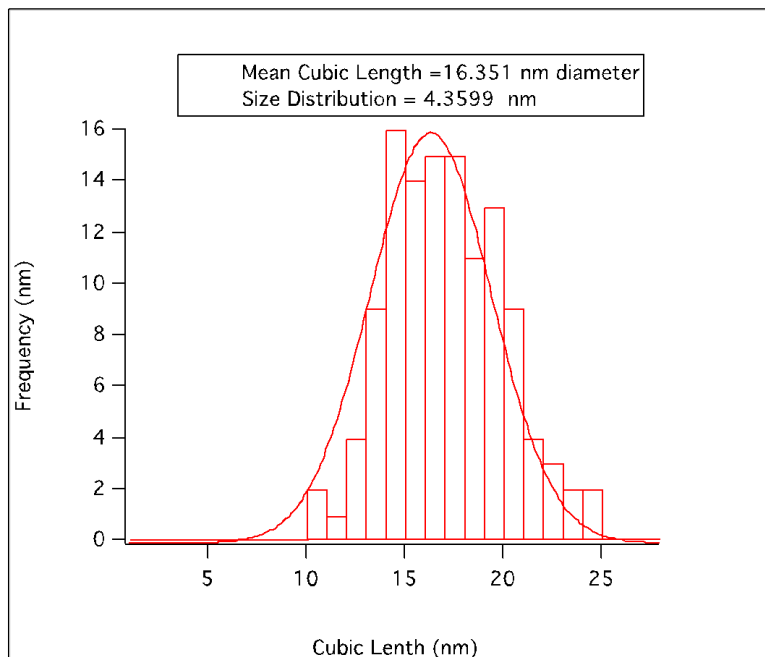


Figure 18: Nanocubes spin cast onto a plasma cleaned TEM grid, annealed at 100°C for 24.0 hr

Table 6: Mean length of nanocubes spincast on plasma cleaned TEM grids, and annealed at 100°C

Plasma Cleaned, Annealed at 100°C		
Annealing Time (hrs)	Mean Length (nm)	Standard Deviation (nm)
0.0	15.8	4.61
0.5	14.6	2.90
1.0	15.0	3.18
1.5	15.4	3.18
2.0	15.0	3.34
6.0	15.6	3.83
12	15.8	3.93
18	16.3	4.25
24	16.4	4.36
Average	15.5	3.73

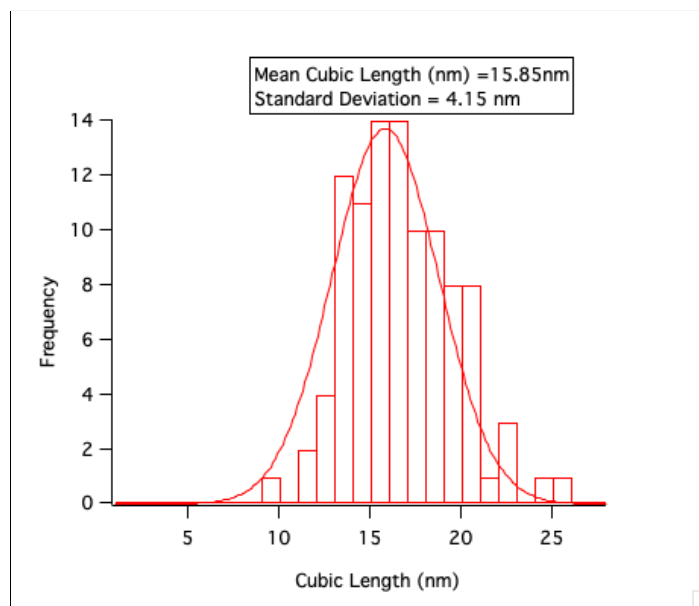


Figure 19: Nanocubes spin cast onto a TEM grid with no surface modification, annealed at 150°C for 0.5hr

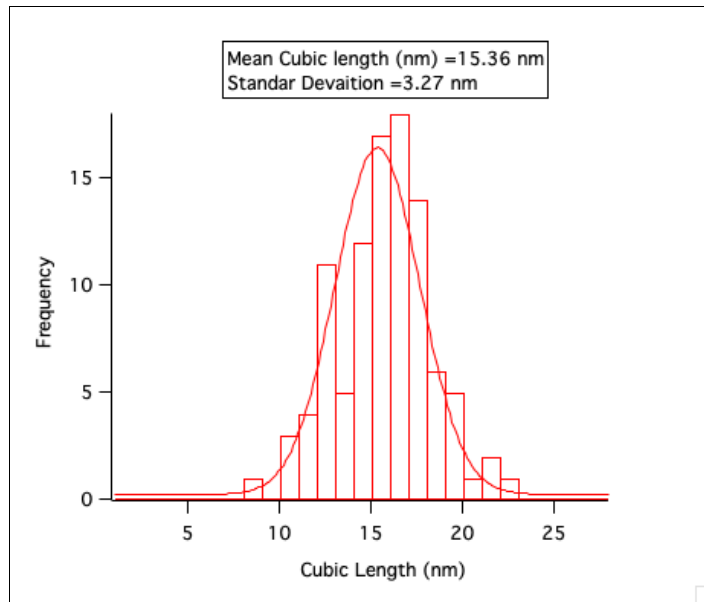


Figure 20: Nanocubes spin cast onto a TEM grid with no surface modification, annealed at 150°C for 1.0 hr

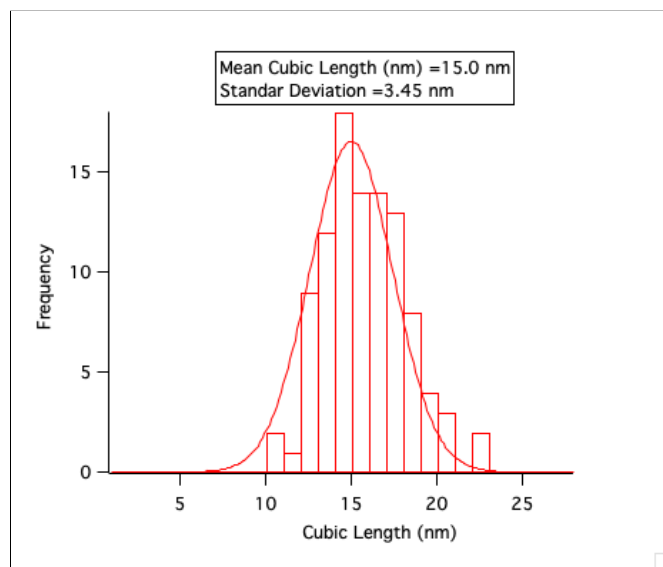


Figure 21: Nanocubes spin cast onto a TEM grid with no surface modification, annealed at 150°C for 1.5hr

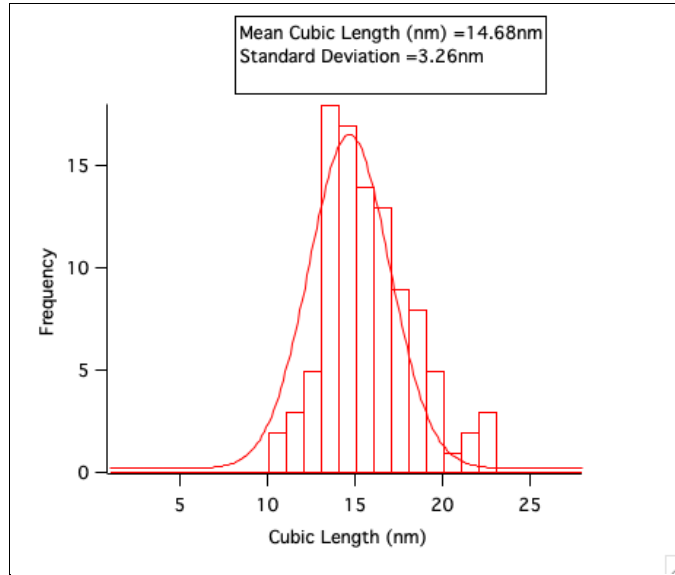


Figure 22: Nanocubes spin cast onto a TEM grid with no surface modification, annealed at 150°C for 2.0 hr

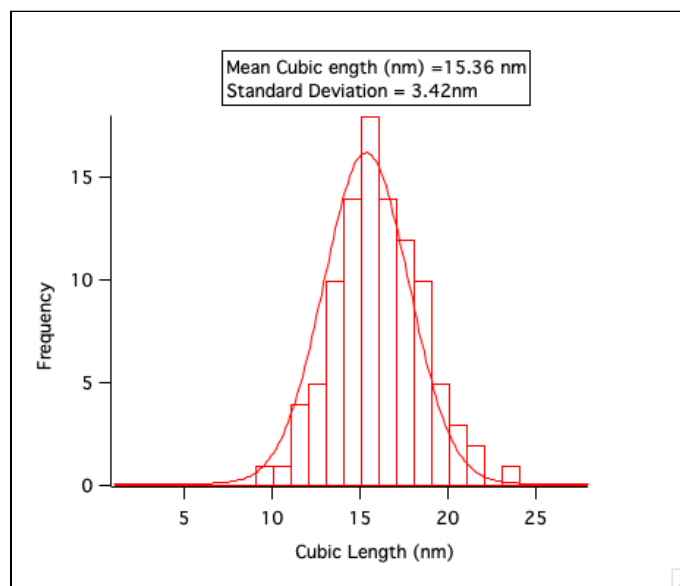


Figure 23: Nanocubes spin cast onto a TEM grid with no surface modification, annealed at 150°C for 6.0 hr

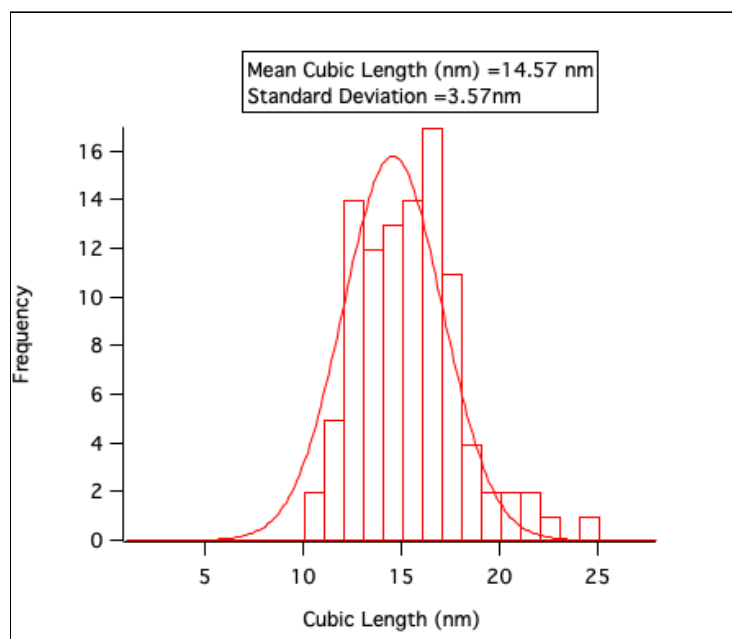


Figure 24: Nanocubes spin cast onto a TEM grid with no surface modification, annealed at 150°C for 12 hr

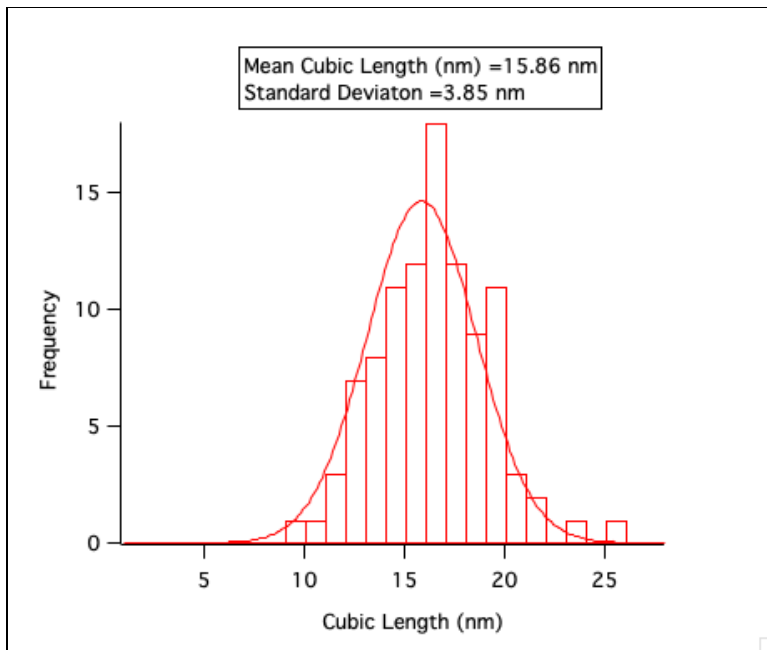


Figure 25: Nanocubes spin cast onto a TEM grid with no surface modification, annealed at 150°C for 18 hr

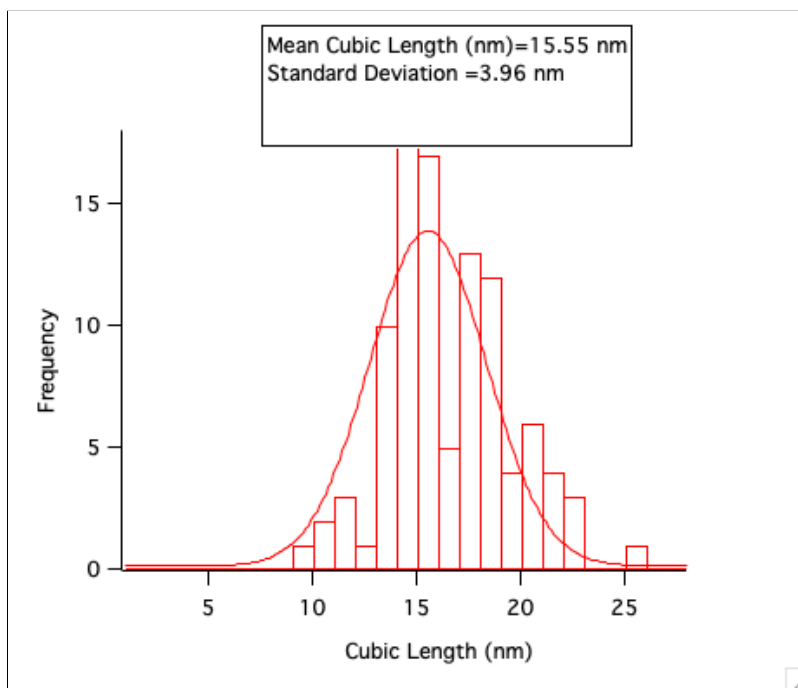


Figure 26: Nanocubes spin cast onto a TEM grid with no surface modification, annealed at 150°C for 24 hr

Table 7: Mean length of nanocubes spincast on TEM grids with no surface modification, and annealed at 150°C

No Surface Modification, Annealed at 150°C		
Annealing Time	Mean Length (nm)	Standard Deviation (nm)
0.0	15.5	3.96
0.5	15.9	3.85
1.0	14.6	3.57
1.5	15.4	3.42
2.0	14.7	3.26
6.0	15.0	3.45
12	15.4	3.27
18	15.9	4.15
Average	15.3	3.62

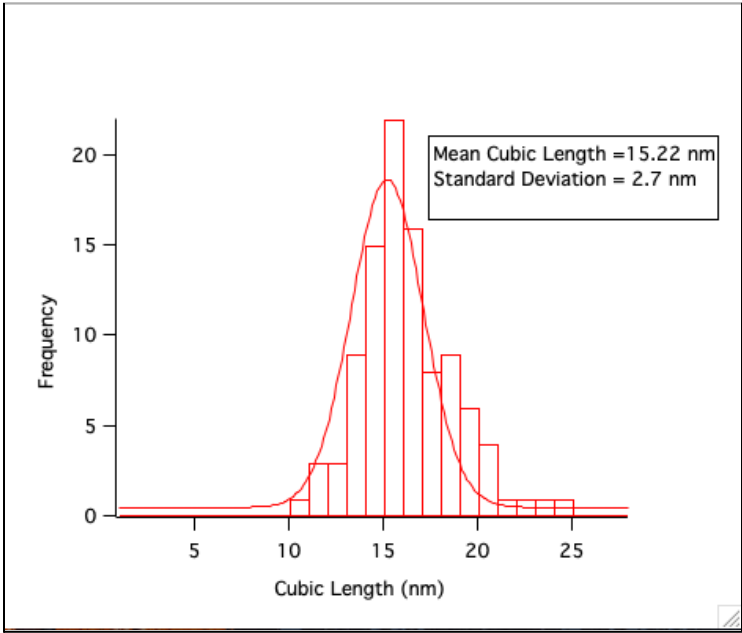


Figure 27: Nanocubes spin cast onto a plasma cleaned TEM grid, annealed at 150°C for 0.5 hr

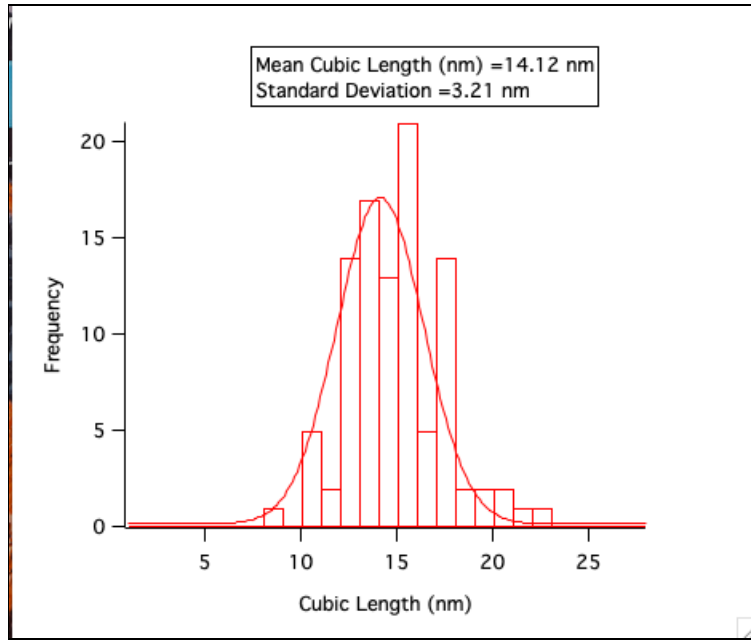


Figure 28: Nanocubes spin cast onto a plasma cleaned TEM grid, annealed at 150°C for 1.0 hr

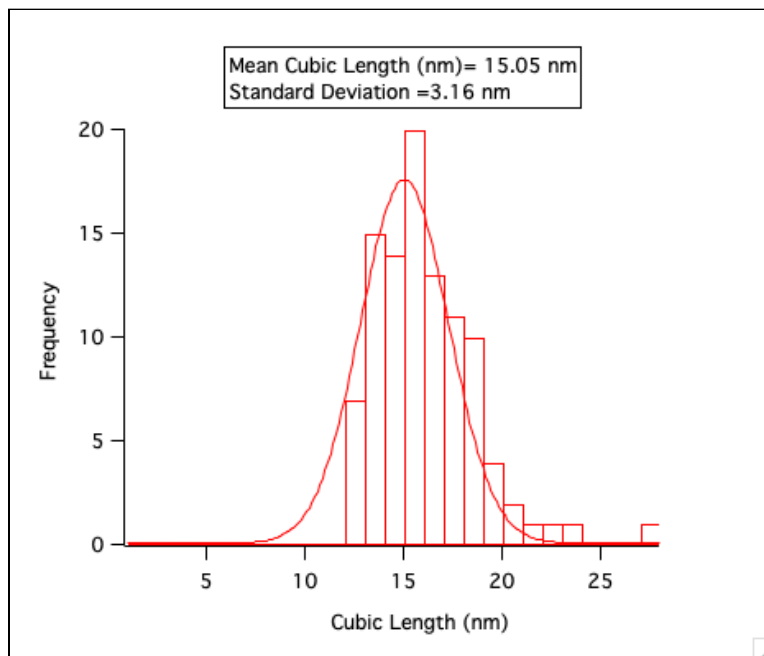


Figure 29: Nanocubes spin cast onto a plasma cleaned TEM grid, annealed at 150°C for 1.5 hr

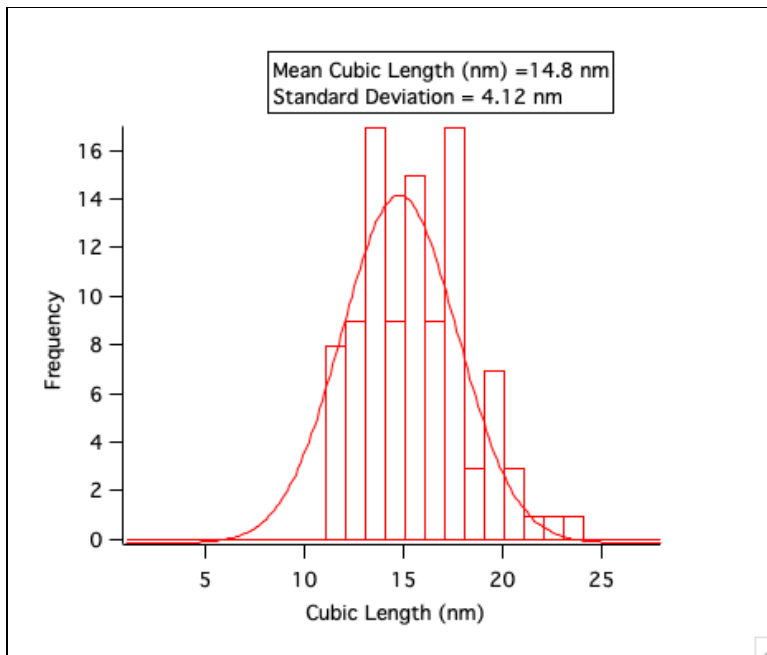


Figure 30: Nanocubes spin cast onto a plasma cleaned TEM grid, annealed at 150°C for 2.0 hr

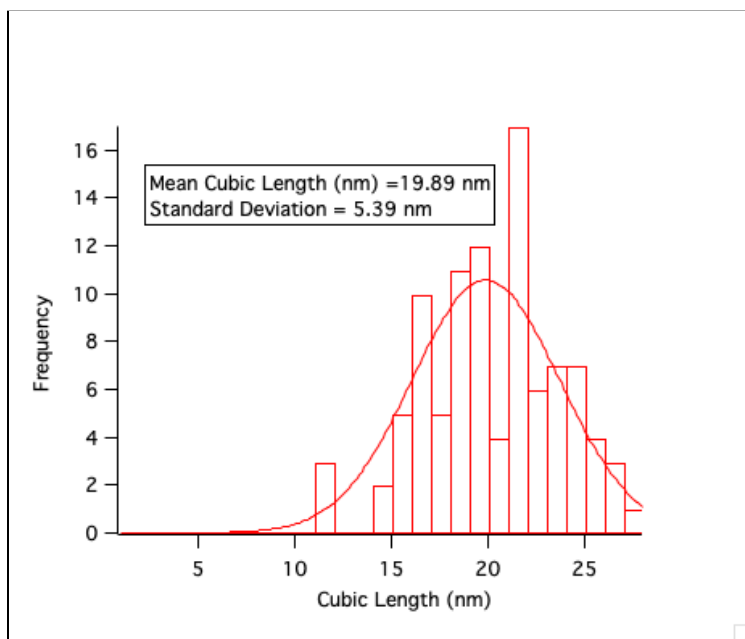


Figure 31: Nanocubes spin cast onto a plasma cleaned TEM grid, annealed at 150°C for 6.0 hr

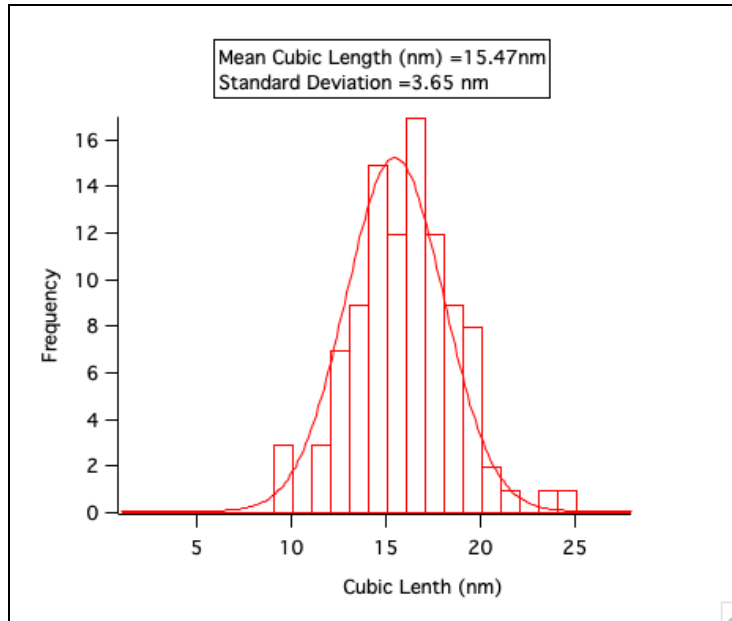


Figure 32: Nanocubes spin cast onto a plasma cleaned TEM grid, annealed at 150°C for 12 hr

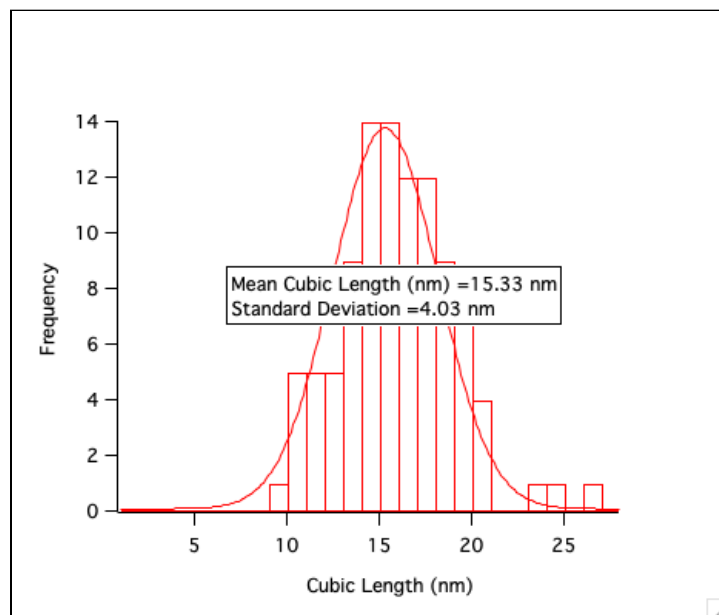


Figure 33: Nanocubes spin cast onto a plasma cleaned TEM grid, annealed at 150°C for 18 hr

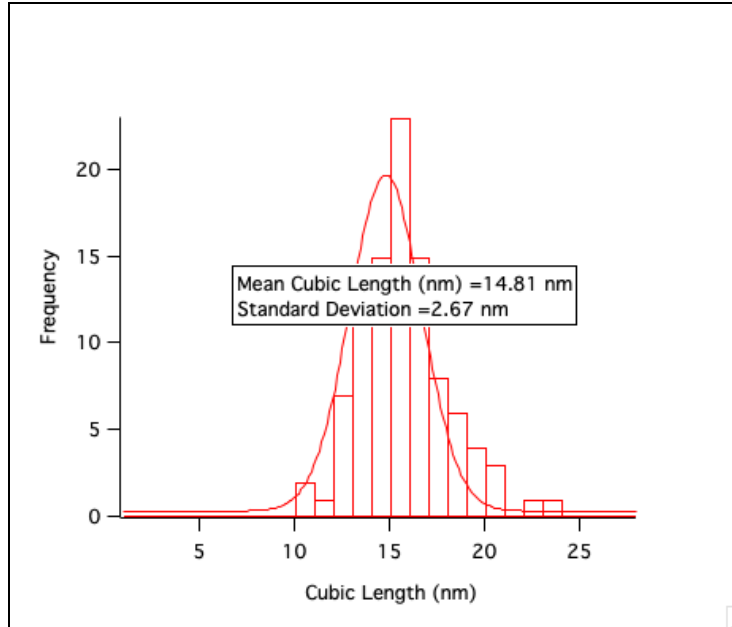


Figure 34: Nanocubes spin cast onto a plasma cleaned TEM grid, annealed at 150°C for 24hr

Table 8: Mean length of nanocubes spincast on plasma cleaned TEM grids, and annealed at 150°C

Plasma Cleaned, Annealed at 150°C		
Annealing Time (hrs)	Mean Length (nm)	Standard Deviation (nm)
0.0	15.5	3.96
0.5	15.2	2.70
1.0	14.1	3.21
1.5	15.1	3.16
2.0	14.8	4.12
6.0	20.0	5.39
12	15.5	3.65
18	15.3	4.03
24	14.8	2.67
Average	15.6	3.62